STRATIGRAPHIC CHANGES IN ICHNOPEDOFACIES OF THE UPPER TRIASSIC CHINLE FORMATION, NORTHEAST CHINLE BASIN, SOUTHEASTERN UTAH: IMPLICATIONS FOR DEPOSITIONAL CONTROLS AND PALEOCLIMATE

By

Sean J. Fischer

Submitted to the graduate degree program in Geology and the Graduate Faculty of the University of Kansas in partial fulfillment of the requirements for the degree of Master of Science.

_____

Chairperson: Dr. Stephen T. Hasiotis

_____

Dr. Evan K. Franseen

_____

Dr. Paul A. Selden

Date Defended: 9/20/16

The Thesis Committee for Sean J. Fischer

certifies that this is the approved version of the following thesis:

STRATIGRAPHIC CHANGES IN ICHNOPEDOFACIES OF THE UPPER TRIASSIC CHINLE FORMATION, NORTHEAST CHINLE BASIN, SOUTHEASTERN UTAH: IMPLICATIONS FOR DEPOSITIONAL CONTROLS AND PALEOCLIMATE

_____

Chairperson: Stephen T. Hasiotis

Date approved: 9/20/16

ABSTRACT

The Upper Triassic Chinle Formation in the Stevens Canyon area, southeastern Utah, represents fluvial, palustrine, and lacustrine strata deposited in a continental back-arc basin on the western edge of Pangea. Previous investigations interpreted a megamonsoonal climate with increasing aridity for the Colorado Plateau towards the end of the Late Triassic. In this study, we systematically integrate ichnologic and pedologic features of the Chinle Formation into ichnopedofacies to interpret paleoenvironmental and paleoclimatic variations in the northeastern part of the Chinle Basin. Seventeen ichnofossil morphotypes and six paleosol orders were combined to form 12 ichnopedofacies. Ichnopedofacies development was controlled by autocyclic and allocyclic processes, and hydrology. In the northeast Chinle Basin, annual precipitation was ~1100–1300 mm in the Petrified Forest Member. Precipitation levels were >1300 mm/yr at the base of the lower Owl Rock Member, decreased to ~700–1100 mm/yr, and then to ~400–700 mm/yr. Two drying upward cycles from ~1100 mm/yr to ~700 mm/yr are observed in the middle and upper Owl Rock members. In the Church Rock Member, precipitation decreased from ~400 mm/yr at the base of the unit to ~25–325 mm/yr at the end of Chinle Formation deposition. Ichnopedofacies indicate monsoonal conditions persisted until the end of the Triassic Period with decreasing precipitation the result of the northward migration of Pangea. Ichnopedofacies in the northeast Chinle Basin indicate both long-term drying of climate and short-term, wet-dry fluctuations. Wet-dry cycles occur at other locations in the Chinle Basin, but variation exists in interpreted precipitation levels across the Chinle Basin due to the use of different climate indices. Overall trends of decreasing paleoprecipitation between the northeast and southeast Chinle Basin during Petrified Forest Member deposition, and between the northeast and central part of the Chinle Basin basin during Owl Rock Member deposition are

recognized. Climate was not consistent across the Chinle Basin during the Late Triassic; there were complex variations in precipitation.

THESIS ACKNOWLEDGEMENTS

I thank the University of Kansas Geology Department for their support during my graduate studies. I especially thank Dr. Stephen Hasiotis for accepting me as his graduate student and his help and direction with my thesis project. Without his insight in ichnology and paleopedology and input during the editing process, this project would not have been possible. I also thank Dr. Evan Franseen and Dr. Paul Selden for being part of my Masters thesis committee, and for their comments and input during the course of the project and on the thesis manuscript.

I thank Aaron Hess, Bob Rader, and Stephen Fischer for their assistance in the field. Thanks is also to Dr. Dan Hirmas for his help in identifying paleosols and feedback concerning XRD data. I also thank Victor Day at the University of Kansas Small Molecule X-Ray Crystallography Lab for his assistance in running and analyzing XRD samples. Thanks also to the University of Kansas IchnoBioGeoSciences group for their review, input, and ideas regarding the thesis project and manuscript.

I thank the graduate students at the University of Kansas for their help, support, and fellowship throughout my graduate studies. I especially thank Andy Connelly, Amanda Falk, Alexa Goers, James Golab, Sean Hammersburg, Josh Hogue, Adam Jackson, Matt Jones, and Bob Rader for their emotional support and wisdom. I could not have finished this project without their encouragement and insight.

Finally, I thank my parents Stephen and Celeste Fischer, brother Eric Fischer, and sister Lindsey Fischer for their love and support throughout this whole process. I could not have completed my Masters thesis without them and their daily phone calls of encouragement kept me on track when progress was tough. I will forever be grateful for their patience and understanding

as I completed my degree, and for believing in me when I myself doubted I would finish. I also thank the rest of my family for their continued encouragement and support during my graduate studies and for their enthusiasm in hearing about my thesis progress.

TABLE OF CONTENTS

INTRODUCTION

Analyses of paleosols and ichnofossils provide a wealth of hydrologic and climatic information in continental sedimentary deposits (e.g., Driese and Foreman 1992; Turner 1993; Hasiotis and Dubiel 1994; Driese et al. 1995; Kraus 1999; Retallack 2001; Driese and Mora 2002; Prochnow et al. 2006a; Hasiotis et al. 2007, Cleveland et al. 2008a; Dubiel and Hasiotis 2011; Hasiotis and Platt 2012). This study combines lithofacies, paleosols, and ichnocoenoses of the Upper Triassic Chinle Formation (Fm) into ichnopedofacies to interpret paleoenvironmental conditions and paleoclimatic changes in the northeast Chinle Basin. These interpretations, in turn, will enable more detailed reconstructions of the variability in sedimentation rate, tectonics, and climate across the Chinle Basin, building a more accurate regional picture of the Chinle Fm through the Late Triassic. This is the first study to systematically integrate pedogenic and ichnologic features in the Chinle Fm to determine local controls on base level, sediment deposition, pedogenesis, groundwater profile, and environments.

Paleosols record the relative influence of soil-forming factors—Climate, Organisms, Topography, Parent material, and Time (Jenny 1941)—that modified sediments deposited on ancient landscapes (e.g., Retallack 2001; Hasiotis 2004, 2008; Hasiotis and Platt 2012). Ichnofossils form through the interaction of organisms with a medium to produce three-dimensional (3D) structures and are influenced by such physiochemical factors as sedimentation rate, depositional energy, groundwater profile, nutrients, and oxygenation (Hasiotis 2007; Hasiotis et al. 2007; Hasiotis and Platt 2012). Combinations of these physiochemical factors, unique to different depositional settings, are indicated by ichnocoenoses (ichnocoenosis, singular)—co-occurring ichnofossil assemblages representing an ancient biological community interacting with the environment (Hasiotis et al. 2012; Hasiotis and Platt 2012). Ichnocoenoses

are useful for identifying continental subenvironments (e.g., Hasiotis 2004, 2008; Hasiotis et al. 2007, 2012; Smith et al. 2008b; Hasiotis and Platt 2012). Combining ichnology and paleopedology to develop ichnopedofacies models—associations of ichnocoenoses and pedogenic features (Hasiotis et al. 2007)—allows for higher resolution interpretations of physiochemical conditions and soil-forming factors in the northeast Chinle Basin during the Late Triassic.

The main objectives of this study are to: 1) determine the variation of depositional systems and paleoenvironmental settings; 2) establish ichnopedofacies and physiochemical conditions; and 3) interpret fine-scale climatic conditions in the northeastern Chinle Basin and compare it to the regional paleoclimate of the southwestern United States. Finer scale sedimentologic studies of the Chinle Fm are needed to more accurately interpret the spatial and temporal differences in sediment deposition, continental subenvironments, and climate between the edge and center of the Chinle Basin during the Late Triassic.

BACKGROUND

The Chinle Fm has been a target for stratigraphic and sedimentologic studies (e.g., Repenning et al. 1969; Stewart et al. 1972; Blakey and Gubitosa 1983; Dubiel 1987, 1992; Blakey 1989; Hazel 1994; Tanner 2000; Woody 2006; Trendell et al. 2012) due to its paleontology (e.g., Colbert 1974; Ash 1975, 1987; Hasiotis and Mitchell 1993; Hasiotis et al. 1993; Schwartz and Gillette 1994; Therrien and Fastovsky 2000; Harris and Downs 2002; Gaston et al. 2003; Parker and Irmis 2006; Irmis et al. 2007; Stocker 2012) and uranium ore (e.g., Abdel-Gawad and Kerr 1963; Lupe 1977; Dubiel 1983). Numerous investigators have interpreted the Chinle Fm as a complex mosaic of continental depositional environments (e.g.,

Stewart et al. 1972; Blakey and Gubitosa 1983; Dubiel 1987, 1989; Dubiel and Hasiotis 2011), which were influenced by sedimentation rate, basin subsidence, and climate. Stewart et al. (1972) conducted one of the first extensive correlations of Chinle Fm members across the Colorado Plateau and identified large incised paleovalleys within Chinle Fm strata. Blakey and Gubitosa (1983) and Dubiel (1987) described cyclic fluvial-lacustrine depositional sequences, and Blakey and Gubitosa (1983) interpreted paleovalleys to separate these cycles. Dubiel and Hasiotis (2011) further interpreted incised paleovalleys as sequence stratigraphic boundaries that separated each member of the Chinle Fm, with each member representing a major degradational–aggradational cycle.

Pedologic and ichnologic studies in the Chinle Fm have been limited in scope. Local investigations of Chinle Fm paleosols have been concentrated in the center of the Chinle Basin around Petrified Forest National Park (PFNP) (e.g., Kraus and Middleton 1987a; Therrien and Fastovsky 2000; Trendell et al. 2012, 2013a, 2013b; Atchley et al. 2013), with other studies conducted in northern New Mexico (Cleveland et al. 2007, 2008a, 2008b), western Colorado (Dubiel et al. 1992), and eastern Utah (Prochnow et al. 2005, 2006a, 2006b). Much of this research utilized paleosols to interpret fluvial architecture and sequence stratigraphy, showing that local fluvial evolution, topographic position, and salt tectonics had as great an, or even greater, influence on sedimentation and pedogenesis as did regional climate (e.g., Kraus and Middleton 1987a; Prochnow et al 2005, 2006b; Cleveland et al. 2007; Trendell et al. 2012, 2013a). Few paleosol studies in the Chinle Fm, though, have been combined with ichnologic observations beyond plant ichnofossils (e.g., Dubiel et al 1992; Cleveland et al. 2008a; Dubiel and Hasiotis 2011; Ash and Hasiotis 2013). Despite numerous descriptions of Chinle Fm ichnofossils from PFNP (e.g., Hasiotis and Dubiel 1993a, 1993b, 1995a, 1995b; Martin and

Hasiotis 1998; Hasiotis and Martin 1999), research beyond this area of the Chinle Basin is limited (e.g., Hasiotis and Mitchell 1993; Hasiotis et al. 1993; Hasiotis and Dubiel 1994; Hasiotis 1995; Gaston et al. 2003; Gillette et al. 2003), and few studies have established detailed local ichnocoenoses (Hasiotis and Dubiel 1993b). More thorough studies combining ichnologic and paleopedologic observations of Chinle Fm strata are imperative to interpret fine-scale climatic conditions across the Chinle Basin.

GEOLOGIC SETTING AND STUDY AREA

Geologic Setting

The Upper Triassic Chinle Fm was deposited in a continental back-arc basin on the western edge of Pangea between 5–30° N paleolatitude (e.g., Van der Voo et al. 1976; Dickinson 1981; Parrish and Peterson 1988; Bazard and Butler 1991) (Fig. 1). Pangea migrated north during Chinle Fm deposition and the Colorado Plateau region reached 30° N paleolatitude by the Early Jurassic (e.g., Cleveland et al. 2008a; Dubiel and Hasiotis 2011). The dominant drainage was to the northwest, and paleoriver systems sourced from the Ouachita orogen in Texas flowed through both the Dockum and Chinle basins (e.g., Dubiel 1994; Riggs et al. 1996; Dickinson and Gehrels 2008; Dubiel and Hasiotis 2011). Sediment sources were the Uncompaghre Uplift, Amarillo-Wichita Highlands, and a magmatic arc on the western coast of Pangea that also supplied ash to the Chinle Basin (Fig. 1; e.g., Stewart et al. 1972, 1986; Blakey and Gubitosa 1983; Riggs et al. 1996). Concurrent salt tectonism in the Salt Anticline Region of eastern Utah and western Colorado locally affected fluvial architecture, depositional geometries, and paleosol development (e.g., Cater 1970; Hazel, 1994; Prochnow et al., 2006b).

The Chinle Fm consists of, in ascending order, the Shinarump, Monitor Butte, Moss Back, Petrified Forest, Owl Rock, and Church Rock members (mbrs), and has a maximum thickness of over 500 m in the southern Four Corners area, thinning to the northwest and northeast (Fig. 2; e.g., Stewart et al. 1972; Dubiel 1987, 1989; Dubiel 1994). Chinle Fm strata are separated from the Lower to Middle (?) Triassic Moenkopi Fm by the T-3 unconformity across the majority of the Colorado Plateau, and also unconformably overlie the Lower Permian DeChelly Sandstone in northern Arizona (e.g., Stewart et al. 1972; Pipiringos and O'Sullivan 1978; Dubiel et al. 1996; Dubiel and Hasiotis 2011). The J-0 unconformity marks the boundary between the Chinle Fm and the overlying Lower Jurassic Wingate Sandstone (e.g., Pipiringos and O'Sullivan 1978; Dubiel 1994; Hazel 1994).

During the Late Triassic, deposition in the Chinle Basin was influenced by a megamonsoonal climate with wet and dry seasons (e.g., Parrish and Peterson 1988; Dubiel et al. 1991; Dubiel 1994; Dubiel and Hasiotis 2011). Conditions became more arid towards the end of Chinle Fm deposition, represented by eolian sand sheet and playa lake strata in the Church Rock and equivalent Rock Point mbrs (Dubiel 1989; Dubiel et al. 1991; Tanner and Lucas 2006; Dubiel and Hasiotis 2011). Chinle Fm sediments were eventually buried by migrating sand dunes of the Lower Jurassic Wingate Sandstone (e.g., Blakey and Gubitosa 1983; Parrish and Peterson 1988; Dubiel 1989). The transition to drier conditions reflects the northward migration of Pangea towards the mid-latitudes (e.g., Dubiel 1994, Cleveland et al. 2008b; Dubiel and Hasiotis 2011).

Study Area

The study area is 56 km south of Moab, Utah, near the southeastern border of Canyonlands National Park (Fig. 3). Outcrops were investigated in Stevens Canyon and Indian

Creek Canyon (Fig. 3). The Upper Triassic Chinle Fm is locally represented by the Monitor Butte, Moss Back, Petrified Forest, Owl Rock, and Church Rock mbrs (Fig. 4). The top of the Chinle Fm is overlain by the Lower Jurassic Wingate Sandstone (e.g., Hasiotis and Mitchell 1993; Hasiotis et al. 1993).

The Monitor Butte Member (Mbr) overlies and locally fills paleochannels incised into the Shinarump Mbr and unconformably overlies the Moenkopi Fm (Stewart et al. 1972; Dubiel and Hasiotis 2011). Only the top of the Monitor Butte Mbr was observed at one measured section and consists of red, yellow, and green-grey mudstone. Volcanic ash is a significant component of clastic sediment, as evidenced by increased amount of bentonite, altered lithic clasts, and relict glass shards (Dubiel 1987, 1989; Dubiel and Hasiotis 2011). The Monitor Butte Mbr is interpreted as a complex mosaic of meandering fluvial, palustrine, lacustrine, and deltaic environments (Blakey and Gubitosa 1983, 1984; Dubiel and Hasiotis 2011).

The Moss Back Mbr is preserved within the Cottonwood Paleovalley, which incised into the underlying Monitor Butte Mbr and Moenkopi Fm (e.g., Stewart et al. 1972; Blakey and Gubitosa 1983, Dubiel and Hasiotis 2011). Strata consist of brown to grey, medium-grained sandstone and carbonate-nodule conglomerate (e.g., Stewart et al. 1972, Dubiel 1987, 1989). Sandstones contain tabular-planar and trough-cross stratification, large-scale lateral accretion, and rarer horizontal lamination, and sandbodies consist of stacked, interconnected, broad sand sheets (e.g., Blakey and Gubitosa 1984; Dubiel 1994; Dubiel and Hasiotis 2011). Depositional environments are interpreted as braided fluvial systems (e.g., Blakey and Gubitosa 1983, 1984; Dubiel 1989; Dubiel et al. 1991).

The Petrified Forest Mbr overlies the Moss Back and Monitor Butte mbrs (e.g., Stewart et al. 1972; Dubiel and Hasiotis 2011). Lithofacies consist of lavender and brown, bentonitic

sandstone and variegated, carbonate-nodule-bearing mudstone (e.g., Dubiel 1989, Therrien and Fastovsky 2000; Dubiel and Hasiotis 2011). Sandstones display trough-cross stratification and lateral accretion, contain thin carbonate-nodule conglomerate lenses, and occur as ribbon and narrow sheet sand bodies encased in mudstone (e.g., Blakey and Gubitosa 1984; Dubiel 1987, 1989). Volcanic ash is a significant component of clastic sediment (Dubiel 1987, 1989; Dubiel and Hasiotis 2011). The Petrified Forest Mbr was deposited in palustrine and high-sinuosity, suspended-load fluvial environments (e.g., Blakey and Gubitosa 1983; Dubiel 1987; Dubiel et al. 1991).

The Owl Rock Mbr overlies the Petrified Forest Mbr. Lithofacies consist of orange and red siltstone (e.g., Stewart et al. 1972; Dubiel 1987). Intraformational carbonate-nodule conglomerate lenses derived from adjacent Owl Rock Mbr paleosols are present and display large-scale, lateral accretion (e.g., Tanner 2000; Dubiel and Hasiotis 2011). The Owl Rock Mbr was deposited in fluvial and lacustrine environments (e.g., Blakey and Gubitosa 1983; Dubiel 1994; Dubiel and Hasiotis 2011).

The Church Rock Mbr overlies the Owl Rock Mbr. Lithofacies consist of red, orange, and brown siltstone and sandstone, with sandstone occurring as broad sheet and ribbon sand bodies that display trough-cross stratification, ripple-cross lamination, horizontal lamination, and lateral accretion (e.g., Stewart et al. 1972; Blakey and Gubitosa 1983, 1984; Dubiel 1989; 1994). The Church Rock Mbr was deposited in fluvial and playa lake environments (e.g., Dubiel 1987; Dubiel et al. 1991).

METHODS

Field

Eight sections along Stevens Canyon and one section in Indian Creek Canyon (see Fig. 3B) were measured using a 1.5-m-long Jacobs Staff. Description of sedimentary facies included unit thickness, color, grain size, grain type, degree of sorting, sedimentary structures, and bedding morphology (e.g., Compton 1985). Lithofacies were separated according to grain size, and then further subdivided based on dominant sedimentary structures (e.g., Miall 1996; van der Kolk et al. 2015). Facies associations were assigned according to Collinson (1986) and Miall (1996). Photographs of outcrop were taken with a Canon PowerShot™ ELPH 115 IS camera. Chinle Fm units were correlated by walking out lithofacies associations at the outcrop and by tracing them out from panoramic photos.

Ichnofossils were described by their architectural and surficial morphology, and internal fill (Hasiotis and Mitchell 1993; Hasiotis et al. 1993; Bromley 1996). Ichnofossils were also assigned to burrowing behaviors defined by Hasiotis (2000, 2004, 2008), which reflect spatial position and moisture zones in the soil profile. Epiterraphilic behavior is displayed by ichnofossils constructed on the surface of the soil profile and include trackways (Hasiotis 2004, 2008). Terraphilic behavior is reflected by ichnofossils constructed above the water table near the surface of the soil-water profile and in the upper vadose zone where 100% soil moisture levels are rarely reached (Hasiotis 2004, 2008; Hasiotis et al. 2007). Hygrophilic behavior reflects burrow construction above the water table in the upper, intermediate, and lower vadose zone (Hasiotis 2004, 2008; Hasiotis et al. 2007). Ichnofossils displaying hygrophilic behavior require specific morphological and reproductive moisture levels in order to form (Hasiotis 2004,

2008; Hasiotis et al. 2007). Ichnofossils constructed in fully saturated conditions at or beneath the water table in the phreatic zone, or beneath the sediment surface under open bodies of water, display hydrophilic behavior (Hasiotis 2004, 2008; Hasiotis et al. 2007). Specific ichnogenera (or ichnofossils) can reflect more than one behavior. Ichnocoenoses were determined through immediate horizontal and vertical associations of ichnofossils along stratigraphic horizons, and named according to the dominant ichnogenus (or ichnofossil) present (Hasiotis 2004, 2008; Hasiotis et al. 2007).

Paleosols were described according to Mack et al. (1993), Kraus (1999), and Retallack (2001). Pedogenic observations included matrix color, mottling color, horizonation, soil structures, slickensides, and calcium carbonate nodules. Color was determined from fresh exposure using Munsell soil color (Munsell Soil Color Book 2009). Stage of calcium carbonate accumulation was described according to Gile et al. (1966) and Machette (1985). Paleosols were classified as Entisols if primary sedimentary structures were present (Hasiotis et al. 2007; Dubiel and Hasiotis 2011). Inceptisols and Calcic Inceptisols were defined as weakly developed paleosols with incipient horizonation and calcium carbonate accumulation (*sensu* Mack et al. 1993) similar to Stages 1–2 of calcic horizon development (Gile et al. 1966; Machette 1985). Inceptisols were differentiated from Entisols by a lack of primary sedimentary structures. Vertisols were identified by slickensides, prismatic peds, and redoximorphic coloration (Dubiel and Hasiotis 2011). Alfisols and Calcic Alfisols were defined as paleosols containing elevated clay horizons (*sensu* Mack et al. 1993) and calcium carbonate accumulation similar to Stages 2–3 of calcic horizon development (Gile et al. 1966; Machette 1985).

Ichnopedofacies were constructed based on vertical and lateral associations of sedimentary facies, ichnofossils, and pedologic features (e.g., Hasiotis et al. 2007). First, the

dominant sedimentary facies were described. Then, horizons were differentiated and the paleosol order was identified. Next, the features of the dominant ichnocoenosis present were incorporated into the pedogenic diagnosis. From this, ichnopedofacies were named by combining the names of the dominant ichnocoenosis and paleosol (if present) comprising the unit.

Laboratory

Twenty-two blue-epoxy-impregnated thin sections (7.62 × 5.08 cm) were observed under a Nikon Eclipse™ E600 POL petrographic polarizing light microscope (1–40×) with attached digital camera for lithologic description. Pedologic micromorphology was described according to Brewer (1976). Rock samples were also observed under a Nikon SMZ™ 1000 binocular scope (1–8×) for lithologic and ichnologic description. Descriptions from microscope supplemented field observations and aided classification of sedimentary facies, ichnocoenoses, and paleosol orders.

Samples were crushed to under 150 μm for X-ray diffraction (XRD) and X-ray fluorescence (XRF) analysis. XRD was performed on 76 samples at the University of Kansas Small Molecule X-Ray Crystallography Lab using a Bruker MicroSTAR™ diffractometer. Qualitative mineralogical data was collected with a scan rate of three, one-minute runs from 5–115° 2θ. Clay mineralogy was determined according to Moore and Reynolds (1997). XRD data was used to determine the clay mineralogy of paleosols and to aid the identification of clay-rich horizons marking Alfisols and Calcic Alfisols. XRF was conducted at Oneida Research Services on 30 samples to determine elemental weight percentages; these values were converted to weight percent oxide and molar ratios. XRF data was used to track changes in elemental composition in

paleosol profiles and to differentiate paleosol horizons, especially calcic horizons. Both XRD and XRF data aided in amending paleosol classifications made in the field.

RESULTS

Lithofacies

Five distinct lithofacies consisting of 11 subfacies were identified from outcrop (Table 1). The mudstone facies contains units composed predominately of mud-sized grains and was not subdivided into subfacies. Siltstone subfacies were subdivided based on the presence of planar lamination and the relative amount of very fine sand grains (Fig. 5). Sandstone and conglomerate subfacies were separated based on the dominant primary sedimentary structures (Figs. 5, 6). Silt and sand grains composed of calcite were common constituents (Table 1).

Ichnology

Seventeen ichnogenera and ichnofossils were identified (Table 2; Figs. 7–9). These ichnofossils form nine reoccurring ichnocoenoses across the northeast Chinle Basin (Table 3). Ichnodiversity and abundance was greatest in the Petrified Forest and Owl Rock mbrs and lowest within the Moss Back Mbr (see Table 2).

Paleosols

Six types of paleosols were identified by pedogenic development: Entisols, Inceptisols, Calcic Inceptisols, Vertisols, Alfisols, and Calcic Alfisols (Table 4). Every member of the Chinle Fm shows some degree of pedogenic modification.

Entisols.—Paleosol profiles consist of compound AC and C horizons. Roots and burrows penetrate parent material, which display primary sedimentary structures. Horizons are dominantly red (10R 5/4, 2.5YR 5/6), pale red (10R 6/3, 6/2), red brown (2.5YR 4/3), and green grey (Gley 1 8/10GY) with pale-red (10R 7/3), brown (2.5Y 7/3, 2.5YR 7/3), and yellow (5Y 6/8, 2.5Y 7/8) mottles and green-grey (Gley 1 7/10Y) reduction haloes. This paleosol contains the highest variety of ichnocoenoses, but most of these ichnocoenoses consist of horizontal, shallow burrows (see Tables 3–4). Entisols are present in the Moss Back, Petrified Forest, Owl Rock, and Church Rock mbrs.

Inceptisols.—These have compound, composite, and cumulative A-C and AC profiles. A horizons contain fine–coarse angular blocky and very fine-granular peds, with granular peds consisting of compressed fecal pellets. The A horizon is red (10R 4/3, 2.5YR 4/6, 5/6) and red brown (2.5YR 3/4, 4/4) with pale-red (10R 6/3) mottles and green-grey (Gley 1 7/10Y) reduction haloes. Inceptisols are observed in the Petrified Forest, Owl Rock, and Church Rock mbrs.

Calcic Inceptisols.—These consist of composite ABk, A-ABk-AB, A-AB-ABk, and A-AB-Bk-C profiles. A horizons consist of fine–coarse angular blocky and very fine-granular peds, which consist of compressed fecal pellets. A horizons are red (2.5YR 4/5, 5/6), pale red (10R 6/2), red brown (5R 5/3, 4/4, 2.5YR 4/4), and brown (7.5YR 4/2) with red (10R 4/2), yellow (5YR 6/6, 10YR 7/3, 2.5YR 4/3), and grey (10R 7/1) mottles and green-grey (Gley 1 7/10Y, Gley 1 8/10GY) reduction haloes. AB horizons consist of fine–coarse angular blocky and very fine-granular peds, with granular peds also composed of compressed fecal pellets. AB horizons have higher red values and hues than the overlying horizon, and are red (10R 5/6) and red brown (10R 4/3) with green-grey (Gley 1 7/10Y) reduction haloes. ABk and Bk horizons consist of fine–coarse angular blocky and very fine-granular peds, and autobrecciation is present. These

horizons are red (10R 5/6, 2/5YR 5/4) and pale red (10R 4/3, 5/2) with red (2.5R 3/6), pale red (10R 6/2), red-brown (2.5R 5/4) and yellow (5YR 6/6, 10YR 7/3, 2.5TR 4/3) mottles and green-grey (Gley 1 7/10Y) reduction haloes. ABk and Bk horizons are 55–95-cm thick and reach Stages 1–2 of calcic paleosol development (Gile et al. 1966; Machette 1985). Carbonate accumulation commonly manifests as nodules 5–8 mm in diameter, and horizons have weight percent CaO from 51.78%–99.50%. Calcic horizons commonly overprint each other to form composite paleosol profiles. Calcic Inceptisols are present in the Petrified Forest, Owl Rock, and Church Rock mbrs.

Vertisols.—These consist of compound to cumulative A-Bss profiles. A horizons consist of medium–coarse angular blocky and fine–medium prismatic peds, and are pale red (5R 5/3). Rhizohaloes in the A horizon are yellow (2.5Y 7/4). Bss horizons consist of fine–medium prismatic peds and contain large slickensides. Strong redoximorphic mottling is present in Bss horizons, which are pale red (5R 5/3) and green grey (Gley 1 7/10GY). Vertisols are observed only in the Owl Rock Mbr.

Alfisols.—These consist of composite and cumulative A-Bt and A-AB-Bt profiles. A horizons consist of fine–coarse angular blocky and very fine-granular peds, which are composed of compressed fecal pellets. A horizons are red (2.5YR 5/6, 10R 6/4, 5/6) with green-grey (Gley 1 7/10Y) reduction haloes. AB horizons consist of fine–coarse angular blocky peds and are red brown (2.5YR 4/4) with green-grey (Gley 1 7/10GY) mottles. Bt horizons consist of fine–medium angular blocky, very fine granular, and fine–medium wedge peds and slickensides. The dominant colors of the Bt horizons are red (10R 4/6, 5/6) and red brown (2.5YR 3/3) with green-grey (Gley 1 7/10Y) reduction haloes. These Bt horizons are characterized by illite and montmorillonite. Alfisols are only found in the Owl Rock Mbr.

Calcic Alfisols.—These consist of composite A-Btk and A-Bt-Btk profiles. A horizons consist of fine–coarse angular blocky peds, and are red (10R 5/4), pale red (10R 6/3), and red brown (7.5YR 5/2) with red (10R 5/6) and grey (10YR 7/2) mottles and green-grey (Gley 1 7/10GY) reduction haloes. Bt horizons consist of fine–medium angular blocky peds and are red (2.5YR 5/6) with red-brown (2.5YR 6/4, 7/3) mottles and green-grey (Gley 1 5G8/1) reduction haloes. Illite and montmorillonite are the main clay component, and these Bt horizons contain increased calcium accumulations. Btk horizons consist of fine–medium blocky peds and have rare slickensides. Horizons are predominantly red (10R 4/4, 5/3, 5/4), pale red (10R 6/3), and red grey (10R 6/1) with red (2.5YR 5/6, 10R 5/3) and red-brown (2.5YR 7/3) mottles and green-grey (Gley 1 8/10GY) reduction haloes. Btk horizons range from 0.12–3 m thick, and contain illite and montmorillonite. Calcium carbonate accumulation match Stages 2–3 of calcic paleosol development (Gile et al. 1966; Machette 1985), and horizons have weight percent CaO from 66.64%–87.43%. The characteristic features of Btk horizons are calcium carbonate nodules 0.5–2.0 cm in diameter. Calcic Alfisols are only present in the Owl Rock Mbr.

Facies Associations

Lithofacies, ichnocoenoses, and paleosols form six-reoccurring facies associations from proximal to distal position on the alluvial plain (Table 5; Fig. 10). Facies associations are interpreted to represent a variety of depositional environments including braided river, meandering river, crevasse-splay and levee, floodplain, palustrine, and lacustrine deposits. FA-1 is most abundant in the Moss Back Mbr, where trough-cross-stratified sandstone occurs as stacked, interconnected, laterally extensive sand sheets. FA-1 is also abundant in the Church Rock Mbr. FA-2 is most abundant in the middle Owl Rock Mbr. Conglomerate beds have

erosive bases and occur as thin, laterally discontinuous, ribbon sand bodies encased in siltstone. Large oncoids are a common component of the clasts of the conglomerate. FA-3 is common in the Owl Rock Mbr, consisting of stacks of interbedded massive siltstone, ripple-cross-laminated sandstone, and laterally discontinuous sandstone and conglomerate beds. FA-4 forms the majority of the Petrified Forest and Owl Rock mbrs, and consists of fine-grained siliciclastic facies. FA-4 is also observed in the Church Rock Mbr. FA-5 is rarely observed in the Petrified Forest and Owl Rock mbrs. FA-5 consists of planar-laminated mudstone and siltstone with ichnofossils along bedding planes. FA-6 is only observed in the Church Rock Mbr, consists of planar-laminated siltstone and very fine-grained sandstone, and is the least abundant facies association. FA-6 is differentiated from FA-5 by rare to absent ichnocoenoses and paleosols.

ICHNOPEDOFACIES

IP-1: Shallowly Burrowed Entisol

Description.—Shallowly Burrowed Entisols retain primary sedimentary structures and contain at least one of the following ichnocoenoses: *Cylindrichum*, *Scoyenia*, *Skolithos*, or *Steinichnus* (see Table 3; Fig. 11). The *Cylindrichum* Ichnocoenosis is common in planar- and ripple-cross-laminated siltstone to very fine-grained sandstone (F-2c and F-3) with abundant desiccation cracks. The *Scoyenia* Ichnocoenosis is mainly associated with massive siltstone (F-2a) and ripple-cross-laminated siltstone to fine-grained sandstone (F-3). The *Skolithos* Ichnocoenosis is associated with lens-shaped sandstone bodies that display planar-laminated bedding (F-2c). The base of these bodies is erosional with a thin bed of conglomerate, and the lenses are surrounded by fine-grained strata. The *Steinichnus* Ichnocoenosis occurs in planar-

laminated mudstone (F-1) with abundant desiccation cracks (Fig. 11). Soil profiles are Entisols and consist of compound AC horizons. Ichnofossils, including few rhizoliths, primarily occur along bedding planes and penetrate <12 cm into the sediment. This ichnopedofacies is commonly associated with crevasse-splay and levee (FA-3) and palustrine (FA-5) deposits.

Interpretation.—*Cylindrichum* in conjunction with F-2c and F-3 suggest subaerially exposed levee, crevasse-splay, and point bar environments with shallow water tables (Hasiotis and Dubiel 1993a; Hasiotis and Demko 1996; Hasiotis 2004, 2008). This is further supported by the association of *Cylindrichum* with desiccation cracks, indicating wetting and drying cycles. *Scoyenia* exhibit hygrophilic behavior, which indicates they formed in shallow water tables with sediment saturation near 100% and where the capillary fringe is close to the surface in either marginal-lacustrine or levee environments (Frey et al. 1984; Hasiotis and Dubiel 1993a; Hasiotis 2004, 2008). The occurrence of *Scoyenia* in F-3 suggests deposition on levees or fluvial bars (e.g., Miall 1996). The occurrence of both *Cylindrichum* and *Scoyenia* within the same beds (see Table 3) indicate fluctuating water-table conditions in these proximal fluvial environments. *Scoyenia* form after initial deposition when water tables and sediment moisture levels are high, then *Cylindrichum* is constructed in the deposits as the water table lowers (Hasiotis and Bown 1992; Hasiotis 2004, 2008). *Skolithos* are not indicative of any specific environment, but the sandstone lenses containing these ichnofossils match the morphology of crevasse-splay deposits (e.g., Miall 1996). *Steinichnus* are associated with palustrine and channel–levee environments with high water tables at or near the sediment-water-air interface (Bromley and Asgaard 1979; Hasiotis and Bown 1992; Hasiotis 2002, 2004, 2008). *Steinichnus* do not show branching, and previous observations of *Steinichnus* in the Morrison Fm associated unbranched forms with deposition in palustrine environments (Hasiotis 2004, 2008). Occurrence of *Steinichnus* in green-

grey mudstone also supports poorly drained, reducing conditions (e.g., Therrien and Fastovsky 2000; Kraus and Hasiotis 2006; Smith et al. 2008b). Desiccation cracks and shallow rhizoliths within these same mudstones indicate there were periods of slightly lower water tables and subaerial exposure (Hasiotis 2004, 2008; Hasiotis et al. 2007). The close proximity of environments to fluvial systems led to more frequent sedimentation, resulting in shorter duration of pedogenesis between depositional events (e.g., Bown and Kraus 1987, 1993a, b; Kraus 1999; Hasiotis 2002; Hasiotis 2007; Hasiotis et al. 2012). The occurrence of *Steinichnus* additionally suggests areas with periods of standing water, such as swamps and lakes (e.g., Hasiotis 2004, 2008; Hasiotis et al. 2012).

IP-2: Rhizolith Entisol

Description.—This ichnopedofacies consists of the Rhizolith Ichnocoenosis (see Table 3; Fig. 12) in ripple-cross-laminated sandstone (F-3), massive medium-grained sandstone (F-4a), and massive pebble conglomerate (F-5b). Ripple-cross-laminated sandstone is red brown and commonly occurs above laterally extensive, stacked, trough-cross-stratified sandstone. Massive medium-grained sandstone and pebble conglomerate bodies form thin, laterally extensive sheets with erosive bases. Paleosol profiles are Entisols with compound AC horizons. Red-brown rhizoliths and green-grey rhizohaloes, which occur along bedding planes, are associated with lithofacies F-4a and F-5b. Deeper penetrating green-grey rhizohaloes, varying from 15–70 cm deep and from 18–85 cm long, occur with *Planolites* and are found in lithofacies F-3. This ichnopedofacies is associated with braided-river (FA-1) and crevasse-splay and levee (FA-3) deposits.

Interpretation.—Rhizoliths and rhizohaloes in F-4a and F-5b suggest crevasse-splay deposits with high water tables near the sediment surface, restricting vertical penetration by roots (e.g., Miall 1996; Hasiotis 2007; Hasiotis et al. 2007; Hasiotis and Platt 2012). Red-brown rhizoliths within drab green-grey matrix indicates poorly drained sediment (Kraus and Hasiotis 2006). Green-grey rhizohaloes within red sediment, however, formed by surface water gleying mobilizing and transporting iron oxides away from the original root in well-drained soils (e.g., Kraus and Hasiotis 2006; Smith et al. 2008b; Chakraborty et al. 2013). Color differences in the paleosol matrix, rhizoliths, and rhizohaloes suggest alternating periods of well- and poorly drained conditions within the crevasse-splay deposits.

The sand-body morphology and stacking pattern of the trough-cross-stratified and ripple-cross-laminated sandstone indicates deposition on bars of braided rivers (e.g., Blakey and Gubitosa 1984; Collinson 1986; Miall 1996). Deep penetration of roots in these facies associations suggests that the fluvial bars became subaerially exposed via falling water level to produce well-drained conditions (Hasiotis 2002; Hasiotis et al. 2007; Hasiotis and Platt 2012; Counts and Hasiotis 2014). Fluvial bars could have also been abandoned during channel migration and became part of the proximal floodplain as colonization by plants occurred (e.g., Kraus 1987; Hasiotis 2004, 2008). The drab colors of the rhizohaloes formed through surface water gleying during short periods of standing water, most likely during and after flooding events (Retallack 2001; Hasiotis 2004, 2008; Kraus and Hasiotis 2006). Rhizohalo depth of penetration decreases upsection from 70 to 15 cm below the sediment surface (Fig. 12), indicating a rise in the water table through time (e.g., Hasiotis 2004, 2008; Hasiotis et al. 2007). Weak paleosol development with preservation of sedimentary structures occurred within close

proximity to the fluvial system, leading to frequent flooding and burial by sediment (Bown and Kraus 1987, 1993a, b; Hasiotis 2002; Hasiotis 2007).

IP-3: Camborygma Entisol

Description.—This ichnopedofacies is characterized by the *Camborygma* Ichnocoenosis (see Table 3; Fig. 13) in ripple-cross-laminated siltstone and sandstone (F-3), massive medium–coarse sandstone (F-4a), and massive pebble conglomerate (F-5b). Paleosol profiles are Entisols with compound AC horizons. The massive sandstones and conglomerates have thin, laterally extensive sheet morphologies. *Camborygma* are ≤0.5 m deep and long in massive, medium sandstone to pebble conglomerate. *Camborygma* are up to 1.3 m deep and 1.45 m long in ripple-cross-laminated sandstone (Fig. 13). *Skolithos* are also observed in association with *Camborygma* in F-3. This ichnopedofacies is associated with crevasse-splay and levee deposits (FA-3).

Interpretation.—*Camborygma* represent hydrophilic behavior, extend into the phreatic zone, and mark the level of the paleowater table (Hasiotis and Mitchell 1993; Hasiotis et al. 1993; Hasiotis 2002, 2004, 2008). *Camborygma* within F-4a and F-5b are assigned to *Camborygma litonomos* due to their simple shaft morphology and length <0.5 m (Hasiotis and Mitchell 1993; Hasiotis et al. 1993; Hasiotis and Honey 2000). *Camborygma litonomos* represent saturated sediments with a high water table in proximal levee, crevasse-splay, and pointbar environments (Hasiotis and Mitchell 1993; Hasiotis et al. 1993; Hasiotis 2004, 2008). This interpretation is supported by sandstone and conglomerate bodies that have morphologies matching proximal fluvial crevasse-splay deposits (e.g., Miall 1996).

Camborygma within F-3 are assigned to *Camborygma eumekenomos* since they show simple bifurcation, and burrow depths are >1 m (Hasiotis and Mitchell 1993; Hasiotis et al. 1993; Hasiotis and Honey 2000). *Camborygma eumekenomos* indicate deeper, highly fluctuating water tables in proximal floodplain environments (Hasiotis and Mitchell 1993; Hasiotis et al. 1993; Hasiotis 2004, 2008). Stacked compound AC horizons first formed on levees during an interval of nonsteady, high sedimentation (Fig. 13; Kraus 1999; Hasiotis and Platt 2012). *Skolithos* burrows formed during short intervals of pedogenesis between depositional episodes and suggest that other bioturbation may have occurred within AC horizons but is not clearly visible (Fig. 13). Close proximity to the fluvial system led to frequent burial by sediment, restricting pedogenic development and preserving primary sedimentary structures (e.g., Bown and Kraus 1987, 1993a, b; Hasiotis et al. 2012). *Camborygma eumekenomos* originated from a stable soil surface during a hiatus in sedimentation, allowing burrows to overprint the underlying AC horizons (Fig. 13; Hasiotis and Honey 2000). Occurrence of *C. eumekenomos* likely marks the migration of the fluvial system away from the depositional area, which led to less frequent sedimentation events and greater pedogenesis (e.g., Bown and Kraus 1987, 1993a, b; Hasiotis and Mitchell 1993; Hasiotis 2004, 2008).

IP-4: Naktodemasis-Camborygma Entisol

Description.—This ichnopedofacies consists of the *Naktodemasis-Camborygma* Ichnocoenosis (see Table 3; Fig. 14) in ripple-cross-laminated very fine-grained sandstone (F-3). These strata form stacked, compound AC horizons and have strong red colors. *Camborygma* are between 20–45 cm deep and 25–55 cm long. *Naktodemasis* are 2–5 mm in diameter and overprint the burrow fill of *Camborygma*. These *Naktodemasis* bioturbate the sediment within

beds and are not just restricted to bedding planes. *Scoyenia* are 3–5.5 mm in diameter and are restricted to bedding planes. Green-grey rhizohaloes extend along bedding planes, are 5–20 cm deep, and 6–25 cm long. This is the only ichnopedofacies that contains occurrences of *Arenicolites*, *Ancorichnus*, and *Treptichnus*. This ichnopedofacies is associated with crevasse-splay and levee deposits (FA-3).

Interpretation.—The Naktodemasis-Camborygma Entisol contains ichnofossils representing both high and low water tables. The occurrence of *Scoyenia*, *Arenicolites*, *Ancorichnus*, and *Treptichnus* along bedding planes supports a shallow water table and even indicates intervals of standing freshwater (Hasiotis 2002, 2004, 2008). *Camborygma* are assigned to *C. litonomos* and also indicate a shallow water table between 20–45 cm beneath the sediment surface (Hasiotis and Mitchell 1993; Hasiotis et al. 1993; Hasiotis and Honey 2000). *Naktodemasis*, however, reflect terraphilic to hygrophilic behavior, which indicates moderate- to well-drained soil conditions (e.g., Hasiotis 2004, 2008; Smith et al. 2008a, 2008b; Counts and Hasiotis 2009, 2014). Green-grey rhizohaloes penetrating up to 20 cm deep in red Entisol profiles further support a thin, well-drained vadose zone (Hasiotis 2004, 2008; Kraus and Hasiotis 2006; Hasiotis et al. 2007; Counts and Hasiotis 2014).

Overprinting of ichnofossils exhibiting terraphilic, hygrophilic, and hydrophilic behaviors are common features in levee deposits and indicate fluctuating water tables (Hasiotis and Bown 1992; Hasiotis 2002). After initial sediment deposition, when standing water was present, the levee was colonized with *Arenicolites*, *Ancorichnus*, and *Treptichnus*. As water level fell beneath the sediment surface, *Scoyenia* and shallow roots bioturbated the levee. Continued pedogenesis and decrease in the water table allowed *C. litonomos* and *Naktodemasis* to bioturbate the sediment and overprint previous burrows. Towards the end of pedogenesis, deeper penetrating

roots, in turn fed on by the organisms producing *Naktodemasis*, overprinted *C. litonomos*. Pedogenesis was brief due to close proximity to the fluvial system, which frequently deposited new sediment onto the levee that underwent pedogenesis after the water level lowered; this pattern was repeated over time (e.g., Bown and Kraus 1987, 1993a, b; Hasiotis and Bown 1992; Hasiotis 2007).

IP-5: Rhizolith Inceptisol

Description.—This ichnopedofacies consists of the Rhizolith Ichnocoenosis (Table 3; Fig. 15) in red and red-brown, massive siltstone to very fine-grained sandstone (F-2b). Paleosols are Inceptisols and form compound A and AC profiles. Red-brown rhizoliths are up to 16.5 cm deep and 17.5 cm long. Green-grey rhizohaloes are up to 25 cm deep and 26 cm long. This ichnopedofacies is associated with floodplain deposits (FA-4).

Interpretation.—Vertically penetrating, green-grey rhizohaloes and red-brown rhizoliths and strong red color of paleosols indicate well-drained conditions (e.g., Kraus and Hasiotis 2006). Root ichnofossils, however, only show a maximum depth of penetration of 25 cm, indicating the vadose zone was thin and the water table was shallow (Fig. 15; e.g., Hasiotis et al. 2007). Paleosol profiles are compound, indicating high, nonsteady sedimentation with pedogenesis occurring in between depositional events (Kraus 1999; Hasiotis and Platt 2012). The AC horizon, though, still contains remnant bedding, indicating shorter pedogenesis than the overlying homogenized A horizon (Fig. 15; e.g., Bown and Kraus 1987, 1993a, b; Hasiotis et al. 2012). Incipient formation of horizons, nonsteady sedimentation, short duration of pedogenesis, and shallow water tables suggest a proximal position on the floodplain (e.g., Bown and Kraus 1987, 1993a, b; Birkeland 1999; Hasiotis 2002; Hasiotis and Platt 2012).

IP-6: Naktodemasis Inceptisol and Calcic Inceptisol

Description.—This ichnopedofacies consists of the *Naktodemasis* Ichnocoenosis (Table 3; Fig. 16) in red and red-brown, massive siltstone to very fine-grained sandstone (F-2b). Paleosols are Inceptisols and Calcic Inceptisols that form composite and cumulative A, AB, and ABk horizons. Calcic horizons reach mature Stage 1 to incipient Stage 2 development with sparse calcium carbonate nodules (Gile et al. 1966; Machette 1985). Green-grey rhizohaloes are 20–95 cm deep, up to 110 cm long, and penetrate into underlying horizons. *Naktodemasis* are 2–5 mm in diameter, extensively bioturbate the entire profile, and overprint rhizohaloes. This ichnopedofacies is associated with floodplain deposits (FA-4).

Interpretation.—Extensive *Naktodemasis* bioturbation, deeply penetrating rhizohaloes, and strong red paleosol coloration suggest well-drained environments with a deep water table (Kraus and Aslan 1993; Kraus and Hasiotis 2006; Hasiotis et al. 2007; Smith et al. 2008a; Counts and Hasiotis 2009, 2014). Calcium carbonate nodules suggest environments where evapotranspiration was greater than precipitation (e.g., Gile et al. 1966; Machette et al. 1985; Dubiel and Hasiotis 2011), and these nodules also support the interpretation of well-drained conditions (Prochnow et al. 2006). Length of pedogenesis was enough to allow roots to crosscut underlying horizons and *Naktodemasis* to form around these roots as feeding behavior (Fig. 16C). Cumulative and composite profiles form when pedogenesis outpaces steady state and nonsteady state sediment deposition respectively, leading to more developed paleosols (e.g., Kraus and Aslan 1993; Kraus 1999; Hasiotis and Platt 2012). Greater duration of pedogenesis suggests a more distal position on the floodplain, where sedimentation events were less frequent (e.g., Bown and Kraus 1987, 1993a, b; Hasiotis 2007; Hasiotis et al. 2012).

IP-7: Camborygma Inceptisol and Calcic Inceptisol

Description.—This ichnopedofacies consists of the *Camborygma* Ichnocoenosis (Table 3; Fig. 17) in red and pale red, massive siltstone, and very fine-grained sandstone (F-2b). Paleosols are Inceptisols and Calcic Inceptisols that contain composite Bk horizons. Calcium carbonate nodules have mature Stage 2 development (Gile et al. 1966; Machette 1985). *Camborygma* reach 110–120 cm deep and 150 cm long. Green-grey rhizoliths and rhizohaloes are 60 cm deep and 70 cm long. This ichnopedofacies is associated with floodplain deposits (FA-4).

Interpretation.—*Camborygma* are assigned to *C. eumekenomos* and indicate a deep, highly fluctuating water table (Hasiotis and Mitchell 1993; Hasiotis et al. 1993; Hasiotis and Honey 2000; Hasiotis 2004, 2008), which was at times >1 m below the sediment surface. *Camborygma eumekenomos* terminate at a pale red Bk horizon (Fig. 17). Pale red coloration is associated with less well-drained paleosol horizons (Kraus and Aslan 1993; Kraus and Hasiotis 2006; Smith et al. 2008), supporting more frequent saturated conditions at this level. Stronger red coloration in overlying horizons, roots, fecal pellets, and calcium carbonate nodules, however, suggest well-drained, oxidizing conditions higher in the paleosol profile (Kraus and Aslan 1993; Kraus and Hasiotis 2006; Prochnow 2006; Hasiotis and Platt 2012). Calcium carbonate nodules overprint *C. eumekenomos* and extend into the pale red Bk horizon. These nodules most likely formed during extended intervals of lower precipitation and a drop in the paleowater table, which would allow for calcium carbonate precipitation (Kraus and Aslan 1993). Calcium carbonate nodules and *C. eumekenomos* suggest evapotranspiration was greater than precipitation at times and moisture was highly seasonal (Machette 1985; Dubiel and Hasiotis 2011). Composite

horizons indicate pedogenesis outpaced nonsteady state sediment deposition, leading to better developed paleosols and suggesting a distal position on the floodplain (e.g., Bown and Kraus 1987, 1993a, b; Kraus 1999; Hasiotis et al. 2007; Hasiotis and Platt 2012).

IP-8: Therapsid Inceptisol and Calcic Inceptisol

Description.—This ichnopedofacies consists of the Therapsid Ichnocoenosis (Table 3; Fig. 18) in red, red-brown, and grey, massive siltstone (F-2a). Paleosols are Inceptisols and Calcic Inceptisols that contain composite ABk horizons. Siltstone is cemented by calcium carbonate and reaches Stage 1 development (Gile et al. 1966; Machette 1985). Therapsid burrows are 175 cm deep, 215 cm long, and can overprint multiple ABk horizons. White and yellow rhizoliths are up to 50 cm deep and 80 cm long. This ichnopedofacies is associated with floodplain deposits (FA-4).

Interpretation.—Therapsid burrows exhibit terraphilic behavior and were constructed above the water table (e.g., Hasiotis 2004, 2008; Hasiotis et al. 2004; Hembree and Hasiotis 2008). Two episodes of colonization by therapsids are observed (Fig. 18). The lower therapsid burrows occur in horizons with duller color values and iron oxide nodules, which are indicators of higher moisture, higher sediment saturation, and more poorly drained conditions (Kraus and Aslan 1993; Mack et al. 1993; Stiles et al. 2001). Therapsid burrows, however, would not be located in water-saturated sediments. These burrows developed during an interval of sediment hiatus and stable landscape with well-drained conditions (e.g., Hasiotis et al. 2004; Hembree and Hasiotis 2008). The lower therapsid burrows, then, formed in soils that underwent shorter duration pedogenesis, preventing the formation of redder color values. The upper two ABk horizons represent two intervals of sedimentation and subsequent bioturbation by roots. Deeply

penetrating rhizoliths and stronger red coloration indicate well-drained paleosols with longer pedogenesis (Kraus and Aslan 1993; Kraus and Hasiotis 2006). A period of stable soil surfaces and hiatus in sedimentation allowed therapsid burrows to overprint horizons and led to the buildup of calcium carbonate in the soil profile, which also supports well-drained conditions (e.g., Kraus and Aslan 1993). Paleosols with composite calcic horizons indicate that pedogenesis outpaced sediment deposition, suggesting a distal position on the floodplain (e.g., Bown and Kraus 1987, 1993a, b; Kraus 1999; Hasiotis et al. 2007; Hasiotis and Platt 2012).

IP-9: Camborygma Vertisol

Description.—This ichnopedofacies consists of the *Camborygma* Ichnocoenosis (Table 3; Fig. 19) in pale red and green-grey, massive siltstone (F-2a). The paleosol is a Vertisol with redoximorphic mottling, slickensides, prismatic peds, and compound to cumulative A-Bss horizons. *Camborygma* are 75 cm deep and 95 cm long, extending into the Bss horizon. Rhizohaloes are bright yellow, 60 cm deep, and 70 cm long. *Fictovichnus* is observed 25 cm below the top of the Bss horizon. This ichnopedofacies is associated with floodplain deposits (FA-4).

Interpretation.—Redoximorphic coloration, prismatic peds, and slickensides are indicative of a Vertisol and support fluctuating water tables and seasonal moisture (e.g., Driese and Foreman 1992; Driese and Mora 1993; Kraus and Hasiotis 2006; Dubiel and Hasiotis 2011). Redoximorphic colors indicate alternating periods of oxidizing and reducing conditions (e.g., Driese et al. 1995; Kraus and Hasiotis 2006), and prismatic peds shrink and expand during alternating wet and dry seasons, forming slickensides (e.g., Retallack 2001; Dubiel and Hasiotis 2011). *Fictovichnus* are cocoons that represent terraphilic behavior in well-drained sediments

and were probably constructed during the dry season when soil moisture and the water table were lower (e.g., Hasiotis 2002, 2003, 2004, 2008; Alonso-Zara et al. 2014). Subsequent water table rise during the wet season aided in preservation of the cocoons (Alonso-Zara et al. 2014). Following an interval of deposition, plants colonized the soil profile, and yellow rhizohaloes formed in saturated, poorly drained sediments with reducing conditions (Kraus and Hasiotis 2006). Another interval of deposition followed bioturbation by these yellow roots, and a subsequent hiatus in sedimentation allowed for *Camborygma* to overprint underlying horizons. *Camborygma* are assigned to *C. eumekenomos* (Hasiotis and Mitchell 1993; Hasiotis et al. 1993; Hasiotis and Honey 2000) and indicate a highly fluctuating water table ~75 cm below the sediment surface, suggesting seasonal moisture. Redoximorphic coloration, compound and cumulative profiles where pedogenesis slightly outpaces sedimentation, and *C. eumekenomos* burrows indicate a proximal position on the floodplain (e.g., Kraus and Bown 1987, 1993a, b; Hasiotis and Mitchell 1993; Kraus 1999; Hasiotis 2004, 2008; Hasiotis and Platt 2012).

IP-10: Naktodemasis Alfisol

Description.—This ichnopedofacies consists of the *Naktodemasis* Ichnocoenosis (Table 3; Fig. 20) in red and red-brown mudstone to siltstone (F-1 and F-2a). Paleosols are Alfisols with composite Bt horizons. Ichnofossils are only discernable in the A horizon. *Naktodemasis* are between 2–5 mm in diameter and green-grey rhizohaloes are 10 cm deep and 12 cm long. This ichnopedofacies is associated with floodplain deposits (FA-4).

Interpretation.—*Naktodemasis* displaying feeding behavior around roots and red matrix coloration indicate well-drained conditions with a low water table (Kraus and Aslan 1993; Kraus and Hasiotis 2006; Smith and Hasiotis 2008; Smith et al. 2008a; Counts and Hasiotis 2009,

2014). Composite Bt horizons formed as pedogenesis outpaced sedimentation, allowing clay to accumulate in the subsurface (e.g., Kraus 1999; Hasiotis and Platt 2012). Longer duration pedogenesis and a more stable soil surface suggest a distal position on the floodplain (Bown and Kraus 1987, 1993a, b; Hasiotis et al. 2007).

IP-11: Naktodemasis Calcic Alfisol

Description.—This ichnopedofacies consists of the *Naktodemasis* Ichnocoenosis (Table 3; Fig. 21) in red, red-brown, and red-grey, massive siltstone (F-2a). Paleosols are Calcic Alfisols with composite Btk horizons. Calcium carbonate horizons reach mature Stage 2 development (Gile et al. 1966; Machette 1985). *Naktodemasis* are between 2–5 mm in diameter and extensively bioturbate the paleosol profile down into the Bt horizon. Green-grey rhizohaloes are 19 cm deep and 22 cm long. *Planolites* are only observed within the A horizon and are <2 mm in diameter. This ichnopedofacies is associated with floodplain deposits (FA-4).

Interpretation.—*Naktodemasis* bioturbation extending down 75 cm, calcium carbonate nodules, and red coloration indicate well-drained conditions with a deep water table (Kraus and Aslan 1993; Kraus and Hasiotis 2006; Prochnow et al. 2006; Smith and Hasiotis 2008; Smith et al. 2008a; Counts and Hasiotis 2009, 2014). Calcium carbonate nodules suggest evapotranspiration was greater than precipitation and moisture was seasonal (Gile et al. 1966; Machette 1985; Dubiel and Hasiotis 2011). Composite Btk profiles indicate that pedogenesis outpaced sedimentation, allowing for clay accumulation and calcium carbonate buildup (Kraus 1999; Hasiotis and Platt 2012). Time of pedogenesis was also long enough for *Naktodemasis* to exhibit feeding behavior around roots. Greater duration of pedogenesis and stable soil surfaces

indicate this ichnopedofacies had a distal position on the floodplain (Bown and Kraus 1987, 1993a, b; Hasiotis 2002, 2007).

IP-12: Rhizolith Calcic Alfisol

Description.—This ichnopedofacies consists of the Rhizolith Ichnocoenosis (Table 3; Fig. 22) in red and red-brown, massive siltstone (F-2a). Paleosols are Calcic Alfisols with composite Btk horizons. Calcium carbonate accumulation reaches Stage 3 development (Gile et al. 1966; Machette 1985) with abundant calcium carbonate nodules up to 2 cm in diameter. Rhizotubules lined with calcium carbonate nodules are 120 cm deep and 135 cm long. Green-grey siltstone fills the inside of rhizotubules. This ichnopedofacies is associated with floodplain deposits (FA-4).

Interpretation.—Red matrix, deeply penetrating rhizotubules, and calcium carbonate nodules indicate well-drained conditions with a deep water table (e.g., Machette 1985; Kraus and Aslan 1993; Kraus and Hasiotis 2006; Counts and Hasiotis 2014). Calcium carbonate nodules suggest this ichnopedofacies developed in environments where evapotranspiration was greater than precipitation and moisture was seasonal (Gile et al. 1966; Dubiel and Hasiotis 2011). Rhizotubules formed as calcium carbonate precipitated on root surfaces during the uptake of nutrients and water (e.g., Klappa 1980; Kraus and Hasiotis 2006). Following the death of the root, the remaining cylindrical rhizotubule created a conduit for water movement in the soil profile (Klappa 1980), leading to reducing conditions within the rhizotubule and gleyed matrix. The Btk horizon above the rooted zone indicates another Calcic Alfisol formed on top of this profile, but it was cut out by the overlying conglomerate (Fig. 22A). Abundant accumulation of calcium carbonate and well-formed, composite Btk horizons indicate greater duration of paleosol

development with pedogenesis outpacing sedimentation (e.g., Bown and Kraus 1987, 1993a, b; Kraus 1999; Hasiotis and Platt 2012). These paleosols formed on the most distal position of the floodplain.

DISTRIBUTION OF PALEOSOLS AND ICHNOPEDOFACIES

Lateral Distribution

Ichnopedofacies show an inverse relationship between paleosol development and proximity to the fluvial system (Fig. 23). Entisol ichnopedofacies (IP-1–4) are restricted to proximal fluvial bar, crevasse-splay, and levee environments. Inceptisol, Calcic Inceptisol, Vertisol, Alfisol, and Calcic Alfisol ichnopedofacies (IP-5–12) are only present in floodplain environments. This lateral distribution of ichnopedofacies on the alluvial plain shows a similar pattern to paleosols of the Paleogene Willwood Fm in Wyoming (Bown and Kraus 1987, 1993a, b). Bown and Kraus (1987, 1993a, b) attributed their observations of paleosol development to decreasing short-term sediment accumulation rates with increasing distance from the channel. Thinning of fluvial deposits away from the channel means distal environments experience less sedimentation and greater duration of pedogenesis (e.g., Bown and Kraus 1987, 1993a, b; Hasiotis 2002, 2007). Rhizolith Inceptisols show greater development than ichnopedofacies in channel bank, crevasse-splay, and levee environments, but pedogenesis did not act long enough for the development of calcic or argillic horizons. This suggests formation on the proximal floodplain (Fig. 23). The strong hydromorphic features of Camborygma Vertisols indicate areas of low topography on the floodplain, leading to higher gleyed matrixes and less well-drained conditions (Kraus and Middleton 1987a; Kraus and Aslan 1993; Prochnow et al 2005). Lack of

calcium carbonate accumulation further supports higher moisture content in this ichnopedofacies. Naktodemasis Inceptisols and Calcic Inceptisols, Camborygma Inceptisols and Calcic Inceptisols, and Therapsid Inceptisols and Calcic Inceptisols display more developed horizonation, supporting formation on the distal floodplain (Fig. 23). Naktodemasis Alfisols, Naktodemasis Calcic Alfisols, and Rhizolith Calcic Alfisols show both thick, well-developed calcic and argillic horizons, also indicating a position on the distal floodplain (Fig. 23).

Vertical Distribution

Stratigraphic changes in ichnologic and pedologic features are observed throughout the Chinle Fm (Figs. 24, 25; see Fig. 10). *Camborygma* decrease in occurrence through Owl Rock Mbr deposition, and are absent from the Church Rock Mbr (Fig. 10). Therapsid burrows, conspicuous in the Petrified Forest Mbr, decrease upsection through the Owl Rock Mbr, and are absent from the Church Rock Mbr (Fig. 10). Root ichnofossils and *Naktodemasis* occur throughout the Petrified Forest and Owl Rock mbrs, though *Naktodemasis* are only present near the base of the Church Rock Mbr, whereas root ichnofossils persist higher into this unit (Fig. 10). Rhizoliths and *Cylindrichum* are the stratigraphically highest occurring ichnofossils in the Chinle Fm (Fig. 10). Overall, ichnofossil diversity increases from the Moss Back Mbr into the lower and middle Owl Rock mbrs, then decreases throughout the rest of the Owl Rock and Church Rock mbrs. Calcium carbonate nodules are most abundant in the Petrified Forest, lower Owl Rock, and base of the middle Owl Rock mbrs and decrease in occurrence upsection (Fig. 10). Ichnopedofacies tend to redden upsection and become dominated by ichnofossils displaying terraphilic behavior (Fig.10).

Proximal fluvial (i.e., channel, levee, crevasse splay) deposits show a stratigraphic shift in ichnopedofacies throughout the Chinle Fm. Rhizolith Entisols in the Moss Back Mbr transition to Camborygma Entisols in the Petrified Forest Mbr (Fig. 25). Camborygma Entisols transition to both (1) Shallowly Burrowed Entisols, dominated by the *Steinichnus* and *Scoyenia* ichnocoenoses, and (2) Camborygma-Naktodemasis Entisols in the Owl Rock Mbr (Fig. 25). Ichnopedofacies transition to (1) Shallowly Burrowed Entisols, dominated by the *Scoyenia* and *Cylindrichum* ichnocoenoses, and (2) Rhizolith Entisols in the Church Rock Mbr (Fig. 25).

Floodplain (i.e., proximal and distal) deposits also display stratigraphic changes in ichnopedofacies. Floodplain ichnopedofacies are absent in the Moss Back Mbr, but the Petrified Forest Mbr contains (1) Naktodemasis Inceptisols and Calcic Inceptisols and (2) Therapsid Inceptisols and Calcic Inceptisols (Fig. 25). These ichnopedofacies transition to (1) Camborygma Vertisols, (2) Rhizolith Inceptisols, (3) Naktodemasis Calcic Alfisols, and (4) Rhizolith Calcic Alfisols in the lower Owl Rock Mbr (Fig. 25). In the middle to upper Owl Rock mbrs, ichnopedofacies consist of (1) Camborygma Inceptisols and Calcic Inceptisols, (2) Naktodemasis Alfisols, and (3) Naktodemasis Inceptisols and Calcic Inceptisols (Fig. 25). Ichnopedofacies transition to (1) Naktodemasis Inceptisols and Calcic Inceptisols and (2) Rhizolith Inceptisols in the Church Rock Mbr (Figs. 10, 25).

INCISED VALLEYS AND CHANNEL FILLS

Pedogenic development was further influenced by topographic position and location within the study area. Stacked paleovalleys are present in all members, and paleosols fill these paleovalleys (see Fig. 24). Depths of paleovalleys vary from ~5–17 m, indicating a significant variation in paleotopography was present during Chinle Fm deposition. In the Petrified Forest,

lower Owl Rock, and upper Owl Rock mbrs less developed paleosols dominate the paleovalleys, and better developed paleosols occur on interfluve positions. A position on the interfluve itself, however, is not indicative of a particular stage of paleosol development. Inceptisols and Vertisols were more common at interfluve locations in the south of the study area. Calcic Inceptisols, Alfisols, and Calcic Alfisols were more common on interfluves located towards the north end of the study area. This indicates a local trend from Petrified Forest Mbr into Owl Rock Mbr deposition, where lower valley fill rates with longer duration of pedogenesis were present in the north, with rate of valley fill increasing to the south. No trend is associated with paleosol development and topographic position for paleovalleys in the Moss Back, middle Owl Rock and Church Rock mbrs.

Petrified Forest Mbr

Inceptisols are found within paleovalleys at S1 and S4 and on interfluves at Southwest Section, East Section, S2, West Section, and S3 (see Fig. 24). Calcic Inceptisols and Calcic Alfisols are present only on the interfluves at S5, West Section, and S3 (Fig. 24). Less-developed paleosols in the paleovalleys at S1 and S4 were likely due to frequent flooding, high sedimentation rates, and shorter durations of pedogenesis. Interfluves are lower topographically in the south of the study area than in the north (Fig. 24; see Fig. 3). Development of Inceptisols on the interfluves at Southwest Section, East Section, and S2 were likely due to higher sedimentation rates, leading to shorter periods of pedogenesis. The better developed paleosols at S5, West Section and S3 indicate the interfluves at these locations had lower sedimentation rates. Lower sedimentation lead to longer durations of pedogenesis that enabled concentration of calcium carbonate nodules. These three measured sections (S5, West Section, and S3) are

clustered in the north of the study area (Fig. 3), suggesting that rate of valley fill was slower and duration of pedogenesis was longer to the north.

Lower Owl Rock Mbr

Inceptisols are observed within the paleovalleys at S1 and S2 and on interfluves at Southwest Section, East Section, S5, and West Section (Fig. 24). Only one Vertisol was observed on an interfluve at Southwest Section (Fig. 24). Alfisols are present within the paleovalley at S2 and on the interfluve at S3 (Fig. 24). Calcic Alfisols are present only on interfluve positions at East Section, West Section, and S4 (Fig. 24). In paleovalleys at S1 and S2, frequent flooding, increased sedimentation, and shorter duration of pedogenesis influenced development of Inceptisols. Alfisols at S2 likely formed during an interval of lower sedimentation and longer duration of pedogenesis. Interfluves become topographically lower towards the south of the study area (Figs. 3, 24), and Inceptisols dominate the profiles at Southwest Section and S5, indicating shorter duration of pedogenesis towards the south. On the topographically lowest interfluve in the lower Owl Rock Mbr, however, the Camborygma Vertisol at Southwest Section contains a cumulative Bss horizon, which suggests intervals of low, steady sediment deposition and longer duration of pedogenesis. (Fig. 24; see Fig. 19). This ichnopedofacies also contains slickensides and high clay content. These pedogenic features, along with a position on the flanks of the lowest paleovalley, indicate imperfectly drained conditions were present at the southernmost location of the study area. These factors resulted in redoximorphic mottling and the construction of *Camborygma* at this location. Interfluves at East Section, S4, West Section, and S3 are dominated by Alfisols and Calcic Alfisols with composite horizons. These paleosols indicate slower, nonsteady sedimentation rates, deeper water table,

slower rates of valley fill, and longer duration of pedogenesis in the north end of the study area. These physiochemical factors were likely influenced by a more elevated position on the alluvial plain.

Upper Owl Rock Mbr

Inceptisols are present in paleovalleys at S1, East Section, S2, S5, and S4 and on interfluves at Southwest Section, East Section, and S3 (Fig. 24). Alfisols are present in paleovalleys at East Section and on the interfluve at West Section (Fig. 24). Calcic Alfisols are only present on the interfluve at West Section (Fig. 24). In paleovalleys at S1, East Section, S2, S5, and S4, higher sedimentation rates and shorter duration of pedogenesis influenced the development of Inceptisols. The occurrence of an Alfisol at East Section marks a short interval of lower sedimentation and greater duration of pedogenesis, allowing for the formation of more developed paleosols. Interfluves in the upper Owl Rock Mbr are near the same topographic level, but only Inceptisols are present at Southwest Section in the south, whereas Alfisols and Calcic Alfisols are found at West Section towards the north. This suggest higher sedimentation and valley fill rates on interfluves in the south of the study area. Towards the north, sedimentation rates decreased and duration of pedogenesis increased, allowing more developed Alfisols and Calcic Alfisols to form on interfluves.

PHYSIOCHEMICAL CONTROLS ON SEDIMENTATION AND ICHNOPEDOLOGIC DEVELOPMENT

Physiochemical conditions controlling sedimentation and ichnopedofacies development in the northeast Chinle Basin can be separated into three main groups: 1) autocyclic controls, 2)

allocyclic controls, and 3) hydrology. Autocyclic processes are determined by energy distribution within the depositional basin and include fluvial channel migration and overbank flooding events (e.g., Beerbower 1964; Allen 1970; Bridge and Leeder 1979; Bridge 1984; Smith et al. 1989; Slingerland and Smith 2004; Cleveland et al. 2007; Trendell et al. 2012). Allocyclic controls are influences from outside of the depositional basin and include tectonism (including halokinesis) and climate (e.g., Beerbower 1964; Cater 1970; Bridge and Leeder 1979; Blakey and Gubitosa 1983; Alexander and Leeder 1987; Hazel 1994; Cecil 2003; Cleveland et al. 2007; Dubiel and Hasiotis, 2011; Trendell et al. 2012). Hydrology is influenced by autocyclic and allocyclic processes and controls the distribution, tiering, and depth of ichnofossils (e.g., Hasiotis and Bown 1992; Hasiotis and Mitchell 1993; Hasiotis and Dubiel 1994; Hasiotis 2002; 2004, 2007, 2008; Hasiotis et al. 2007, 2012).

Autocyclic Processes

Within the Chinle Fm, meandering river, braided river, crevasse-splay, and levee deposits commonly overlie floodplain deposits (see Fig. 10). This depositional pattern has been interpreted to record overbank flooding and channel migration on the alluvial plain, with pedogenesis occurring between depositional events (e.g., Bridge and Leeder 1979; Bridge 1984; Kraus 1987, 1999, 2002; Smith et al. 1989; Slingerland and Smith 2004).

Overbank Flooding.—This depositional process is preserved in the Petrified Forest, middle Owl Rock, and Church Rock mbrs where massive siltstone (F-2a) and very fine-grained sandstone (F-2b) are overlain by beds of ripple-cross-laminated sandstone (F-3) and massive sandstone (F-4a) <0.5 m thick (see Table 1; Figs. 10, 24). Sandstone facies are ribbon sand bodies surrounded by siltstone. The thin, discontinuous nature of such sandstone facies indicates

deposition on the distal ends of prograding crevasse-splay and levee complexes (e.g., Bridge 1984; Bown and Kraus 1987). Frequency of overbank flooding influenced upsection changes in paleosol development. Alfisols occur between depositional episodes in the Petrified Forest and middle Owl Rock mbrs (Fig. 24). Alfisols decrease upsection and no Alfisols are found within the Church Rock Mbr (Figs. 10, 24, 25). Alfisols in the Petrified Forest and middle Owl Rock mbrs indicates these units had longer duration of pedogenesis between depositional events. The frequency and magnitude of sedimentation by overbank flooding increased in the Church Rock Mbr (e.g., Bown and Kraus 1993a, b; Hasiotis 2007; Hasiotis et al. 2007), which reduced the duration of pedogenesis and resulted in a transition from the formation of Calcic Inceptisols to the formation of Inceptisols and Entisols.

Channel Migration.—This depositional process is preserved in the Moss Back and Church Rock mbrs where trough cross-bedded conglomerate (F-5a) transitions upsection through massive conglomerate, trough-cross-bedded sandstone (F-4b), massive sandstone (F-4c), and ripple-cross-laminated sandstone (F-3) (see Table 1; Figs. 10, 24). Channel migration is also preserved in the Petrified Forest and Owl Rock mbrs where massive siltstone (F-2a) and very fine-grained sandstone (F-2b) are overlain by beds of ripple-cross-laminated sandstone (F-3), massive sandstone (F-4a), trough-cross-bedded sandstone (F-4b), planar-bedded sandstone (F-4c), trough-cross-bedded conglomerate (F-5a), massive conglomerate (F-5b), and incline-bedded conglomerate (F-5c) up to 7-m thick (see Table 1; Figs. 10, 24). Sandstone and conglomerate facies occur as discontinuous ribbons and laterally extensive sheets. Channel migration of braided and meandering rivers influenced sediment deposition and duration of pedogenesis. Channel migration towards distal positions on the floodplain led to more frequent sedimentation events and laid levee and crevasse-splay deposits over floodplain deposits, interrupting

pedogenesis. Subsequent fluvial migration away from the area resulted in less frequent sedimentation and greater duration of pedogenesis, allowing crevasse-splay and levee deposits to be topped by ichnopedofacies (e.g., Kraus 1987; Bown and Kraus 1993a, b; Hasiotis et al., 2007). For example, Naktodemasis-Camborygma Entisols formed on levee deposits in the upper Owl Rock Mbr due to channel migration away from the soil profile (see Figs. 10, 14, 25).

Frequency of channel migration changed through Chine Fm deposition, affecting the development of paleosols and ichnopedofacies. In the Moss Back Mbr, frequent migration of braided rivers led to the abandonment of fluvial bars and the development of Rhizolith Entisols on bar tops (see Figs. 10, 12, 25). Channel migration frequency then decreased during deposition of the Petrified Forest and lower Owl Rock mbrs. One instance of levee deposits from channel migration was observed in the Petrified Forest Mbr at East Section; none were observed in the lower Owl Rock Mbr (Fig. 24). Decreased reworking by meandering fluvial systems with low, nonsteady sedimentation allowed for greater duration of pedogenesis and the development of Calcic Inceptisols and Calcic Alfisols (Figs. 10, 24, 25). Numerous channel migration deposits in the middle Owl Rock Mbr indicate an increase in migration frequency upsection (Fig. 24). A well-preserved example occurs at West Section (Figs. 10, 24, 25). At this location, incline-bedded conglomerate represents lateral accretion of pointbar deposits, which cut into underlying Rhizolith Calcic Alfisols (see Fig. 22A). Increasing fluvial migration and nonsteady sedimentation led to a shift from composite, calcic paleosols at the base of the middle Owl Rock Mbr to compound and composite, noncalcic Alfisols, Inceptisols, and Entisols upsection (Figs. 10, 24, 25). Frequency of channel migration then decreased during upper Owl Rock Mbr deposition, with only one channel migration event observed near the top of the unit, which contains Naktodemasis-Camborygma Entisols (see Fig. 14). Less frequent channel migration,

and a shift to relatively steady sediment deposition allowed for the accumulation of composite and cumulative Naktodemasis Inceptisol and Calcic Inceptisol profiles (see Figs. 10, 16, 25). Channel migration frequency then increased once again during Church Rock Mbr deposition. Increased channel migration and increasing nonsteady sediment deposition led to shorter duration of pedogenesis and a transition from composite Naktodemasis Inceptisols and Calcic Inceptisols to compound Rhizolith Inceptisols and Shallowly Burrowed Entisols (Figs. 10, 25).

Comparison to FACs.—In the northeast Chinle Basin, overbank flooding and channel migration deposits fine upward and are similar to the meter-scale fluvial aggradational cycles (FACs) observed in the Chinle Fm of Arizona, New Mexico, and eastern Utah (e.g., Prochnow et al. 2006b; Cleveland et al. 2007; Trendell et al. 2012). FACs are attributed to overbank flooding and channel migration (e.g., Prochnow et al. 2006b; Cleveland et al. 2007; Trendell et al. 2012). Fining-upward FACs stack into fluvial aggradational cycle sets, which in turn stack into fluvial sequences (e.g., Prochnow et al. 2006b; Cleveland et al. 2007). In the study area, however, such nested fluvial cycles were not identified. Channel migration and overbank flooding did affect finer scale sedimentation patterns in the study area. The absence of nested fluvial cyclicity, however, indicates that autocyclic processes were neither as common nor the dominant control on sedimentation as at other locations in the Chinle Basin.

Allocyclic Processes

Regional Tectonism.—Changes in rates of basin subsidence and accommodation are indicated by shifting styles of fluvial deposition and ichnopedofacies development. Fluvial-lacustrine depositional phases similar to those described by Blakey and Gubitosa (1983) and Dubiel (1987) were observed in the northeast Chinle Basin. Blakey and Gubitosa (1983)

attributed these depositional phases to changes in regional tectonism. Multistory sand sheets of braided river deposits in the Moss Back Mbr are interpreted to reflect low rates of basin subsidence (e.g., Blakey and Gubitosa 1983, 1984; Kraus 1987; Hazel 1994; Cleveland et al. 2007). Low subsidence rates led to decreased accommodation, causing increased reworking of sediment by fluvial systems (e.g., Kraus and Middleton 1987b). Frequent reworking of sediment resulted in poor preservation of ichnopedofacies in the Moss Back Mbr, and those that were preserved were less developed due to short duration of pedogenesis (Figs. 10, 25). Fluvial styles evolved into meandering streams in the Petrified Forest and Owl Rock mbrs. The thick floodplain deposits and ribbon sand bodies of these units support rapid subsidence rates, which allowed for greater accommodation in the basin (e.g., Blakey and Gubitosa 1984; Kraus 1987; Kraus and Middleton 1987b; Hazel 1994; Cleveland et al. 2007). Greater accommodation meant less frequent sediment reworking by rivers and longer duration of pedogenesis (e.g., Bown and Kraus 1987; Blakey and Gubitosa 1984; Kraus 2002). This aided in the formation and preservation of more developed ichnopedofacies in the Petrified Forest and lower Owl Rock mbrs. During intervals of higher sedimentation, there was aggradation of the floodplain and fluvial systems (e.g., Smith et al. 1989; Slingerland and Smith 2004). Intervals of higher nonsteady and steady sedimentation explain the formation of compound and composite ichnopedofacies in the middle Owl Rock Mbr and composite and cumulative ichnopedofacies in the upper Owl Rock Mbr. Sand sheets in the Church Rock Mbr indicate a shift to lower basin subsidence rates at the end of Chinle Fm deposition (Blakey and Gubitosa 1983, 1984; Kraus 1987; Hazel 1994; Cleveland et al. 2007). Ribbon sand bodies in the Church Rock Mbr, however, indicate basin subsidence rate was not as low as during Moss Back Mbr deposition. These slightly higher subsidence rates allowed for the accommodation needed for the

preservation of playa lake deposits in the Church Rock Mbr. As basin subsidence decreased, accommodation also decreased, and sediment reworking by fluvial systems increased (e.g., Kraus and Middleton 1987b). Shorter duration of pedogenesis led to less developed ichnopedofacies upsection, though frequent cannibalization of sediment by rivers meant some ichnopedofacies were not preserved in Church Rock Mbr deposits.

Incised valleys were formed through base-level changes (Fig. 24), and ichnopedofacies filling these valleys were influenced by temporal and spatial changes in sedimentation rate. Drops in base level cut valleys into Chinle Fm units and mark the breaks between members. Valleys were subsequently filled during rises in base level, which created accommodation for sedimentation. During Moss Back Mbr deposition, high, nonsteady sedimentation rates and increased fluvial migration during reduced accommodation influenced the formation of Rhizolith Entisols (Figs. 10, 25). During Petrified Forest, lower Owl Rock, and upper Owl Rock Mbr deposition, relative rates of valley fill were higher in the south of the study area than in the north, creating a trend of increasing duration of pedogenesis on interfluves located to the north. Overall sedimentation rates remained fairly low during deposition of the Petrified Forest and lower Owl Rock mbrs. Low, nonsteady sedimentation, along with rare channel migration, further enhanced the formation of well-developed ichnopedofacies including compound and composite Therapsid Calcic Inceptisols and Rhizolith and Naktodemasis Calcic Alfisols (Figs. 10, 25). Sedimentation rates than increased and remained predominantly nonsteady during middle Owl Rock Mbr deposition, resulting in a transition from composite Camborygma Calcic Inceptisols to numerous overbank flooding and channel migration deposits containing compound and composite paleosols (Fig. 10). Sedimentation remained high, but decreased slightly and become relatively steady in the upper Owl Rock Mbr. This steady sedimentation, with decreased channel

migration, influenced the formation of composite and cumulative Naktodemasis Alfisols and Naktodemasis Inceptisols and Calcic Inceptisols (Figs. 10, 25). Sedimentation rates increased in the Church Rock Mbr and also shifted to nonsteady deposition. This change in sedimentation, in conjunction with decreased basin accommodation and more frequent channel migration, resulted in a shift from composite Naktodemasis Inceptisols and Calcic Inceptisols at the base of the member to poorly developed, compound Shallowly Burrowed Entisols and Rhizolith Inceptisols (Figs. 10, 25).

Halokinesis.—This process influenced facies distribution and preservation in the study area. The northeast Chinle Basin is located at the western edge of the Salt Anticline Region, and previous investigations have noted that halokinesis influenced sedimentary architecture and paleosol development (e.g., Blakey and Gubitosa 1983; Hazel 1994; Prochnow et al. 2005, 2006b). Across the Four Corners region, including southeastern Utah, extensive lacustrine limestone beds have been identified within the Owl Rock Mbr (e.g., Stewart et al. 1972; Blakey and Gubitosa 1983; Dubiel 1987; Tanner 2000; Tanner and Lucas 2006). The Owl Rock Mbr in the study area, however, does not contain those extensive lacustrine limestone beds. A laterally accreted conglomerate bed containing oncoid clasts occurs instead in that stratigraphically equivalent position (Figs. 10, 24, 25). Increased basin subsidence during lower Owl Rock Mbr deposition created the accommodation needed for lakes to form. Oncolites then developed within this local lacustrine system (e.g., Abell et al. 1982; Rosell and Obrador 1982; Parcerisa et al. 2006; Arenas et al. 2007). Following lake development, a drop in local base level caused by salt diapirism led to fluvial incision and reworking of the lacustrine deposits (Blakey and Gubitosa 1983, 1984; Hazel 1994). The only preserved evidence of the lacustrine system are the oncolites that compose the gravel in the lateral accretion beds.

Climate.—Climatic trends are observed in vertical changes of floodplain ichnopedofacies, particularly those with pedogenic carbonate. As any stage of carbonate development can be found under a range of precipitation regimes, the modern locations of India and Tanzania were selected as analogues to Chinle Fm paleosols since they are effected by monsoonal conditions and have similar environments and latitudinal positions to Chinle Fm deposits.

Therapsid Inceptisols and Calcic Inceptisols in the Petrified Forest Mbr show deeply penetrating rhizoliths and precipitation of calcium carbonate within bright red horizons, indicating well-drained sediments and low moisture (Figs. 10, 25; see Fig. 18; Machette et al. 1985; Kraus and Aslan 1993; Kraus and Hasiotis 2006; Dubiel and Hasiotis 2011). This ichnopedofacies has Stage I carbonate development with weight percent CaO of 80.43% and is interpreted to have formed under seasonal climatic conditions. Compound profiles shifting upsection to composite ABk horizons suggests a shift to lower nonsteady sedimentation rates and longer duration of pedogenesis (Fig. 18; Kraus 1999; Hasiotis and Platt 2012). Stage 1 buildup of carbonate in the ichnopedofacies, therefore, was primarily influenced by precipitation levels. Modern soils in central India (~20–30°N) under monsoonal conditions with Stage 1 carbonate development form under precipitation regimes from 1100–1300 mm/year (Shrivastava et al. 2002). Modern calcic soils on the Serengeti of Tanzania (~1–5°S) under monsoonal conditions show a similar relationship between carbonate buildup and precipitation. Carbonate nodules become rarer as precipitation levels approach 1100 mm/year, and the primary indication of carbonate buildup is effervescence of matrix material under hydrochloric acid (Jager 1982). Modern precipitation values suggest that during Petrified Forest Mbr deposition, Therapsid Inceptisols and Calcic Inceptisols formed under an annual precipitation of ~1100–1300 mm/year.

At the base of the lower Owl Rock Mbr, a Camborygma Vertisol occurs above the Therapsid Inceptisols and Calcic Inceptisols (Figs. 10, 25). Slickensides, prismatic peds, and redoximorphic coloration observed in this ichnopedofacies indicate seasonal precipitation (see Fig. 19; e.g., Driese and Foreman 1992; Driese and Mora 1993; Dubiel and Hasiotis 2011). *Camborygma eumekenomos* that are 75 cm deep further support a highly fluctuating water table and seasonal moisture (Fig. 19; Hasiotis and Mitchell 1993; Hasiotis et al. 1993; Hasiotis and Honey 2000; Hasiotis 2004, 2008). Lack of carbonate in the profile could be due to high precipitation levels or high sedimentation rates preventing longer duration of pedogenesis (Machette 1985; Kraus 1999; Shrivastava et al. 2002; Hasiotis and Platt 2012). Compound and cumulative A-Bss horizons suggest higher rates of sedimentation (Fig. 19; Kraus 1999; Hasiotis and Platt 2012); however, slickensides indicate longer duration of pedogenesis and the buildup of clay in the subsurface (e.g., Driese and Foreman 1992; Driese and Mora 1993). Precipitation, therefore, also played a large role in influencing ichnopedofacies development. In contemporary central India (~20–30°N), Vertisols are found under precipitation regimes from 500–1300 mm/yr (Shrivastava et al. 2002). These Vertisols also display various levels of carbonate buildup, with heavy carbonate dissolution occurring in Vertisols where annual precipitation is 1000–1300 mm (Shrivastava et al. 2002). The lack of carbonate in the Camborygma Vertisol in the study area suggests (1) precipitation levels were >1300 mm/yr, precluding carbonate formation and buildup, and (2) a shift to more humid conditions across the Petrified Forest Mbr–Owl Rock Mbr transition.

Higher within the lower Owl Rock Mbr, ichnopedofacies transition to Naktodemasis Calcic Alfisols and Rhizolith Calcic Alfisols (Figs. 10, 25). Abundant calcium carbonate nodules, clay accumulation, strong red coloration, and deep roots in both of these

ichnopedofacies suggest well-drained conditions, a deep water table, and seasonal precipitation (see Figs. 21, 22; Gile et al. 1966; Machette 1985; Kraus and Aslan 1993; Kraus and Hasiotis 2006; Dubiel and Hasiotis 2011; Counts and Hasiotis 2014). Carbonate development is at Stage 2 in Naktodemasis Calcic Alfisols with weight percent CaO of 66.64%, and reaches Stage 3 in Rhizolith Calcic Alfisols where carbonate nodules occur throughout the entire profile and weight percent CaO is 87.43%. Both ichnopedofacies contain composite Btk horizons, which suggests low, nonsteady sedimentation and long duration of pedogenesis (Figs. 21, 22; Kraus 1999; Hasiotis and Platt 2012). Differences in carbonate nodule development, then, between the two ichnopedofacies was not due to differences in duration of pedogenesis, but variations in precipitation levels. Modern soils with Stage 2 carbonate development under monsoonal conditions form on the Serengeti Plain (~1–5°S) under precipitation regimes from 700–1100 mm/yr (Jager 1982). This suggests Naktodemasis Calcic Alfisols formed under an annual precipitation of ~700–1100 mm. Modern soils with Stage 3 carbonate development and carbonate nodules similar in size to those in the Rhizolith Calcic Alfisols are found in southern India (~10–12°N) under precipitation regimes between 400–500 mm/yr (Shankar and Achyuthan 2007). Carbonate nodules are also present throughout the whole profile of modern calcic soils forming under monsoonal conditions in central India (~20–30°N) under precipitation regimes of 500–700 mm/yr (Shrivastava et al. 2002). This suggests the Rhizolith Calcic Alfisols formed under an annual precipitation of ~400–700 mm. Thick Btk horizons in the lower Owl Rock Mbr also suggest smaller scale cycles of decreasing precipitation, allowing the top of the calcic horizon to move upward over time (e.g., Birkeland 1999). Higher precipitation would have allowed water to flow deeper into the soil profile, washing out and dissolving the carbonate nodules (e.g., Gile et al. 1966; Shrivastava et al. 2002). The preservation of thick calcic horizons

indicates precipitation decreased and rainfall reached shallower and shallower levels, recording small scale drying cycles during monsoonal conditions. The change from Camborygma Vertisols to Naktodemasis Calcic Alfisols and then Rhizolith Calcic Alfisols marks a clear shift to drier conditions during lower Owl Rock Mbr deposition, from >1300 mm/yr to ~700–1100 mm/yr to finally ~400–700 mm/yr.

In the middle Owl Rock Mbr, ichnopedofacies shift to Camborygma Inceptisols and Calcic Inceptisols (Figs. 10, 25). Gleyed horizons and *Camborygma* 110–120 cm deep at the base of the unit indicate seasonal precipitation and fluctuating water tables >1 m beneath the paleosol surface (see Fig. 17; Hasiotis and Mitchell 1993; Hasiotis et al. 1993; Hasiotis 2004, 2008). Stage 2 calcium carbonate nodules then overprint *Camborygma* and the gleyed horizon, suggesting a decrease in precipitation during paleosol formation (Fig. 17; i.e., polygenetic; Kraus and Aslan 1993; Kraus 1999; Dubiel and Hasiotis 2011). Composite Bk horizons indicate low rates of nonsteady sedimentation and longer duration of pedogenesis (Fig. 17; Kraus 1999; Hasiotis and Platt 2012), further suggesting that precipitation was the main control on carbonate accumulation. *Camborygma* likely formed during annual precipitation of ~1100 mm (Jager 1982); Stage 2 carbonate nodules then formed and moved upward in the profile as precipitation dropped towards ~700 mm/yr (Jager 1982). Despite a decrease in precipitation during formation of the Camborygma Inceptisols and Calcic Inceptisols, precipitation levels were still higher than during formation of the Rhizolith Calcic Alfisols observed lower in the section (e.g., Birkeland 1999; Shrivastava et al. 2002). The reappearance of *Camborygma* at the top of the middle Owl Rock Mbr suggests a return to precipitation levels of ~1100 mm/yr heading into the middle Owl Rock Mbr-upper Owl Rock Mbr contact.

Ichnopedofacies shift to Naktodemasis Alfisols and Naktodemasis Inceptisols and Calcic Inceptisols in the upper Owl Rock Mbr (Figs. 10, 25). Bioturbation by *Naktodemasis*, deeply penetrating rhizohaloes, and lack of dissolution around carbonate nodules in these two ichnopedofacies indicate a well-drained, deep water table (see Figs. 16, 20; e.g., Shrivastava et al. 2002; Kraus and Hasiotis 2006; Hasiotis et al. 2007; Smith et al. 2008a; Counts and Hasiotis 2014). Naktodemasis Inceptisols and Calcic Inceptisols contain Stage 2 calcium carbonate nodules; however, nodules occur more shallowly in profile and are less common than in the underlying Camborygma Inceptisols and Calcic Inceptisols. Weight percent CaO in Bk horizons of the Naktodemasis Calcic Inceptisol is 51.78%, which is lower than the weight percent CaO of 66.64% of the Stage 2 calcic horizon in Naktodemasis Calcic Alfisols. Fewer nodules and decreased carbonate accumulation may indicate less precipitation to carry carbonate deeper into the subsurface, or that sedimentation rate was too fast to allow for more advanced pedogenic development (e.g., Gile et al. 1966; Machette 1985; Kraus 1999; Hasiotis and Platt 2012). Evidence for both decreased precipitation and high sedimentation rate were observed in the upper Owl Rock Mbr. *Camborygma* are found in Naktodemasis Inceptisols and Calcic Inceptisols at the base of the upper Owl Rock Mbr, but are not found in this ichnopedofacies in the rest of the unit. The lack of *Camborygma* in the rest of the upper Owl Rock Mbr, except in levee deposits, supports a decrease in soil saturation conditions and the water table upsection (e.g., Hasiotis and Mitchell 1993; Hasiotis et al. 1993; Hasiotis and Honey 2000). Naktodemasis Alfisols are present only at the base of the upper Owl Rock Mbr and contain composite Bt horizons (Figs. 20, 25). Naktodemasis Inceptisols and Calcic Inceptisols are composed of cumulative to composite A and ABk horizons (Fig. 16). The shift from composite Alfisols to cumulative and composite Inceptisols and Calcic Inceptisols suggests a shift from high rates of

nonsteady sedimentation to steady sedimentation with decreased duration for pedogenesis (e.g., Kraus 1999; Hasiotis and Platt 2012). Precipitation levels were likely ~1100 mm/yr at the base of the upper Owl Rock Mbr, then decreased to ~700 mm/yr upsection (Jager 1982). Increasing sediment deposition during drier climate, however, shortened the duration of pedogenesis and precluded the formation of more numerous calcium carbonate nodules in the Naktodemasis Inceptisols and Calcic Inceptisols.

Ichnopedofacies shift from Naktodemasis Inceptisols and Calcic Inceptisols to Rhizolith Inceptisols and Shallowly Burrowed Entisols in the Church Rock Mbr (Figs. 10, 25). Dark red-brown matrix colors and numerous desiccation cracks indicate well-drained soil conditions and more pronounced drying of sediment (Dubiel 1987; Kraus and Aslan 1993; Kraus and Hasiotis 2006). Other than rhizoliths, *Naktodemasis* at the base of the unit, and shallowly burrowed ichnofossils, however, ichnopedologic features are rare and there are no occurrences of *Camborygma* or carbonate nodules (Figs. 10, 25), suggesting high sedimentation rates and low precipitation (e.g., Gile et al. 1966; Machette 1985; Hasiotis and Mitchell 1993; Hasiotis et al. 1993; Kraus 1999; Hasiotis and Platt 2012). Naktodemasis Inceptisols and Calcic Inceptisols show Stage 1 carbonate development and weight percent CaO of 99.50%. Despite the lack of carbonate nodules, this weight percent CaO is higher than values seen in Stage 1–3 calcic horizons in underlying units. Carbonate accumulation greater than Stage 3 weight percent CaO values and lack of *Camborygma* in this ichnopedofacies likely indicates precipitation levels of ~400 mm/yr (Shankar and Achyuthan 2007). High rates of steady sedimentation and shorter duration of pedogenesis likely precluded the formation of Stage 3 nodules and kept carbonate dispersed in the paleosol matrix. The shift from composite Naktodemasis Inceptisols and Calcic Inceptisols to compound Entisols and Inceptisols indicates a change from high, steady

sedimentation to higher, nonsteady sedimentation rates and shorter duration of pedogenesis (Kraus 1999; Hasiotis and Platt 2012). Common sediment reworking by meandering and braided rivers, frequent overbank flooding, and proximity to the fluvial channel prevented the formation of better developed paleosols and deeper burrowing ichnofossils higher in the member. Shallowly Burrowed Entisols are associated with playa lake deposits. In modern Australia (~35°S), shallow playa lakes form under precipitation regimes of 325 mm/yr (Teller and Last 1990). This modern precipitation value suggests that Shallowly Burrowed Entisols in playa lake deposits formed under an annual precipitation of ~325 mm. Rhizoliths in Church Rock Mbr ichnopedofacies gives a lower limit for precipitation levels. In the modern Namib desert of Namibia (~23–24°S), the precipitation limit of vegetated surfaces is ~25 mm/yr (Amit et al. 2010). This suggests mean annual precipitation towards the end of Church Rock Mbr deposition was ~25–325 mm. The shift from Naktodemasis Inceptisols and Calcic Inceptisols to Shallowly Burrowed Entisols and Rhizolith Inceptisols suggests precipitation levels decreased in the Church Rock Mbr from ~400 mm/yr to ~25–325 mm/yr. Despite these lower precipitation levels, moisture still entered the environment until the very end of Chinle Fm deposition (Dubiel 1987; Dubiel et al. 1991).

Hydrology

Groundwater and soil moisture conditions, influenced by climate and proximity to alluvial and lacustrine systems (e.g., Hasiotis 2002, 2004, 2008; Hasiotis et al. 2007, 2012), varied during Chinle Fm deposition, which affected stratigraphic distribution of ichnofossils and depths of burrowing. The wettest intervals in the Chinle Fm are the Petrified Forest, base of the lower Owl Rock, base and top of the middle Owl Rock, and base of the upper Owl Rock mbrs

(Fig. 10). These units also have the greatest occurrences of *Camborygma* (Figs. 10, 25), which penetrate below the water table into the phreatic zone and reflect the hydrophilic behavior of crayfish (Hasiotis and Mitchell 1993; Hasiotis et al. 1993; Hasiotis 2002, 2004, 2008). Higher precipitation in the Petrified Forest, base of the lower Owl Rock, base and top of the middle Owl Rock, and base of the upper Owl Rock mbrs resulted in a shallower water table, and more common burrowing by crayfish. Times of decreased precipitation outside of these intervals, however, resulted in deepened water tables, and less common burrowing by crayfish (Fig. 10). No *Camborygma* are present in the Church Rock Mbr; precipitation was too low and the water table was too deep for *Camborygma* to form. A likely overall decrease in the water table during Chinle Fm deposition caused *Camborygma* to occur less often upsection and have greater burrowing depths (Figs. 10, 25). *Camborygma* penetrate a depth of only 75 cm in Camborygma Vertisols of the lower Owl Rock Mbr, but penetrate 110–120 cm in Camborygma Inceptisols and Calcic Inceptisols of the middle Owl Rock Mbr.

The only instances where hydrophilic and hygrophilic behavior, including *Camborygma*, are observed during times of decreased precipitation are in levee deposits (Fig. 10). For example, in the middle Owl Rock Mbr, Naktodemasis-Camborygma Entisols containing *Ancorichnus*, *Arenicolites*, *Camborygma*, and *Treptichnus* occur in levee deposits under an estimated precipitation of ~700 mm/yr (Fig. 10). These ichnofossils are not observed in floodplain deposits of the middle Owl Rock Mbr under the same precipitation levels. At the top of the upper Owl Rock Mbr, another Naktodemasis-Camborygma Entisol with *Camborygma* and *Scoyenia* occurs in levee deposits under an estimated precipitation of ~700 mm/yr (Figs. 10, 25; see Fig. 14). These traces are absent in the rest of the unit except for *Camborygma* at the base of the upper Owl Rock Mbr in floodplain deposits, which reflects the higher precipitation estimate of ~1100

mm/yr and resulted in higher water tables. In the Church Rock Mbr, hydrophilic behavior is not observed at all, instead hygrophilic behavior and shallow water tables are indicated by *Scoyenia* (Figs. 10, 25). Restriction of deep burrowing to proximal fluvial deposits—specifically levees—in the middle and upper Owl Rock mbrs and the predominance of hygrophilic behaviors in the Church Rock Mbr indicate lower precipitation levels and fluvial systems that likely fed the groundwater.

Ichnofossils displaying terraphilic behavior become more dominant upsection during Chinle Fm deposition. In the Petrified Forest, lower Owl Rock, and middle Owl Rock mbrs, a variety of ichnofossils displaying all four burrowing behaviors are observed in floodplain and palustrine deposits (Figs. 10, 25). By upper Owl Rock Mbr deposition, *Naktodemasis* and root ichnofossils dominate paleosol profiles (Figs. 10, 25). Root ichnofossils become the only ichnofossils present in floodplain deposits of the Church Rock Mbr (Fig. 10). Decreasing water tables through Chinle Fm deposition—due to decreasing precipitation levels—expanded the vadose zone and created conditions favorable to terraphilic burrowers. By the time of Church Rock Mbr deposition, soil moisture conditions on the floodplain became too dry to support organisms other than occasional plants.

Terraphilic, hygrophilic, and hydrophilic behaviors can all coexist in the vadose zone, but in some Chinle Fm units *Naktodemasis* commonly overprint the burrow fill of *Camborygma*. This overprinting indicates separate episodes of burrowing and changing groundwater conditions (e.g., Hasiotis and Bown 1992, Hasiotis 2002). In floodplain deposits at the top of the middle Owl Rock Mbr, this type of overprinting reflects decreasing soil moisture and water tables during soil formation (e.g., Hasiotis and Bown 1992; Hasiotis 2002). *Naktodemasis* overprinting the burrow fill of *Camborygma* are also observed in levee deposits of the middle Owl Rock,

upper Owl Rock, and Church Rock mbrs, reflecting deepening water tables following flooding events.

CLIMATIC VARIATION IN THE CHINLE BASIN

Numerous investigations support increasing aridity throughout Chinle Fm deposition, but there is disagreement concerning the details and cause of this climate shift (e.g., Blakey and Gubitosa 1983; Dubiel et al. 1991; Prochnow et al. 2006a; Cleveland et al. 2008; Atchley et al. 2013; Dubiel and Hasiotis 2011; Nordt et al. 2015). Previous studies corroborate a transition from humid to subhumid and semiarid conditions during deposition of the Petrified Forest Mbr (Prochnow et al. 2006a; Tanner and Lucas 2006; Cleveland et al. 2008a; Atchley et al. 2013; Nordt et al. 2015). Atchley et al. (2013) and Nordt et al. (2015) suggested timing of this climate transition as a result of a complete collapse of the Pangean megamonsoon due to uplift of the Cordilleran magmatic arc. Nordt et al. (2015) also cites magnetostratigraphic studies that suggest Pangea remained in the tropics throughout Chinle Fm deposition (Steiner and Lucas 2000; Loope et al. 2004; Rowe et al. 2007; Zeigler and Geissman 2011). This explanation is in contrast to Dubiel (1987, 1989) and Dubiel et al. (1991), which interpreted a monsoonal climate that persisted until the end of the Late Triassic with a decrease in precipitation caused by the northward movement of Pangea.

Monsoonal indicators in ichnopedofacies of the Petrified Forest and Owl Rock mbrs in this study indicate that paleomonsoon circulation did not collapse during deposition of either of these members. Playa lake, braided river, and meandering river deposits in the Church Rock Mbr further suggest strongly seasonal moisture until the end of Chinle Fm deposition, supporting the continuation of monsoonal conditions until the end of the Triassic Period. The gradual drying

seen at the study area was probably due to the migration of Pangea into the midlatitudes (e.g., Dubiel et al 1991; Dubiel and Hasiotis 2011).

Upsection changes in paleosols and ichnopedofacies of the northeast Chinle Basin indicate finer scale fluctuations in precipitation during an overall drying of climate. The Petrified Forest and lower Owl Rock mbrs at West Section and S3 show 6–15-m-scale alternations between calcic and noncalcic paleosols, suggesting wet-dry climate cycles (Fig. 24). In the lower Owl Rock Mbr, short-term drying cycles are suggested by the upward increase of carbonate nodules within individual Naktodemasis Calcic Alfisols and Rhizolith Calcic Alfisols. At the base of the middle Owl Rock Mbr, Camborygma Inceptisols and Calcic Inceptisols suggest shallower water tables 1 m from the sediment surface, supporting a period of more humid conditions than the underlying Calcic Alfisols. Carbonate nodules overprinting *Camborygma* and gleyed soil horizons in the Camborygma Inceptisols and Calcic Inceptisols also suggest short-term drying during ichnopedofacies formation. In the upper Owl Rock Mbr, loss of *Camborygma* upsection and the presence of carbonate nodules in Naktodemasis Inceptisols and Calcic Inceptisols indicate decreasing precipitation.

Repetition of paleosol successions and lacustrine deposits in continental strata has been attributed to Milankovitch cyclicity. For example, Kraus and Riggins (2007) suggested that drying episodes observed in paleosols in the Upper Paleocene–Lower Eocene Willwood Fm of Wyoming may correspond to precessional cyclicity observed in equivalent marine deposits. Abdul Aziz et al. (2008) attributed 8-m-scale paleosol cycles in the Willwood Fm to precession cycles and 3-m-scale cycles to sub-Milankovitch cycles similar to those described by Bond et al. (1993), Steenbrink et al. (2003), and Becker et al. (2005). Olsen and Kent (1996, 1999), Olsen et al. (1996), and Olsen (1997) identified precession cycles nested within eccentricity cycles in

Upper Triassic lacustrine deposits of the Newark Basin. Recent research in the Chinle Basin of similarly aged alluvial and lacustrine deposits did not identify any Milankovitch cyclicity (e.g., Prochnow et al. 2006a; Tanner and Lucas 2006; Cleveland et al. 2008a; Atchley et al. 2013; Nordt et al. 2015). The lack of well-preserved cyclicity in paleosols and ichnopedofacies in the Moss Back, middle Owl Rock, and Church Rock mbrs in the northeastern Chinle Basin are attributed to autocyclic channel migration and overbank flooding episodes. These sedimentation events would interrupt ichnopedofacies development within these three units and mask any Milankovitch signatures. The cut and fill nature of Chinle Fm deposits in the northeast Chinle Basin would also obscure the preservation of Milankovitch cycles throughout the entire formation. This depositional architecture makes the already problematic task of working out Milankovitch signatures even more difficult.

Climate at locations across the Chinle Basin display wet-dry patterns. In eastern Utah, Prochnow et al. (2006a) suggested precipitation decreased from >1400 mm/yr to ~400 mm/yr during Petrified Forest Mbr deposition, and increased from ~400 mm/yr to ~600 mm/yr during deposition of the Owl Rock and Church Rock mbrs. Atchley et al. (2013) and Nordt et al. (2015) interpreted highly fluctuating moisture during deposition of the upper Petrified Forest and Owl Rock mbrs at PFNP and the surrounding vicinity, with highs of ~1000 mm/yr during wet periods and lows of ~200 mm/yr during dry periods. Nordt et al. (2015) additionally identified a humid period with mean annual precipitation (MAP) of ~900 mm near the base of the Owl Rock Mbr. In northern New Mexico, Cleveland et al. (2008a) determined MAP between ~200–450 mm for Petrified Forest Mbr to Rock Point Mbr deposition, and the Rock Point Mbr contained wet-dry fluctuations. This research, however, did not address the mechanism behind these wet-dry cycles,

instead focusing on longer term climatic trends and controls (Cleveland et al. 2008a; Atchley et al. 2013; Nordt et al. 2015).

Despite the presence of wet-dry cycles within Chinle Fm deposits in the northeast Chinle Basin, PFNP, and northern New Mexico, great variation exists between interpreted precipitation levels. The main reason for this variation is the use of different indicators to estimate annual precipitation. Some of these studies did attempt to assign modern soil classifications to paleosols, but none combined both the ichnologic and pedogenic features, nor compared paleosols to modern environmental, behavioral, and latitudinal analogs. Prochnow et al. (2006a), Atchley et al. (2013), and Nordt et al. (2015) used geochemical weathering indices to calculate MAP, but did not incorporate ichnologic evidence into their estimates. Cleveland et al. (2008a), while incorporating some pedogenic and ichnologic features, determined MAP using depth-to-carbonate functions and stated that, as a consequence, MAP values were likely minimum estimates. Prochnow et al. (2006a) also used depth-to-carbonate functions for some of their MAP estimates.

Estimated precipitation values determined in our study by utilizing ichnopedofacies and modern environmental and latitudinal analogs were, in general, higher than MAP values determined through geochemical methods alone in previous research elsewhere in the Chinle Basin. For the Petrified Forest Mbr, Prochnow et al. (2006a), Atchley et al. (2013), and Nordt et al. (2015) do have precipitation estimates of ~1000 mm/yr, and even up to ~1400 mm/yr in the case of Prochnow et al. (2006a). Their MAP estimates are similar to the ~1100–1300 mm/yr precipitation levels determined in our study. Cleveland et al. (2008), however, only estimated ~200–450 MAP for Petrified Forest Mbr equivalent deposits, well below our estimates for the northeast Chinle Basin. For Owl Rock Mbr deposits in eastern Utah, the estimated ~400–500

mm MAP by Prochnow et al. (2006a) is significantly lower than the ~400–1300 mm/yr range in precipitation levels suggested by ichnopedofacies. Atchley et al. (2013) and Nordt et al. (2015), however, estimate MAP up to ~1000 mm/yr during wet intervals in the Owl Rock Mbr at PFNP, which is within our range of estimates for the northeast Chinle Basin. Their MAP estimates for dry intervals, however, are as low as ~200 mm/yr, which is half of the estimates based on ichnopedofacies. Cleveland et al. (2008a) has even lower precipitation estimates for the Chinle Fm in New Mexico. For example, paleosols (in the Rock Point Mbr) at Ghost Ranch, New Mexico, have estimated MAP of ~200–450 mm based on depth-to-carbonate functions. These paleosols also exhibit gleyed soil matrix, wedge-shaped peds, abundant semiplasmic fabrics, and *Camborygma eumekenomos* 20–80 cm deep that are lined with carbonate nodules (Cleveland et al. 2008a). These paleosols have similar appearance to Camborygma Calcic Inceptisols in the northeast Chinle Basin, which have an estimated MAP of ~700–1100 mm. Furthermore, strata interpreted as the Rock Point Mbr (Lucas 1993; Lucas et al. 1997) was originally defined separately as the "siltstone member" by Stewart et al. (1972) and is more likely correlative to the Owl Rock Mbr—which is dominated by siltstone around Canyonlands (see Fig. 24)—based on regional stratigraphy, sedimentology, paleontology, and ichnology (e.g., Stewart et al. 1972; Hasiotis and Mitchell 1993; Schwartz and Gillette 1994; Dubiel and Hasiotis 2011, personal observations). These variations in MAP interpretations highlight the importance to integrate ichnologic and pedogenic features—to create ichnopedofacies—into paleoprecipitation estimates that are correlated to modern environmental and latitudinal analogs in order to build more accurate climate models.

Low MAP values from previous research are at odds with the location of the Chinle Basin in sub-30° paleolatitudes under a megamonsoonal regime in greenhouse conditions (e.g.,

Dickinson 1981; Parrish and Peterson 1988; Bazard and Butler 1991; Dubiel et al. 1991; Dubiel 1994; Dubiel and Hasiotis 2011). Modern near-equatorial environments affected by monsoons, such as the Serengeti plains of Tanzania, have precipitation levels of ~500 mm/yr to as high as 1200 mm/yr (e.g., Oliver 1973; Jager 1982; Lydolph 1985; Aber and Melillo 1991; Sinclair et al. 2007). Modern subtropical environments, such as central India, have precipitation levels of ~400 mm/yr to 1300 mm/yr (e.g., Shrivastava et al. 2002; Shankar and Achyuthan 2007).

Despite the use of different climate indices, overall trends of paleoprecipitation variation across the Chinle Basin are recognized. Although MAP values from New Mexico paleosols may be underestimates, the lack of *Camborygma* from Petrified Forest Mbr equivalent units does suggest lower water tables and decreased precipitation was present south of the northeast Chinle Basin during this time period. An east–west trend in precipitation values is also recognized. In the northeast Chinle Basin, a Camborygma Vertisol is observed within the lower Owl Rock Mbr at Southwest Section (Fig. 24) and represents the highest precipitation levels in our study area at >1300 mm/yr. This ichnopedofacies appears to occur in the same stratigraphic interval as the ~900 mm/yr humid pulse at PFNP, which falls well within the precipitation estimates from our study. Both the center and northeast edge of the Chinle Basin contain evidence for a pulse of wetter conditions, but estimated precipitation was higher during the wetter interval in the northeast Chinle Basin. Precipitation levels in the northeast Chinle Basin varied from levels towards the southeast and central parts of the basin. Climatic conditions, therefore, were not consistent across the Chinle Basin during the Late Triassic.

CONCLUSIONS

Twelve ichnopedofacies, constructed from seventeen ichnofossil morphotypes and six paleosol orders, were identified in the Chinle Fm of the northeast Chinle Basin: 1) Shallowly Burrowed Entisols; 2) Rhizolith Entisols; 3) Camborygma Entisols; 4) Naktodemasis-Camborygma Entisols; 5) Rhizolith Inceptisols; 6) Naktodemasis Inceptisols and Calcic Inceptisols; 7) Camborygma Inceptisols and Calcic Inceptisols; 8) Therapsid Inceptisols and Calcic Inceptisols; 9) Camborygma Vertisols; 10) Naktodemasis Alfisols; 11) Naktodemasis Calcic Alfisols; and 12) Rhizolith Calcic Alfisols.

Ichnopedofacies development and their lateral and vertical distribution reveal that the northeast Chinle Basin was influenced by a variety of physiochemical controls:

1. Higher frequency of channel migration and overbank flooding in the Moss Back Mbr resulted in poorly developed and preserved ichnopedofacies. Reduced influence of autocyclic processes in the Petrified Forest and lower Owl Rock mbrs resulted in more developed, calcic ichnopedofacies. Increasing frequency of autocyclic events during middle Owl Rock Mbr deposition resulted in a transition from composite, calcic ichnopedofacies at the base of the unit to less developed, compound, noncalcic Alfisols and Inceptisols between channel migration and overbank flooding deposits. Frequency of autocyclic events decreased during the upper Owl Rock Mbr, resulting in the formation of more developed cumulative and composite, calcic ichnopedofacies. Increasing frequency of channel migration and overbank flooding in the Church Rock Mbr resulted in a shift from more developed, calcic ichnopedofacies to poorly developed, compound Inceptisols and Entisols.

2. Basin subsidence controlled the development of fluvial systems. Sand sheets of braided river deposits suggest decreased subsidence, decreased accommodation, frequent fluvial

reworking, and reduced duration of pedogenesis in the Moss Back Mbr. A shift to ribbon sand bodies in the Petrified Forest and Owl Rock mbrs suggest meandering rivers with increased subsidence, increased accommodation, less fluvial reworking, and greater duration of pedogenesis. Sheet and ribbon sand deposits in the Church Rock Mbr suggest a decrease in basin subsidence, leading to decreased accommodation, more fluvial reworking, and shorter duration of pedogenesis. Ribbon sand deposits in the Church Rock Mbr, however, indicate accommodation was still greater than in the Moss Back Mbr, allowing for the preservation of playa lake deposits.

3. Changes in base level cut and filled paleovalleys. These paleovalleys preserve the paleotopography present during Chinle Fm deposition. Topographic position and changes in rate of valley fill influenced ichnopedologic development. High, nonsteady sedimentation and decreased accommodation in the Moss Back Mbr resulted in compound Entisols. Low, nonsteady sedimentation during Petrified Forest Mbr and lower Owl Rock Mbr deposition resulted in more developed, compound and composite ichnopedofacies. An increase in nonsteady sedimentation led to more frequent autocyclic deposits in the middle Owl Rock Mbr and a transition from composite, calcic ichnopedofacies to compound and composite, noncalcic ichnopedofacies. Sedimentation rate slightly decreased and shifted to steady state sedimentation in the upper Owl Rock Mbr, resulting in cumulative and composite ichnopedofacies. A shift back to nonsteady sediment deposition in the Church Rock Mbr and increasing sedimentation rates resulted in a transition from composite, calcic ichnopedofacies to compound Entisols and Inceptisols. Overall, a south to north trend of decreasing rates of valley fill is observed in the Petrified Forest, lower Owl Rock, and upper Owl Rock mbrs.

4. Salt tectonism led to the uplift and cannibalization of lacustrine deposits. Increased accommodation in the lower Owl Rock Mbr enabled the formation of lakes with oncoids. Following halokinetic uplift and erosion, oncoids were redeposited in laterally accreted conglomerate beds. These beds remain the only indicator of the previous presence of lacustrine systems in the study area.

5. Climate overall became drier during Chinle Fm deposition with multiple smaller wet-dry cycles. This pattern is reflected in the alternations between calcic and noncalcic ichnopedofacies, and polygenetic paleosol formation with calcium carbonate nodules overprinting gleyed horizons and ichnofossils.

6. Groundwater and soil moisture conditions largely mirror changes in climate. The water table, influenced by precipitation, decreased upsection during Chinle Fm deposition, and ichnofossils reflecting hydrophilic and hygrophilic behavior also decreased upsection. Where ichnofossils displaying hydrophilic and hygrophilic behavior are common during periods of decreased precipitation, they indicate a shallower water table fed by nearby rivers. No ichnofossils displaying hydrophilic behavior are present in the Church Rock Mbr; instead hygrophilic behavior is observed in levee deposits where local water tables were higher. Ichnofossils displaying terraphilic behavior become more dominant upsection, and root ichnofossils become the only ichnofossils observed in Church Rock Mbr floodplain deposits. *Naktodemasis* overprinting the burrow fill of *Camborygma* in Owl Rock Mbr and Church Rock Mbr levee and floodplain deposits reflect drops in the water table following flooding events or due to small-scale drying cycles.

Signatures of seasonality and decreasing precipitation are seen throughout Chinle Fm deposition in the northeast Chinle Basin. Therapsid Inceptisols and Calcic Inceptisols in the

Petrified Forest Mbr suggest an annual precipitation of ~1100–1300 mm with calcium carbonate buildup during drier periods. The lower Owl Rock Mbr contains a Camborygma Vertisol, which indicates highly seasonal precipitation >1300 mm/yr with fluctuating water tables. Thick Btk horizons with Stage 2–3 calcium carbonate nodules in overlying Naktodemasis Calcic Alfisols and Rhizolith Calcic Alfisols indicate a decrease in precipitation from ~700–1100 mm/yr to ~400–700 mm/yr and suggest short-term drying cycles. In the middle Owl Rock Mbr, Camborygma Inceptisols and Calcic Inceptisols contain *Camborygma* >1 m deep that are overprinted by Stage 2 carbonate nodules. These features suggest highly fluctuating water tables and a decrease in annual precipitation from ~1100 mm to ~700 mm. The reappearance of *Camborygma* at the top of the middle Owl Rock Mbr indicates precipitation increased to ~1100 mm/yr heading into the upper Owl Rock Mbr. In the upper Owl Rock Mbr, deposits show another drying cycle from ~1100 mm/yr to ~700 mm/yr. The decrease in precipitation is suggested by the transition from Naktodemasis Alfisols and Naktodemasis Inceptisols and Calcic Inceptisols with *Camborygma* at the base of the upper Owl Rock Mbr to Naktodemasis Inceptisols and Calcic Inceptisols with Stage 2 carbonate nodules. This Stage 2 calcium carbonate also suggests that seasonal precipitation continued. Near the base of the Church Rock Mbr, Naktodemasis Inceptisols and Calcic Inceptisols with high weight percent CaO and Stage 1 horizon development suggest precipitation levels of ~400 mm/yr. Rhizolith Inceptisols and playa lake deposits with Shallowly Burrowed Entisols suggest a precipitation decrease to ~25–325 mm/yr near the end of Chinle Fm deposition. Despite the extended dry periods during Church Rock Mbr deposition, the presence of braided river, meandering river, and playa lake deposits indicate that moisture was still present until the end of the Triassic Period. Ichnopedofacies suggest monsoonal circulation continued throughout Chinle Fm deposition and did not fully

collapse until the end of the Triassic Period and the migration of Wingate Sandstone eolian dunes into the area of the Colorado Plateau.

Some overall precipitation trends at different locations during the same time period across the Chinle Basin are recognized. Decreasing precipitation from the northeast Chinle Basin to the southeast toward the basin center is suggested during Petrified Forest Mbr deposition. There is also a decrease in precipitation levels from the northeast edge to the center of the Chinle Basin during Owl Rock Mbr deposition. The Late Triassic in the Chinle Basin was characterized by complex climatic patterns which greatly influenced local depositional environments, paleotopography, hydrology, pedogenic development, and ichnofossil distribution.

Most variations in the estimates of precipitation levels across the Chinle Basin can be attributed to the use of different climate indices between studies. The use of ichnopedofacies and modern soil, environmental, behavioral, and latitudinal analogs in our study resulted in higher MAP values in general than previous studies of the Chinle Basin, which utilized geochemical weathering indices and depth-to-carbonate functions. Variations between MAP values highlights the need to incorporate ichnopedologic features and modern environmental, behavioral, and latitudinal analogs into precipitation estimates to develop more accurate climate models. MAP estimates from previous studies are too low for the interpretation of the Chinle Basin being deposited in sub-30° paleolatitudes under a megamonsoonal regime in greenhouse conditions.

This is the first study to establish ichnopedofacies in the Chinle Fm. Ichnopedofacies have proved to be useful tools for interpreting fine-scale climatic, hydrologic, and sedimentologic conditions of Chinle Fm deposits. Future use in other Chinle Fm localities will aid in working out detailed interpretations of the timing of climatic changes and cyclicity in precipitation. More detailed climate studies at locations across the Chinle Basin will further the

understanding of the spatial and temporal variations in climatic conditions in the southwest United States during the Late Triassic. Ichnopedofacies, however, are not confined for use only in the Chinle Formation. There is great potential in expanding ichnopedofacies to other continental strata.

ACKNOWLEDGEMENTS

We thank Aaron Hess, Robert Rader, and Stephen Fischer for their assistance in the field. Thanks also to Dan Hirmas for his help in identifying paleosols, and to Victor Day for his assistance in XRD sample analysis. Thanks to the Geological Society of America and the American Association of Petroleum Geologists for providing funds to SJF for this project. Finally, we thank the IchnoBioGeoSciences Group at the University of Kansas for their help and support during this project. We thank xxx and xxx for their comments and suggestions, which improved the manuscript.

REFERENCES

ABDELL–GAWAD, A.M., AND KERR, P., 1963, Alteration of Chinle siltstone and uranium emplacement, Arizona and Utah: Geological Society of America Bulletin, v. 44, p. 23–46.

ABDUL AZIZ, H., HILGEN, F.J., VAN LUIJK, G.M., SLUIJS, A., KRAUS, M.J., PARES, J.M., AND GINGERICH, P.D., 2008, Astronomical climate control on paleosol stacking patterns in the Upper Paleocene-Lower Eocene Willwood Formation, Bighorn Basin, Wyoming: Geology, v. 36, p. 531-534.

ABELL, P.I., AWRAMIK, S.M., OSBORNE, R.H., AND TOMELLINI, S., 1982, Plio-Pleistocene lacustrine Stromatolites from Lake Turkana, Kenya: Morphology, stratigraphy, and stable isotopes: Sedimentary Geology, v. 32, p. 1–26.

ABER, J.D., AND MELILLO, J.M., 1991, Terrestrial Ecosystems: Philadelphia, PA, Saunders, 429 p.

ALEXANDER, J., AND LEEDER, M.R., 1987, Active tectonic controls in alluvial architecture, *in* Ethridge, F.G., Flores, R.M., and Harvey, M.D., eds., Recent Developments in Fluvial Sedimentology: SEPM Special Publication No. 39, p. 243–252.

ALLEN, J.R.L., 1970, Studies in fluviatile sedimentation: A comparison of fining-upwards cyclothems, with special references to coarse-member composition and interpretation: Journal of Sedimentary Petrology, v. 40, p. 298–323.

ALONSO-ZARA, A.M., GENISE, J.F., AND VERDE, M., 2014, Paleoenvironments and ichnotaxonomy of insect trace fossils in continental mudflat deposits of the Miocene Calatayud-Daroca Basin, Zaragoza, Spain: Palaeogeography, Palaeoclimatology, and Palaeoecology, v. 414, p. 342–351.

AMIT, R., ENZEL, Y., GRODEK, T., CROUVI, O., PORAT, N., AND AYALON, A., 2010, The role of rare rainstorms in the formation of calcic soil horizons on alluvial surfaces in extreme deserts: Quaternary Research, v. 74, p. 177–187.

ARENAS, C., CABRERA, L., AND RAMOS, E., 2007, Sedimentology of tufa facies and continental microbialites from the Paleogene of Mallorca Island (Spain): Sedimentary Geology, v. 197, p. 1–27.

ASH, S.R., 1975, The Chinle (Upper Triassic) flora of southeastern Utah: Four Corners Geological Society Guidebook, 8th Field Conference, Canyonlands, p. 143–148.

ASH, S.R., 1987, The Upper Triassic Red Bed Flora of the Colorado Plateau, western United States: Journal of the Arizona–Nevada Academy of Science, v. 22, p. 95–105.

Ash, S.R., and Hasiotis, S.T., 2013, New occurrences of the controversial Late Triassic plant fossil *Sanmiguelia* BROWN and associated ichnofossils in the Chile Formation of Arizona and Utah, USA: N. Jb. Geol. Palaont. Abh., v. 268, p. 65–82.

ATCHLEY, S.C., NORDT, L.C., DWORKIN, S.I., RAMEZANI, J., PARKER, W.G., ASH, S.R., AND BOWRING, S.A., 2013, A linkage among Pangean tectonism, cyclic alluviation, climate change, and biologic turnover in the Late Triassic: The record from the Chinle Formation, southwestern United States: Journal of Sedimentary Research, v. 83, p. 1147–1161.

BAZARD, D.R., AND BUTLER, R.F., 1991, Paleomagnetism of the Chinle and Kayenta Formations, New Mexico and Arizona: Journal of Geophysical Research, v. 96, p. 9847–9871.

BEERBOWER, J. R., 1964, Cyclothems and cyclic depositional mechanisms in alluvial plain sedimentation, *in* D. F. Merriam, ed., Symposium on Cyclic Sedimentation: State Geological Survey of Kansas Bulletin, v. 2, p. 31–42.

BECKER, J., HILGEN, F.J., LOURENS, L.J., KOUWENHOVEN, T., AND VAN DER LAAN, E., 2005, Late Pliocene climate variability on Milankovitch to millennial time scales: High-resolution study of MIS100 from the Mediterranean: Palaeogeography, Palaeoclimatology, Palaeoecology, v. 228, p. 338–360.

BIRKELAND, P.W., 1999, Soils and Geomorphology, Third Edition: New York, NY, Oxford University Press, 430 p.

BLAKEY, R.C., 1989, Triassic and Jurassic geology of the southern Colorado Plateau, *in* Jenny, J.P., and Reynolds, S.J., eds., Geologic Evolution of Arizona: Tucson, Arizona Geological Society Digest 17, p. 369–396.

BLAKEY, R.C., AND GUBITOSA, R., 1983, Late Triassic paleogeography and depositional history of the Chinle Fm, southern Utah and northern Arizona, *in* Reynolds, M. W., and Dolly, E. D., eds., Mesozoic paleogeography of the west-central United States: Rocky Mountain Sec., Soc. Econ. Paleontologists, Mineralogists, Rocky Mountain Paleogeography Symposium 2, p. 57–76.

BLAKEY, R.C., AND GUBITOSA, R., 1984, Controls of sandstone body geometry and architecture in the Chinle Formation (Upper Triassic), Colorado Plateau: Sedimentary Geology, v. 38, p. 51–86.

BOND, G., BROECKER, W., JOHNSON, S., MCMANUS, J., LABEYRIE, L., JOUZEL, J., AND BONANI, G., 1993, Correlations between climate records from North Atlantic sediments and Greenland Ice: Nature, v. 365, p. 143–147.

BOWN, T.M., AND KRAUS, M.J., 1987, Integration of channel and floodplain suites, I. Developmental sequence and lateral relations of alluvial paleosols: Journal of Sedimentary Petrology, v. 57, p. 587–601.

BOWN, T.M., AND KRAUS, M.J., 1993a, Time-stratigraphic reconstruction and integration of paleopedologic, sedimentologic, and biotic events (Willwood Formation, Lower Eocene, northwest Wyoming, U.S.A.): PALAIOS, v. 8, p. 66–80.

BOWN, T.M., AND KRAUS, M.J., 1993b, Soils, time, and primate paleoenvironments: Evolutionary Anthropology, v. 2, p. 11–21.

BREWER, R., 1976, Fabric and Mineral Analysis of Soils, Third Edition: New York, New York, Kreiger, 470 p.

BRIDGE, J.S., 1984, Large-scale facies sequences in alluvial overbank environments: Journal of Sedimentary Petrology, v. 54, p. 583–588.

BRIDGE, J.S., AND LEEDER, M.R., 1979, A simulation model of alluvial stratigraphy: Sedimentology, v. 26, p. 617–644.

BROMELY, R.G., 1996, Trace Fossils: Biology, Taphonomy, and Applications, Second Edition: Special Topics in Paleontology: London, UK, Chapman and Hall, no. 3, 361 p.

BROMLEY, R.G., AND ASGAARD, U., 1979, Triassic freshwater ichnocoenoses from Carlsberg Fjord, east Greenland: Palaeogeography, Palaeoclimatology, Palaeoecology, v. 28, p. 39–80.

CATER, F.W., 1970, Geology of the Salt Anticline Region in southwestern Colorado: Geological Survey Professional Paper 637, 80 p.

CECIL, C.B., 2003, The concept of autocyclic and allocyclic controls on sedimentation and stratigraphy, emphasizing the climatic variable, *in* Cecil, C.B., and Edgar, T.N., eds., Climate Controls on Stratigraphy: SEPM Special Publication No. 77, pp. 13–20.

CHAKRABORTY, A., HASIOTIS, S.T., GHOSH, B., AND BHATTACHARYA, H.N., 2013, Fluvial trace fossils in the Middle Siwalik (Sarmation-Pontian) of Darjeeling Himalayas, India: Journal of Earth System Science, v. 122, p. 1023–1033.

CLEVELAND, D.M., ATCHLEY, S.C., AND NORDT, L.C., 2007, Continental sequence stratigraphy of the Upper Triassic (Norian-Rhatien) Chinle strata, northern New Mexico, USA: Allocyclic and autocyclic origins of paleosols-bearing alluvial successions: Journal of Sedimentary Research, v. 77, p. 909–924.

CLEVELAND, D.M., NORDT, L.C., AND ATCHLEY, S.C., 2008a, Paleosols, trace fossils, and precipitation estimates of the Uppermost Triassic strata in northern New Mexico: Palaeogeography, Palaeoclimatology, Palaeoecology, v. 257, p. 421–444.

CLEVELAND, D.M., NORDT, L.C., ATCHLEY, S.C., AND DWORKIN, S., 2008b, Pedogenic carbonate isotopes as evidence for extreme climate events preceding the Triassic-Jurassic boundary: Implications for the biotic crisis?: Geological Society of America Bulletin, v. 120, p. 1408–1415.

COLBERT, E.H., 1974, Triassic Paleontology of Ghost Ranch: New Mexico Geological Society Guidebook, 25th Field Conference, Ghost Ranch (Central-Northern N.M.) p. 175–178.

COLLINSON, J.D., 1986, Chapter 3: Alluvial Sediments, *in* Reading, H.G., ed., Sedimentary Environments and Facies, Second Edition: Blackwell Scientific Publications, p. 20–62.

COMPTON, R.R., 1985, Geology in the Field: New York, New York, John Wiley and Sons, Inc., 398 p.

COUNTS, J.W., AND HASIOTIS, S.T., 2009, Neoichnological experiments with masked chafer beetles (Coleoptera: Scarabaeidae): Implications for backfilled continental trace fossils: PALAIOS, v. 24, p. 74–91.

COUNTS, J.W., AND HASIOTIS, S.T., 2014, Distribution, paleoenvironmental implications, and stratigraphic architecture of paleosols in Lower Permian continental deposits of western Kansas, U.S.A.: Journal of Sedimentary Research, v. 84, p. 144–167.

DICKINSON, W.R., 1981, Plate Tectonic evolution of the southern Cordillera, *in* Dickinson, W. R., and Payne, W. D., eds., Relations of Tectonics to Ore Deposits in the Southern Cordillera: Arizona Geological Society, Digest v. 14, p. 113–135.

DICKINSON, W.R., AND GEHRELS, G.E., 2008, U-Pb ages of detrital zircons in relation to paleogeography: Triassic paleodrainage networks and sediment dispersal across southwest Laurentia: Journal of Sedimentary Research, v. 78, p. 745–764.

DRIESE, S.G., AND FOREMAN J.L., 1992, Paleopedology and paleoclimatic implications of Late Ordovician vertic paleosols, Juniata Formation, southern Appalachians: Journal of Sedimentary Petrology, v. 62, p. 71–83.

DRIESE, S.G., AND MORA, C.I., 1993, Physico-chemical environment of pedogenic carbonate formation in Devonian vertic paleosols, central Appalachians, USA: Sedimentology, v. 40, p. 199–216.

DRIESE, S.G., AND MORA, C.I., 2002, Paleopedology and stable isotope geochemistry of Late Triassic (Carnian-Norian) paleosols, Durham Sub-basin, North Carolina, U.S.A.: Implications for paleoclimate and paleoatmospheric PCO_2: SEPM Special Publication No. 73, p. 207–218.

DRIESE, S.G., SIMPSON E.L., AND ERIKSSON, K.A., 1995, Redoximorphic paleosols in alluvial and lacustrine deposits, 1.8 GA Lochness Formation, Mount Isa, Australia: Pedogenic processes and implications for paleoclimate: Journal of Sedimentary Research, v. A65, p. 675–689.

DUBIEL, R.F., 1983, Sedimentology of the lower part of the Upper Triassic Chinle Formation and its relationship to uranium deposits, White Canyon area, southeastern Utah: U.S. Geological Survey Open-File Report No. 83–459, 48 p.

DUBIEL, R.F., 1987, Sedimentology of the Upper Triassic Chinle Fm, southeastern Utah – Paleoclimatic implications, *in* Morales, M., and Elliott, D. K., eds., Triassic Continental Deposits of the American Southwest: Journal of the Arizona-Nevada Academy of Science, v. 22, p. 35–45.

DUBIEL, R.F., 1989, Depositional and climatic setting of the Upper Triassic Chinle Fm, Colorado Plateau, *in* Lucas, S. G., and Hunt, A. P., eds., Dawn of the Age of Dinosaurs in the American Southwest: New Mexico Museum of Natural History, 1989 Spring Field Conference Guidebook, p. 171–187.

DUBIEL, R.F., 1992, Sedimentology and depositional history of the Upper Triassic Chinle Formation in the Uinta, Piceance, and Eagle Basins, northwestern Colorado and northeastern Utah: U.S. Geological Survey Bulletin 1787-W, 25 p.

DUBIEL, R.F., 1994, Triassic deposystems, paleogeography, and paleoclimate of the Western Interior, *in* Caputo, M.V., Peterson, J.A., and Franczyk, K.J., eds., Mesozoic Systems of the Rocky Mountain Region, USA: Denver, SEPM (Society for Sedimentary Geology), Rocky Mountain Section, p. 133–168.

DUBIEL, R.F., BLODGETT, R.H., AND BOWN, T.M., 1987, Lungfish burrows in the Upper Triassic Chinle and Dolores Formations, Colorado Plateau: Journal of Sedimentary Petrology, v. 57, p. 512–521.

DUBIEL, R.F., AND HASIOTIS, S.T., 2011, Deposystems, paleosols, and climatic variability in a continental system: The Upper Triassic Chinle Fm, Colorado Plateau, USA: SEPM Special Publication No. 97, p. 393–421.

DUBIEL, R.F., PARRISH, J.T., PARRISH, J.M., AND GOOD, S.C., 1991, The Pangaean megamonsoon – Evidence from the Upper Triassic Chinle Fm, Colorado Plateau: PALAIOS, v. 6, p. 347–370.

DUBIEL, R.F., SKIPP, G., AND HASIOTIS, S.T., 1992, Continental depositional environments and tropical paleosols in the Upper Triassic Chinle Fm, Eagle Basin, western Colorado, *in* Flores, R.M., ed., SEPM Mid-Year Meeting on the Mesozoic of the Western Interior, Fieldtrip Guidebook, p. 21–37.

FREY, R.W., PEMBERTON, S.G., AND FAGERSTROM, J.A., 1984, Morphological, ethological, and environmental significance of the ichnogenera *Scoyenia* and *Ancorichnus*: Journal of Paleontology, v. 58, p. 511–528.

GASTON, R., LOCKLEY, M.G., LUCAS, S.G., AND HUNT, A.P., 2003, *Grallator*–dominated fossil footprint assemblages and associated enigmatic footprints from the Chinle Group (Upper Triassic), Gateway area, Colorado: Ichnos, v. 10, p. 153–163.

GILE, L.H., PETERSON, F.F., AND GROSSMAN, R.B., 1966, Morphological and genetic sequences of carbonate accumulation in desert soils: Soil Science, v. 101, p. 347–360.

GILLETTE, L., PEMBERTON, S.G., AND SARJEANT, W., 2003, A Late Triassic invertebrate ichnofauna from Ghost Ranch, New Mexico: Ichnos, v. 10, p. 141–151.

HARRIS, J.D., AND DOWNS, A., 2002, A drepanosaurid pectoral girdle from the Ghost Ranch (Whitaker) *Coelophysis* quarry (Chile Group, Rock Point Formation, Rhaetian), New Mexico: Journal of Vertebrate Paleontology, v. 22, p. 70–75.

HASIOTIS, S.T., 1995, Crayfish fossils and burrows from the Upper Triassic Chinle Formation, Canyonlands National Park, Utah, *in* Santucci, V.L., and McClelland, L., eds., National Park Service Paleontological Research, Technical Report NPS/NRPO/NRTR-95/16, p. 49–53.

HASIOTIS, S.T., 2000, The invertebrate invasion and evolution of Mesozoic soil ecosystems: the ichnofossil record of ecological innovations, *in* Gastaldo, R.A., and Dimichele, W.A., eds., Phanerozoic Terrestrial Ecosystems: Paleontological Society Short Course, v. 6, p. 141–169.

HASIOTIS, S.T., 2002, Continental Trace Fossils: SEPM, Short Course Notes Number 51, Tulsa, OK, 132 p.

HASIOTIS, S.T., 2003, Complex ichnofossils of solitary and social soil organisms: understanding their evolution and roles in terrestrial paleoecosystems: Palaeogeograpy, Palaeoclimatology, Palaeoecology, v. 192, p. 259–320.

HASIOTIS, S.T., 2004, Reconnaissance of Upper Jurassic Morrison Formation ichnofossils, Rocky Mountain Region, USA: paleoenvironmental, stratigraphic, and paleoclimatic significance of terrestrial and freshwater ichnocoenoses: Sedimentary Geology, v. 167, p. 177–268.

HASIOTIS, S.T., 2007, Continental ichnology: Fundamental processes and controls on trace fossil distribution, *in* Miller, W. III., ed., Trace Fossils—Concepts, Problems, Prospects, Elsevier Press, p. 268–284.

HASIOTIS, S.T., 2008, Reply to the Comments by Bromley et al. of the paper "Reconnaissance of the Upper Jurassic Morrison Formation ichnofossils, Rocky Mountain Region, USA: Paleoenvironmental, stratigraphic, and paleoclimatic significance of terrestrial and

freshwater ichnocoenoses" by Stephen T. Hasiotis: Sedimentary Geology, v. 208, p. 61–68.

HASIOTIS, S.T., AND BOWN, T.M., 1992, Invertebrate trace fossils: The backbone of continental ichnology, *in* Maples, C.G., and West, R.R., eds., Trace Fossils, Short Courses in Paleontology, Number 55: The Paleontological Society, p. 64–101.

HASIOTIS, S.T., AND DEMKO T.M., 1996, Terrestrial and freshwater trace fossils, Upper Jurassic Morrison Formation, Colorado Plateau, *in* Morales, M., ed., The Continental Jurassic: Museum of Northern Arizona Bulletin 60, p. 355–370.

HASIOTIS, S.T., AND DUBIEL, R.F., 1993a, Continental trace fossils of the Upper Triassic Chinle Formation, Petrified Forest National Park, Arizona, *in* Lucas, S.G., and Morales, M., eds., The Nonmarine Triassic: The New Mexico Museum of Natural History and Science Bulletin No. 3, p. 175–178.

HASIOTIS, S.T., AND DUBIEL, R.F., 1993b, Trace fossil assemblages in Chinle Formation alluvial deposits at the Tepees, Petrified Forest National Park, Arizona, *in* Lucas, S.G., and Morales, M., eds., The Nonmarine Triassic: The New Mexico Museum of Natural History and Science Bulletin No. 3, p. G42–43.

HASIOTIS, S.T., AND DUBIEL, R.F., 1994, Ichnofossil tiering in Triassic alluvial paleosols: Implications for Pangean continental rocks and paleoclimate, *in* Embry, A.F., Beauchamp, B., and Glass, D., eds., Carboniferous to Jurassic Pangea: Global Environments and Resources: Canadian Society of Petroleum Geologists, Memoir 17, p. 311–317.

HASIOTIS, S.T., AND DUBIEL, R.F., 1995a, Continental trace fossils, Petrified Forest National Park, Arizona: Tools for paleohydrologic and paleoecosystem reconstructions, *in*

Santucci, V.L., and McClelland, L., eds., National Park Service Paleontological Research, Technical Report NPS/NRPO/NRTR-95/16, p. 82–88.

HASIOTIS, S.T., AND DUBIEL, R.F., 1995b, Termite (Insecta: Isoptera) nest ichnofossils from the Triassic Chinle Formation, Petrified Forest National Park, Arizona: Ichnos, v. 4, p. 119–130.

HASIOTIS, S.T., AND HONEY, J.G., 2000, Paleohydrologic and stratigraphic significance of crayfish burrows in continental deposits: Examples from several Paleocene Laramide basins in the Rocky Mountains: Journal of Sedimentary Research, v. 70, p. 127–139.

HASIOTIS, S.T., KRAUS, M.J., AND DEMKO, T.M., 2007, Climatic controls on continental trace fossils, *in* Miller, W. III., ed., Trace Fossils—Concepts, Problems, Prospects, Elsevier Press, p. 172–195.

HASIOTIS, S.T., AND MARTIN, A.J., 1999, Probable reptile nests from the Upper Triassic Chinle Formation, Petrified Forest National Park, Arizona, *in* Santucci, V.L., and McClelland, L., eds., National Park Service Paleontological Research, Technical Report, NPS/NRGRD/GRDTR-99/03, p. 85–90.

HASIOTIS, S.T., AND MITCHELL, C.E., 1989, Lungfish burrows in the Upper Triassic Chinle and Dolores Formations, Colorado Plateau – Discussion: New evidence suggests origin by a burrowing decapod crustacean: Journal of Sedimentary Petrology, v. 59, p. 871–875.

HASIOTIS, S.T., AND MITCHELL, C.E., 1993, A comparison of crayfish burrow morphologies: Triassic and Holocene fossil, paleo- and neo-ichnological evidence, and the identification of their burrowing signatures: Ichnos, v. 2, p. 291–314.

HASIOTIS, S.T., MITCHELL, C.E., AND DUBIEL, R.F., 1993, Application of morphologic burrow interpretations to discern continental burrow architects: Lungfish or crayfish: Ichnos, v. 2, p. 315–333.

HASIOTIS, S.T., AND PLATT, B.F., 2012, Exploring the sedimentary, pedogenic, and hydrologic factors that control the occurrence and role of bioturbation in soil formation and horizonation in continental deposits: an integrative approach: The Sedimentary Record, v. 10, no. 3, p. 4–9.

HASIOTIS, S.T., PLATT, B.F., REILLY, M., AMOS, K., LANG, S., KENNEDY, D., TODD, D.A., AND MICHEL, E., 2012, Actualistic studies of the spatial and temporal distribution of terrestrial and aquatic organism traces in continental environments to differentiate lacustrine from fluvial, eolian, and marine deposits in the geologic record, *in* Baganz, O.W., Bartov, Y., Bohacs, K., and Nummedal, D., eds., Lacustrine sandstone reservoirs and hydrocarbon systems: AAPG Memoir 95, p. 433–489.

HASIOTIS, S.T., WELLNER, R.W., MARTIN, A.J., AND DEMKO, T.M., 2004, Vertebrate burrows from Triassic and Jurassic continental deposits in North America and Antarctica: Their paleoenvironmental and paleoecological significance: Ichnos, v. 11, p. 103–124.

HAZEL, J.E., JR., 1994, Sedimentary response to intrabasinal salt tectonism in the Upper Triassic Chinle Fm, Paradox Basin, Utah: U. S. Geological Survey Bulletin 2000-F, pp. 34.

HEMBREE, D.I., AND HASIOTIS, S.T., 2008, Miocene vertebrate and invertebrate burrows defining compound paleosols in the Pawnee Creek Formation, Colorado, U.S.A.: Palaeogeography, Palaeoclimatology, Palaeoecology, v. 270, p. 349–365.

IRMAS, R.B., NESBITT, S.J., PADIAN, K., SMITH, N.D., TURNER, A.H., WOODY, D., AND DOWNS, A., 2007, A Late Triassic dinosauromorph assemblage from New Mexico and the rise of dinosaurs: Science, v. 317, p. 358–361.

JAGER, T.J., 1982, Soils of the Serengeti woodlands, Tanzania: Wageningen, Pudoc, 239 p.

JENNY, H., 1941, Factors of Soil Formation: A System of Quantitative Pedology: New York, McGraw-Hill, 281 p.

KLAPPA, C.F., 1980, Rhizoliths in terrestrial carbonates: classification, recognition, genesis and significance: Sedimentology, v. 27, p. 613–629.

KRAUS, M.J., 1987, Integration of channel and floodplain suites II. Vertical relations of alluvial paleosols: Journal of Sedimentary Petrology, v. 57, p. 602–612.

KRAUS, M.J., 1999, Paleosols in clastic sedimentary rocks: Their geologic applications: Earth Science Reviews, v. 47, p. 41–70.

KRAUS, M.J., 2002, Basin scale changes in floodplain paleosols: Implications for interpreting fluvial architecture: Journal of Sedimentary Research, v. 72, p. 500–509.

KRAUS, M.J., AND ASLAN, A., 1993, Eocene hydromorphic paleosols: Significance for interpreting ancient floodplain processes: Journal of Sedimentary Petrology, v. 63, p. 453–463.

KRAUS, M.J., AND HASIOTIS, S.T., 2006, Significance of different modes of rhizolith preservation to interpreting paleoenvironmental and paleohydrologic settings: Examples from Paleogene paleosols, Bighorn Basin, Wyoming, U.S.A.: Journal of Sedimentary Research, v. 76, p. 633–646.

KRAUS, M.J., AND MIDDLETON, L.T., 1987a, Dissected paleotopography and base-level changes in a Triassic fluvial system: Geology, v. 15, p. 18–21.

KRAUS, M.J., AND MIDDLETON, L.T., 1987b, Contrasting architecture of two alluvial suites in different structural settings *in* Ethridge, F.G., Flores, R.M., and Harvey, M.D., eds., Recent Developments in Fluvial Sedimentology: SEPM Special Publication No. 39, p. 253–262.

KRAUS, M.J., AND RIGGINS, S., 2007, Transient drying during the Paleocene-Eocene Thermal Maximum (PETM): Analysis of paleosols in the Bighorn Basin, Wyoming: Palaeogeography, Palaeoclimatology, and Palaeoecology, v. 245, p. 444-461.

LOOPE, D.B., STEINER, M.B., ROWE, C.M., AND LANCASTER, N., 2004, Tropical westerlies over Pangaean sand seas: Sedimentology, v. 51, p. 315–322.

LOUGHNEY, K.M., FASTOVSKY, D.E., AND PARKER, W.G., 2011, Vertebrate fossil preservation in blue paleosols from the Petrified Forest National Park, Arizona, with implications for vertebrate biostratigraphy in the Chinle Fm: Palaios, v. 26, p. 700–719.

LUCAS, S.G., HECKERT, A.B., ESTEP, J.W., AND ANDERSON, O.J., 1997, Stratigraphy of the Upper Triassic Chinle Group, Four Corners Region, *in* Anderson, O.J., Kues, B., and Lucas, S.G., eds., Mesozoic Geology and Paleontology of the Four Corners Region: New Mexico Geological Society, Guidebook, p. 81–108.

LUPE, R., 1977, Depositional environments as a guide to uranium mineralization in the Chinle Formation, San Rafael Swell, Utah: U.S Geological Survey Journal of Research 5, p. 665–372.

LYDOLPH, P.E., 1985, The Climate of Earth: Totowa, NJ, Rowman and Allanheld Publishers, 386 p.

MACHETTE, M.N., 1985, Calcic soils of the southwestern United States: Geological Society of America Special Paper, v. 203, p. 1–21.

MACK, G.H., JAMES, W.C., AND MONGER, H.C., 1993, Classification of paleosols: Geological Society of America Bulletin, v. 105, p. 129–136.

MARTIN, A.J., AND HASIOTIS, S.T., 1998, Vertebrate tracks and their significance in the Chinle Formation (Late Triassic) Petrified Forest National Park, Arizona, *in* Santucci, V.L., and McClelland, L., eds., National Park Service Paleontological Research, Technical Report NPS/NRGRD/GRDTR-98/01, p. 138–143.

MIALL, A.D., 1996, The Geology of Fluvial Deposits: Sedimentary Facies, Basin Analysis, and Petroleum Geology: Berlin, Springer-Verlag, 582 p.

MOORE, D.M., AND REYNOLDS, R.C., 1997, X-Ray Diffraction and the Identification and Analysis of Clay Minerals, Second Edition: New York, New York, Oxford University Press, 378 p.

MUNSELL®, 2009, Soil Color Book, Revised Edition.

NORDT, L., ATCHLEY, S., AND DWORKIN, S., 2015, Collapse of the Late Triassic megamonsoon in western equatorial Pangea, present-day American southwest: Geological Society of America Bulletin, B31186–1.

OLIVER, J.E., 1973, Climate and Man's Environment: An Introduction to Applied Climatology: New York, NY, Wiley, 517 p.

OLSEN, P.E., 1997, Stratigraphic record of the Early Mesozoic breakup of Pangea in the Laurasia-Gondwana rift system: Annu. Rev. Earth Planet. Sci., v. 25, p. 337–401.

OLSEN, P.E., AND KENT, D.V., 1996, Milankovitch climate forcing in the tropics of Pangea during the Late Triassic: Palaeogeography, Palaeoclimatology, and Palaeoecology, v. 122, p. 1–26.

OLSEN, P.E., AND KENT, D.V., 1999, Long-period Milankovitch cycles from the Late Triassic and Early Jurassic of eastern North America and their implications for the calibration of the Early Mesozoic time-scale and the long-term behaviour of the plants: Phil. Trans. R. Soc. Lond., v. 357, p. 1761–1786.

OLSEN, P.E., KENT, D.V., CORNET, B., WITTE, W.K., AND SCHLISCHE, R.W., 1996, High-resolution stratigraphy of the Newark rift basin (early Mesozoic, eastern North America): GSA Bulletin, v. 108, p. 40–77.

PARCERISA, D., GOMEZ-GRAS, D., AND MARTIN-MARTIN, J.D., 2006, Calcretes, oncolites, and lacustrine limestones in Upper Oligocene alluvial fans of the Montgat area (Catalan Coastal Ranges, Spain), *in* Alonso-Zarza, A.M., and Tanner, L.H., eds., Paleoenvironmental Record and Applications of Calcretes and Palustrine Carbonates: Geological Society of America Special Paper 416, p. 105–118.

PARKER, W.G., AND IRMIS, R.B., 2006, A new species of the Late Triassic phytosaur *Pseudopalatus* (Archosauria: Pseudosuchia) from Petrified Forest National Park, Arizona, *in* Parker, W.G., Ash, S.R., and Irmis, R.B., eds., A Century of Research at Petrified Forest National Park: Geology and Paleontology: Museum of Northern Arizona Bulletin No. 62, p. 126–143.

PARRISH, J.T., AND PETERSON, F., 1988, Wind directions predicted from global circulation models and wind directions determined from eolian sandstones of the western United States – A comparison: Sedimentary Geology, v. 56, p. 261–282.

PIPIRINGOS, G.N., AND O'SULLIVAN, R.B., 1978, Principle unconformities in Triassic and Jurassic rocks, Western Interior United States–A preliminary study: Geological Survey Professional Paper 1035-A, 29 p.

PROCHNOW, S.J., NORDT, L.C., ATCHLEY, S.C., HUDEC, M., AND BOUCHER, T.E., 2005, Triassic paleosol catenas associated with a salt-withdrawal minibasin in southeastern Utah, U.S.A.: Rocky Mountain Geology, v. 40, p. 25–49.

PROCHNOW, S.J., NORDT, L.C., ATCHLEY, S.C., AND HUDEC, M.R., 2006a, Multi-proxy paleosol evidence for Middle and Late Triassic climate trends in eastern Utah: Palaeogeography, Palaeoclimatology, and Palaeoecology, v. 232, p. 53–72.

PROCHNOW, S.J., ATCHLEY, S.C., BOUCHER, T.E., NORDT, L.C., AND HUDECS, M.R., 2006b, The influence of salt withdrawal subsidence on paleosol maturity and cyclic fluvial deposition in the Upper Triassic Chinle Formation, Castle Valley, Utah: Sedimentology, v. 53, p. 1319–1345.

REPENNING, C.A., COOLEY, M.E., AND AKERS, J.P., 1969, Stratigraphy of the Chinle and Moenkopi Formations, Navajo and Hopi Indian Reservations Arizona, New Mexico, and Utah: Geological Survey Professional Paper 521-B, 34 p.

RETALLACK, G.J., 1988, Field recognition of paleosols, *in* Reinhardt, J., and Sigleol, W.R., eds., Paleosols and weathering through geologic time: principles and applications: Geological Society of America Special Papers, vol. 216, p. 1–20.

RETALLACK, G.J., 2001, Soils of the Past: An Introduction to Paleopedology, Second Edition: Oxford, U.K., Blackwell Science, 404 p.

RIGGS, N.R., LEHMAN, T.M., GEHRELS, G.E., AND DICKINSON, W.R., 1996, Detrital zircon link between headwaters and terminus of the Upper Triassic Chinle-Dockum paleoriver system: Science, v. 273, p. 97–100.

RINDSBERG, A.K., AND KOPASKA-MERKEL, D.C., 2005, *Treptichnus* and *Arenicolites* from the Steven C. Minkin Paleozoic Footprint Site (Langsettian, Alabama, USA), *in* Buta, R.J.,

Rindsberg, A.K., and Kopaska-Merkel, D.C., eds., Pennsylvanian Footprints in the Black Warrior Basin of Alabama: Alabama Paleontological Society Monograph no. 1, p. 121–141.

ROSELL, J., AND OBRADOR, A., 1982, Oncolites from lacustrine sediments in the Cretaceous of north-eastern Spain: Sedimentology, v. 29, p. 433–436.

ROWE, C.M., LOOPE, D.B., OGLESBY, R.J., VAN DER VOO, R., AND BROADWATER, C.E., 2007, Inconsistencies between Pangean reconstructions and basic climate controls: Science, v. 318, p. 1284–1286.

SCHWARTZ, H.L., AND GILLETTE, D.D., 1994, Geology and taphonomy of the *Coelophysis* quarry, Upper Triassic Chinle Formation, Ghost Ranch, New Mexico: Journal of Paleontology, v. 68, p. 1118–1130.

SHANKAR, N., AND ACHYUTHAN, H., 2007, Genesis of calcic and petrocalcic horizons from Coimbatore, Tamil Nadu: Micromorphology and geochemical studies: Quaternary International, v. 175, p. 140–154.

SHRIVASTAVA, P., BHATTACHARYYA, T., AND PAL, D.K., 2002, Significance of the formation of calcium carbonate minerals in the pedogenesis and management of cracking clay soils (Vertisols) of India: Clays and Clay Minerals, v. 50, p. 111–126.

SINCLAIR, A.R.E., MDUMA, S.A.R., HOPCRAFT, J.G.C., FRYXELL, J.M., HILBORN, R., AND THIRGOOD, S., 2007, Long-term ecosystem dynamics in the Serengeti: Lessons for conservation: Conservation Biology, v. 21, p. 580–590.

SLINGERLAND, R., AND SMITH, N.D., 2004, River avulsions and their deposits: Annu. Rev. Earth Planet. Sci., v. 32, p. 257–285.

SMITH, J.J., HASIOTIS, S.T., KRAUS, M.J., AND WOODY, D.T., 2008b, Relationship of floodplain ichnocoenoses to paleopedology, paleohydrology, and paleoclimate in the Willwood Formation, Wyoming, during the Paleocene-Eocene Thermal Maximum: PALAIOS, v. 23, p. 683–699.

SMITH, N.D., CROSS, T.A., DUFFICY, J.P., AND CLOUGH, S.R., 1989, Anatomy of an avulsion: Sedimentology, v. 36, p. 1–23.

SOIL SURVEY STAFF, 2014, Keys to soil taxonomy, Twelfth Edition: USDA-National Resources Conservation Service, Washington D.C., 360 p.

STEENBRINK, J., KLOOSTERBOER-VAN HOEVE, M.L., AND HILGEN, F.J., 2003, Millennial scale climate variations recorded in early Pliocene colour reflectance time series from the lacustrine Ptolemais Basin (NW Greece): Global and Planetary Change, v. 36, p. 47–75.

STEINER, M.B., AND LUCAS, S.G., 2000, Paleomagnetism of the Late Triassic Petrified Forest Formation, Chinle Group, western United States: Further evidence of 'large' rotation of the Colorado Plateau: Journal of Geophysical Research, ser. B, Solid Earth and Planets, v. 105, p. 25,791–25,808.

STEWART, J.H., ANDERSON, T.H., HAXEL, G.B., SILVER, L.T., AND WRIGHT, J.E., 1986, Late Triassic paleogeography of the southern Cordillera: The problem of a source for voluminous volcanic detritus in the Chinle Fm of the Colorado Plateau region: Geology, v. 14, p. 567–570.

STEWART, J.H., POOLE, F.G., AND WILSON, R.F., 1972, Stratigraphy and origin of the Chinle Fm and related Upper Triassic strata in the Colorado Plateau region. U. S.: Geological Survey Professional Paper 690, 336 p.

STILES, C.A., MORA, C.I., AND DRIESE, S.G., 2001, Pedogenic iron-manganese nodules in Vertisols: A new proxy for paleoprecipitation?: Geology, v. 29, p. 943–946.

STOCKER, M.R., 2012, A new phytosaur (Archosauriformes, Phytosauria) from the Lot's Wife Beds (Sonsela Mbr) within the Chinle Formation (Upper Triassic) of Petrified Forest National Park, Arizona: Journal of Vertebrate Paleontology, v. 32, p. 573–586.

TANNER, L.H., 2000, Palustrine–lacustrine and alluvial facies of the (Norian) Owl Rock Formation (Chinle Group), Four Corners region, southwestern U.S.A: Implications for Late Triassic paleoclimate: Journal of Sedimentary Research, v. 70, p. 1280–1289.

TANNER, L.H., AND LUCAS, S.G., 2006, Calcareous paleosols of the Upper Triassic Chinle Group, Four Corners region, southwestern United States: Climatic implications, *in* Alonso-Zarza, A.M., and Tanner, L.H., eds., Paleoenvironmental Record and Applications of Calcretes and Palustrine Carbonates: Geological Society of America Special Paper 416, p. 53–74.

TELLER, J.T., AND LAST, W.M., 1990, Paleohydrological indicators in playas and salt lakes, with examples from Canada, Australia, and Africa: Palaeogeography, Palaeoclimatology, Palaeoecology, v. 76, p. 215–240.

THERRIEN, F., AND FASTOVSKY, D.E., 2000, Paleoenvironments of early theropods, Chinle Fm (Late Triassic), Petrified Forest National Park, Arizona: PALAIOS, v. 15, p. 194–211.

TRENDELL, A.M., ATCHLEY, S.C., AND NORDT, L.C., 2012, Depositional and diagenetic controls on reservoir attributes within a fluvial outcrop analog: Upper Triassic Sonsela Mbr of the Chinle Fm, Petrified Forest National Park, Arizona: AAPG Bulletin, v. 96, p. 679–707.

TRENDELL, A.M., ATCHLEY, S.C., AND NORDT, L.C., 2013a, Facies analysis of a probable large-fluvial-fan depositional system: The Upper Triassic Chinle Fm at Petrified Forest National Park, Arizona, U.S.A.: Journal of Sedimentary Research, v. 83, p. 873–895.

TRENDELL, A.M., NORDT, L.C., ATCHLEY, S.C., LEBLANC, S.L., AND DWORKIN, S.I., 2013b, Determining floodplain plant distributions and populations using paleopedology and fossil root traces: Upper Triassic Sonsela Mbr of the Chinle Fm at Petrified Forest National Park, Arizona: PALAIOS, v. 28, p. 471–490.

TURNER, B.R., 1993, Paleosols in Permo-Triassic continental sediments from Prydz Bay, East Antarctica: Journal of Sedimentary Petrology, v. 63, p. 694–706.

VAN DER VOO, R., MAUK, F.J., AND FRENCH R.B., 1976, Permian-Triassic continental configurations and the origin of the Gulf of Mexico: Geology, v. 4, p. 177–180.

VAN DER KOLK, D.A., FLAIG, P.P., AND HASIOTIS, S.T., 2015, Paleoenvironmental reconstruction of a Late Cretaceous, muddy, river-dominated polar deltaic system: Schrader Bluff-Prince Creek Formation transition, Shivugak Bluffs, North Slope of Alaska, U.S.A: Journal of Sedimentary Research, v. 85, p. 903–936.

WOODY, D.T., 2006, Revised stratigraphy of the lower Chinle Formation (Upper Triassic) of Petrified Forest National Park, Arizona, *in* Parker, W.G., Ash, S.R., and Irmis, R.B., eds., A Century of Research at Petrified Forest National Park: Museum of Northern Arizona Bulletin No. 62, p. 17–45.

ZEIGLER, K.E., AND GEISSMAN, J.W., 2011, Magnetostratigraphy of the Upper Triassic Chinle Group of New Mexico: Implications for regional and global correlations among Upper Triassic sequences: Geosphere, v. 7, p. 802–829.

FIGURE CAPTIONS

Figure 1.—Paleogeography map and tectonic setting of the Western Interior during deposition of the Chinle Fm, along with major patterns of fluvial systems and sediment transport (modified from Dickinson 1983; Blakey and Gubitosa 1983; Blakey 1989; Dubiel 1989, 1994; Dubiel et al. 1991; Riggs et al. 1996; Dickinson and Gehrels 2008). Red star marks location of study area.

Figure 2.—Generalized stratigraphic column for the Chinle Fm in southeastern Utah, including major unconformities. Members outlined by red box are investigated in this study.

Figure 3.—Field location. **A)** Map of southeastern Utah showing field location (modified from Stewart et al. 1972). Red box shows location of B. **B)** Map of Stevens Canyon and Indian Creek Canyon and their relative position to Canyonlands National Park, Utah. White balloons mark measured sections: S1-Stick Section 1, S2-Stick Section 2, S3-Stick Section 3, S4-Stick Section 4, S5-Stick Section 5, S6-Stick Section 6, SW-Southwest Measured Section, W-West Measured Section, E-East Measured Section.

Figure 4.—Overall stratigraphy at Stevens and Indian Creek Canyon. **A)** S1 stratigraphic section location. **B)** West Measured Section. Chinle Fm members: Moss Back Member (MB), Petrified Forest Member (PFM), Owl Rock Member (ORM), Church Rock Member (CRM). The Chinle Fm is overlain by the Wingate Sandstone (Wg).

Figure 5.—Lithofacies of the Chinle Fm. Jacobs staff in 10 cm intervals. Grain size card 15 cm tall. Rock hammer 33 cm long. **A)** Massive to finely laminated mudstone (F-1). **B)** Massive siltstone (F-2a). **C)** Massive siltstone to very fine-grained sandstone (F-2b). **D**) Planar-laminated siltstone to very fine-grained sandstone (F-2c). **E)** Ripple cross-

laminated siltstone to very fine-grained sandstone (F-3). **F)** Massive fine- to very coarse-grained sandstone (F-4a).

Figure 6.—Lithofacies of the Chinle Fm, continued. Jacobs staff in 10 cm intervals. Rock hammer 33 cm long. **A)** Trough cross-stratified fine- to coarse-grained sandstone (F-4b). **B)** Planar-laminated fine- to coarse-grained sandstone (F-4c). **C)** Trough cross-stratified conglomerate (white arrow) (F-5a). **D**) Massive to planar-laminated conglomerate (F-5b). **E)** Incline-bedded conglomerate (F-5c). **F1)** Close up of incline-bedded conglomerate showing pebble-sized quartz and limestone clasts. **F2)** Large oncoid clast from the incline bedded conglomerate.

Figure 7.—Ichnofossils of the Chinle Fm. **A)** *Ancorichnus* (An), *Arenicolites* (Ar), and *Treptichnus* (Tr). **B)** Branching form of *Camborygma* (Ca). **C)** *Camborygma* (Ca) with a straight, cylindrical morphology. **D)** *Cylindrichum* (Cy). **E)** *Fictovichnus* (Fv). **F)** *Naktodemasis* (Nk).

Figure 8.—Ichnofossils of the Chinle Fm, continued. Grains size card 15 cm tall. **A)** *Planolites* (Pl). **B)** Tetrapod footprint (Rf). **C)** Rhizocretion (Rc). **D)** Rhizolith (Rh). **E)** Rhizotubule (Rt). **F)** *Scoyenia* (Sc).

Figure 9.—Ichnofossils of the Chinle Fm, continued. Rock hammer 33 cm long. **A)** *Skolithos* (Sk). **B)** *Steinichnus* (St). **C)** Therapsid burrow (Tb). **D)** Therapsid burrows (Tb).

Figure 10.—Distribution of lithofacies, facies associations, ichnofossils, pedogenic features, and paleosols in the Chinle Fm with estimated mean annual precipitation. Overall, precipitation decreases through time with shorter term wet-dry cyclicity observed in the Petrified Forest, lower Owl Rock, and middle Owl Rock mbrs.

Figure 11.—Shallowly Burrowed Entisol. **A)** Stacked AC and C horizons. **B)** *Steinichnus* (St) covering the bottom of bedding planes. **C)** Ichnopedofacies measured section.

Figure 12.—Rhizolith Entisol. Jacobs staff in 10 cm intervals. Grain size card 15 cm tall. **A)** AC horizons in outcrop with rhizohaloes (Rh). **B)** Rhizohaloes (Rh) in the basal AC horizon. **C)** Ichnopedofacies measured section.

Figure 13.—Camborygma Entisol. Jacobs staff in 10 cm intervals. **A)** 1.1 m deep *Camborygma* (Ca) penetrating stacked AC horizons. **B)** Close-up of *Camborygma* (Ca). Note the ripple-lamination still preserved around the burrow. **C)** Ichnopedofacies measured section.

Figure 14.—Naktodemasis-Camborygma Entisol. **A)** *Camborygma* (Ca) penetrating stacked AC horizons of ripple cross-laminated very fine-grained sandstone. **B)** *Naktodemasis* (Nk) and rhizoliths (Rh) along bedding planes. **C)** Close-up of *Camborygma* (Ca) burrow. **D)** Ichnopedofacies measured section.

Figure 15.—Rhizolith Inceptisol. Rock hammer 33 cm long. **A**) Green-grey rhizohalo (Rh) in A horizon. **B)** Paleosol profile in outcrop. **C)** Ichnopedofacies measured section.

Figure 16.—Naktodemasis Calcic Inceptisol. **A, B)** Profile of paleosol in outcrop. Paleosols form composite profiles consisting of cumulative horizons. **C)** *Naktodemasis* (Nk) bioturbation around a rhizohalo (Rh). **D)** Ichnopedofacies measured section.

Figure 17.—Camborygma Calcic Inceptisol. Jacobs staff in 10 cm intervals. **A)** Paleosol profile in outcrop. **B)** Close-up of *Camborygma* (Ca) in branching and nonbranching forms. **C)** Ichnopedofacies measured section.

Figure 18.—Therapsid Calcic Inceptisol. Jacobs staff in 10 cm intervals. **A)** Paleosol profile in outcrop. **B)** Close up of therapsid burrow (Tb) and rhizoliths (Rh). **C)** Ichnopedofacies measured section.

Figure 19.—Camborygma Vertisol. **A)** Paleosol profile in outcrop. **B)** Yellow rhizohaloes (Rh) penetrating an A horizon with prismatic peds. **C)** Close up of *Fictovichnus* (Fv) in the Bss horizon. **D)** *Camborygma* from the A horizon. **E)** Ichnopedofacies measured section.

Figure 20.—Naktodemasis Alfisol. Grains size card 15 cm tall. **A)** *Naktodemasis* (Nk) and rhizohaloes in the A horizon. **B, C)** Paleosol profile in outcrop. **D)** Ichnopedofacies measured section.

Figure 21.—Naktodemasis Calcic Alfisol. Jacobs staff in 10 cm intervals. **A)** Paleosol profile in outcrop. **B)** Ichnopedofacies measured section.

Figure 22.—Rhizolith Calcic Alfisol. Jacobs staff in 10 cm intervals. **A)** Btk horizon with numerous calcium carbonate nodules. Top of horizon cut off by overlying conglomerate. **B)** ABtk horizon with rhizotubules (Rt) lined by calcium carbonate nodules. **C)** Lower half of paleosol profile in outcrop. Note the sharp contrast between the calcium carbonate bearing Btk horizon and the underlying A horizon. **D)** Ichnopedofacies measured section.

Figure 23.—Ichnopedofacies depositional model for the Chinle Fm. Lateral distribution of ichnopedofacies on the alluvial plain. Cross section runs from A to A’ on the landscape block diagram and shows variations in physiochemical conditions along different positions on the alluvial plain. Water table marked by black triangle. Shallower burrows are located closer to the fluvial channel. Deeper burrows and calcium carbonate nodules are found on the distal floodplain.

Figure 24.—Correlated measured stratigraphic sections. Red boxes highlight Chinle Fm paleovalleys. Paleovalleys are cut into all members during base-level fall and filled during base-level rise. See Figure 3 for location of measured columns in study area.

Figure 25.—Composite stratigraphic column showing vertical distribution of ichnopedofacies in the Chinle Fm along with prominent sedimentary features.

TABLE CAPTIONS

Table 1.—Chinle Formation Lithofacies

Table 2.—Chinle Formation Ichnofossils

Table 3.—Chinle Formation Ichnocoenoses, traces listed in order of abundance

Table 4.—Chinle Formation Paleosols

Table 5.—Chinle Formation Facies Associations

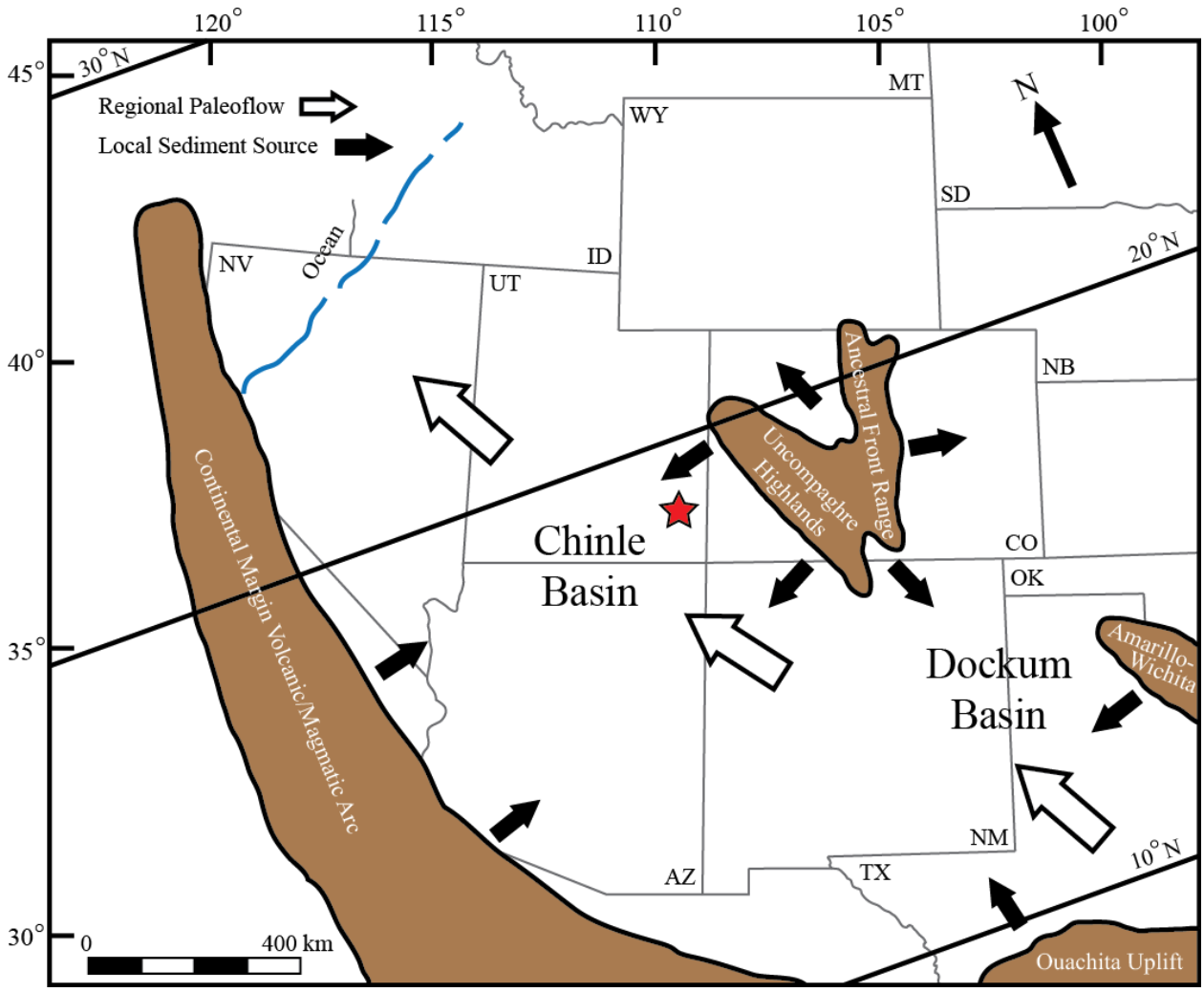
120°
115°
110°
105°
100°
45°
40°
35°
30°
30°N
20°N
10°N
Regional Paleoflow
Local Sediment Source
Ocean
NV
UT
ID
WY
MT
SD
NB
CO
OK
NM
AZ
TX
N
Continental Margin Volcanic/Magmatic Arc
Uncompaghre Highlands
Ancestral Front Range
Chinle Basin
Dockum Basin
Amarillo-Wichita
Ouachita Uplift
0
400 km

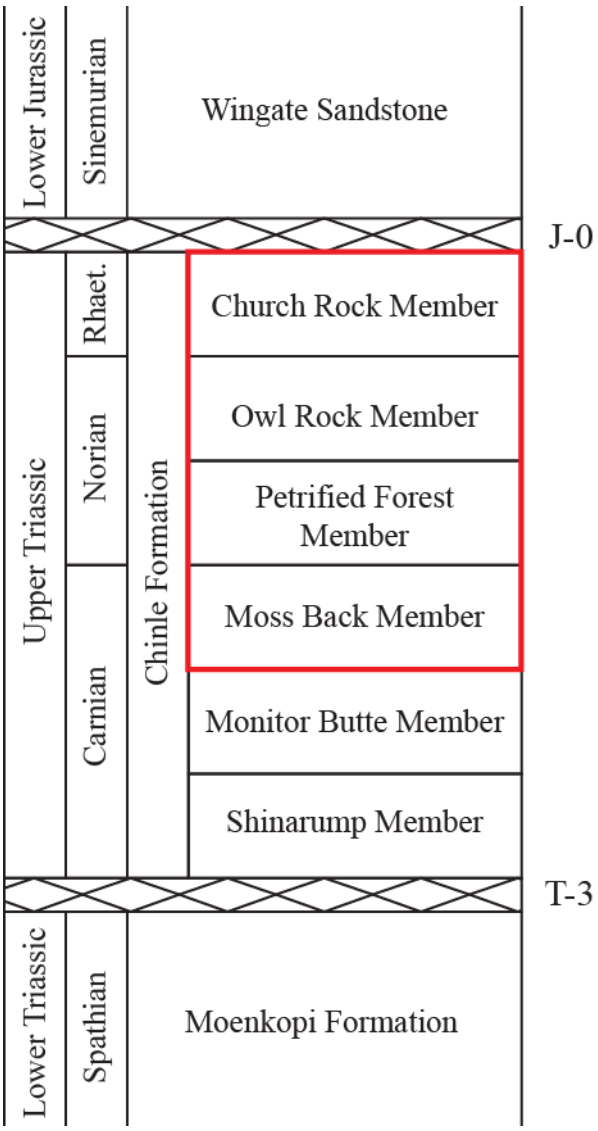
Lower Jurassic
Sinemurian
Wingate Sandstone
J-0
Upper Triassic
Rhaet.
Norian
Carnian
Chinle Formation
Church Rock Member
Owl Rock Member
Petrified Forest Member
Moss Back Member
Monitor Butte Member
Shinarump Member
T-3
Lower Triassic
Spathian
Moenkopi Formation

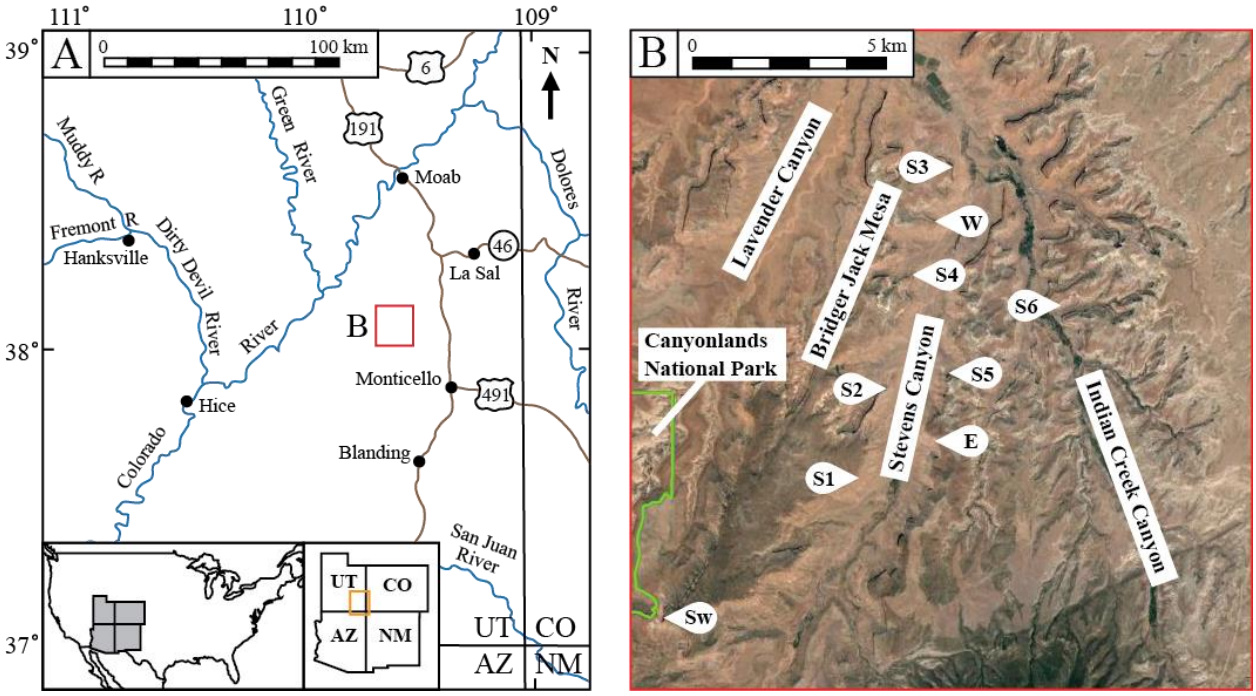
111°
110°
109°
39°
38°
37°
A
0
100 km
N
6
191
46
491
Moab
La Sal
Monticello
Blanding
Hice
Hanksville
Fremont R
Muddy R
Dirty Devil River
Green River
River
Colorado
Dolores
River
San Juan River
B
UT
CO
AZ
NM
UT
CO
AZ
NM
B
0
5 km
Lavender Canyon
Bridger Jack Mesa
Stevens Canyon
Indian Creek Canyon
Canyonlands National Park
S1
S2
S3
S4
S5
S6
W
E
Sw

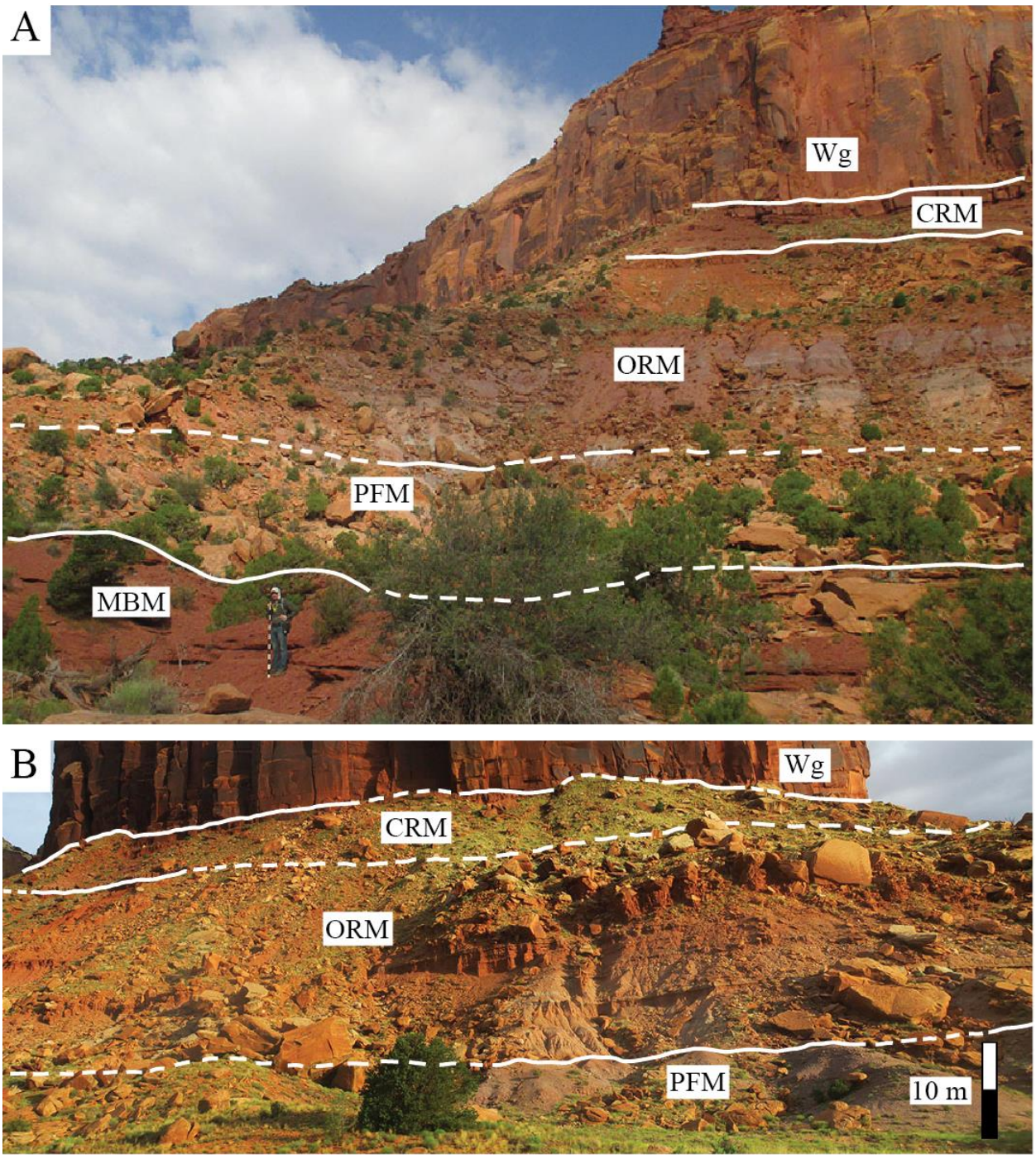
A
Wg
CRM
ORM
PFM
MBM
B
Wg
CRM
ORM
PFM
10 m

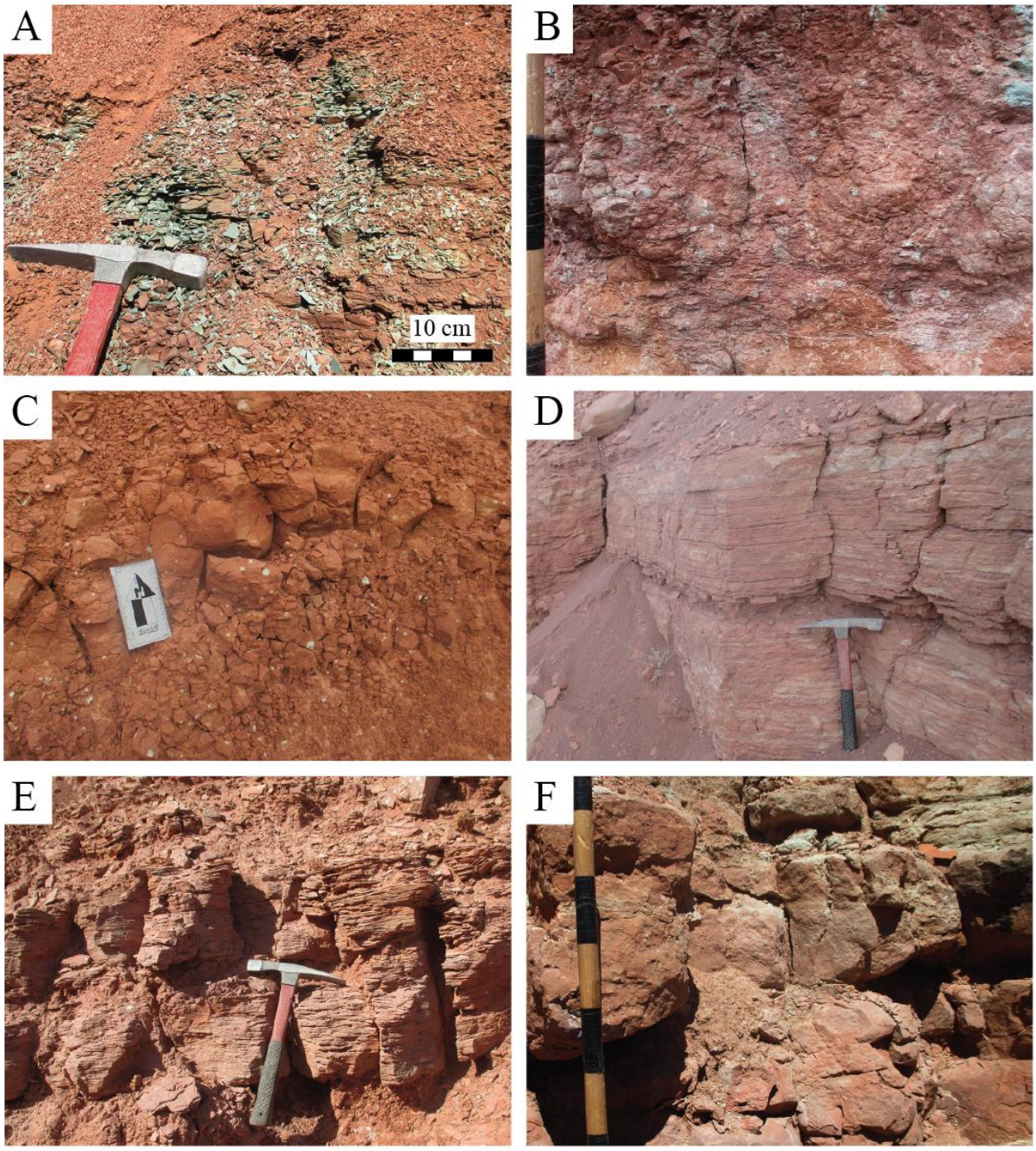
A
10 cm
B
C
D
E
F

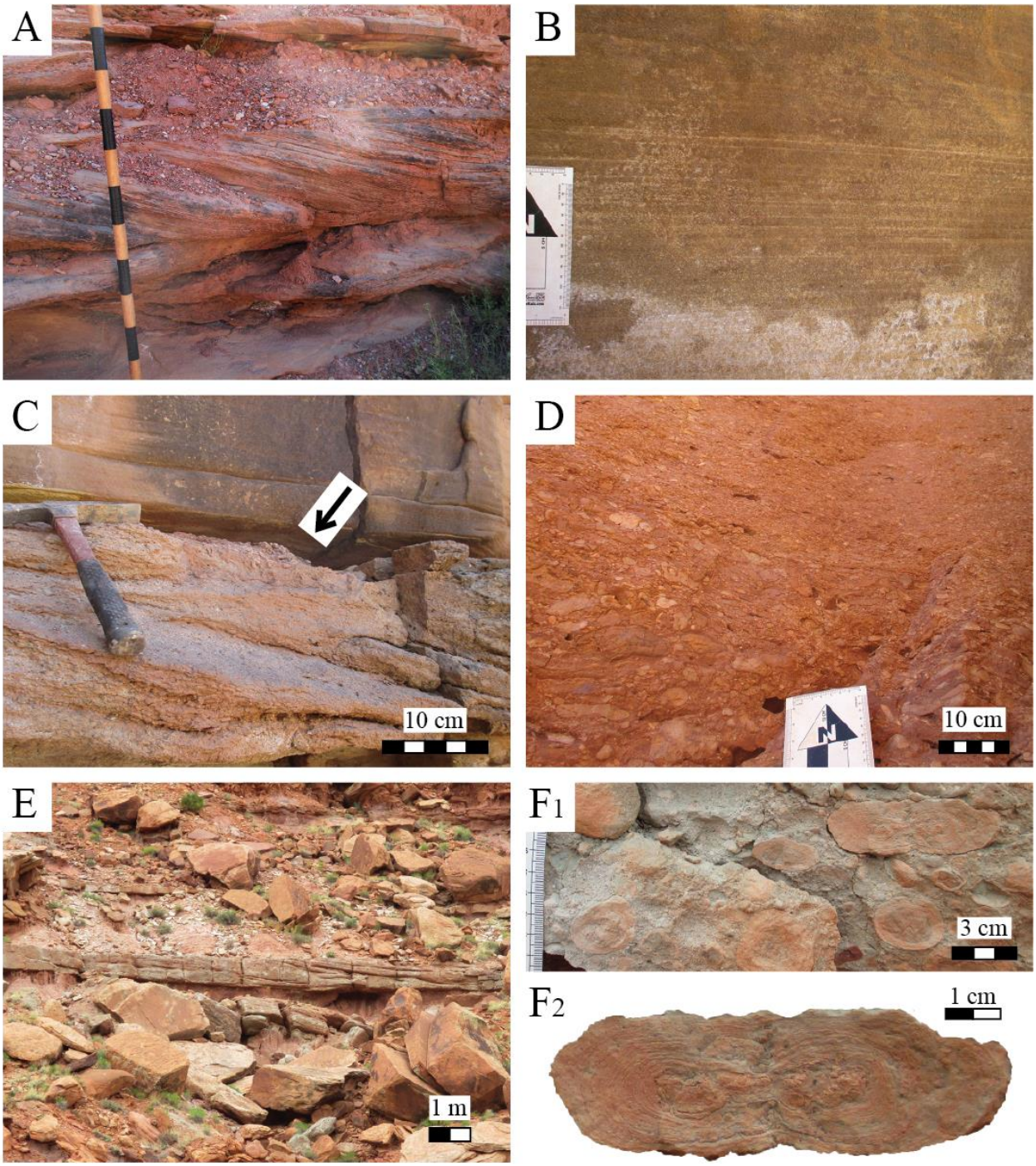
A
B
C
10 cm
D
10 cm
E
1 m
F1
3 cm
F2
1 cm

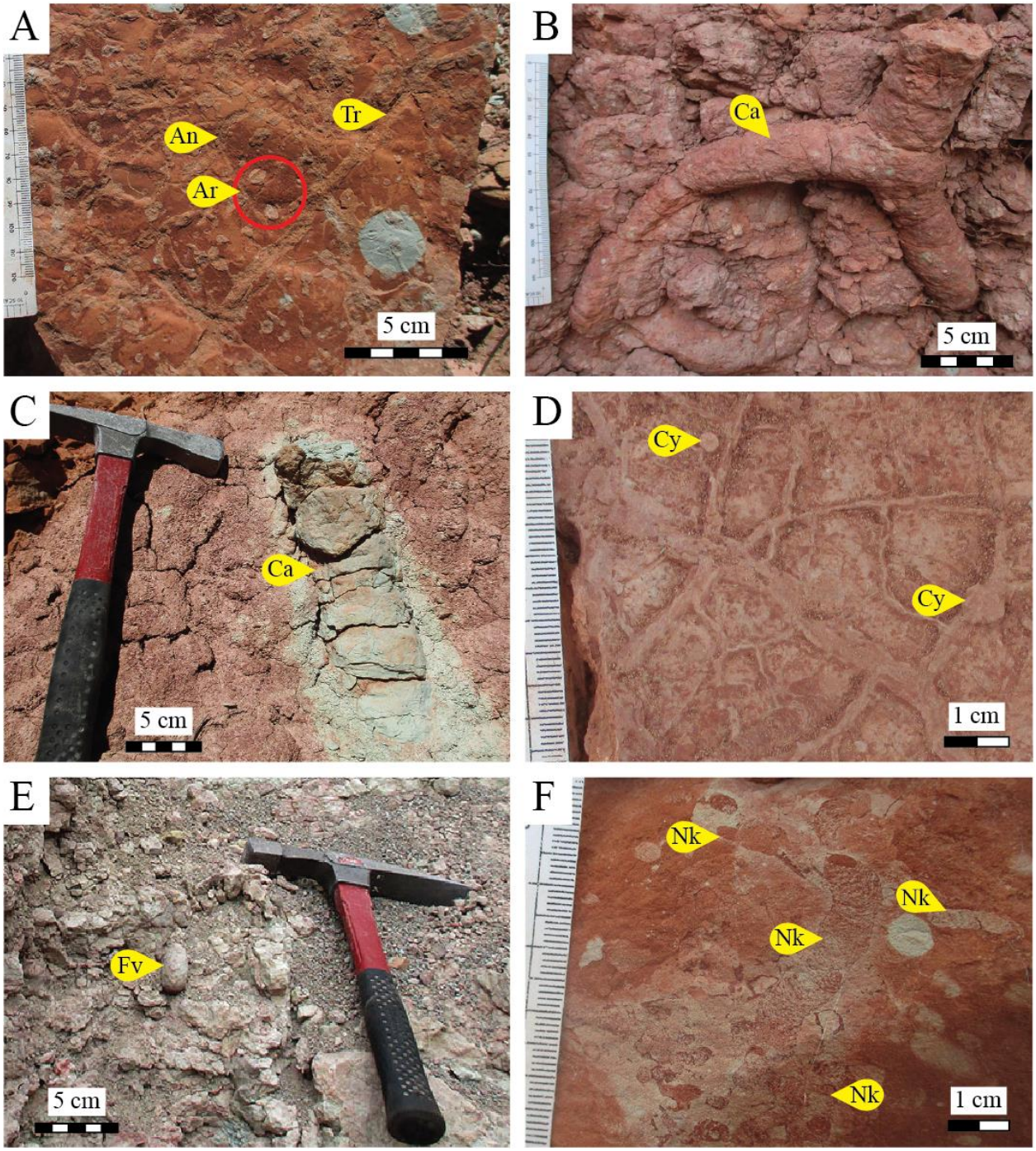
A
An
Tr
Ar
5 cm
B
Ca
5 cm
C
Ca
5 cm
D
Cy
Cy
1 cm
E
Fv
5 cm
F
Nk
Nk
Nk
Nk
1 cm

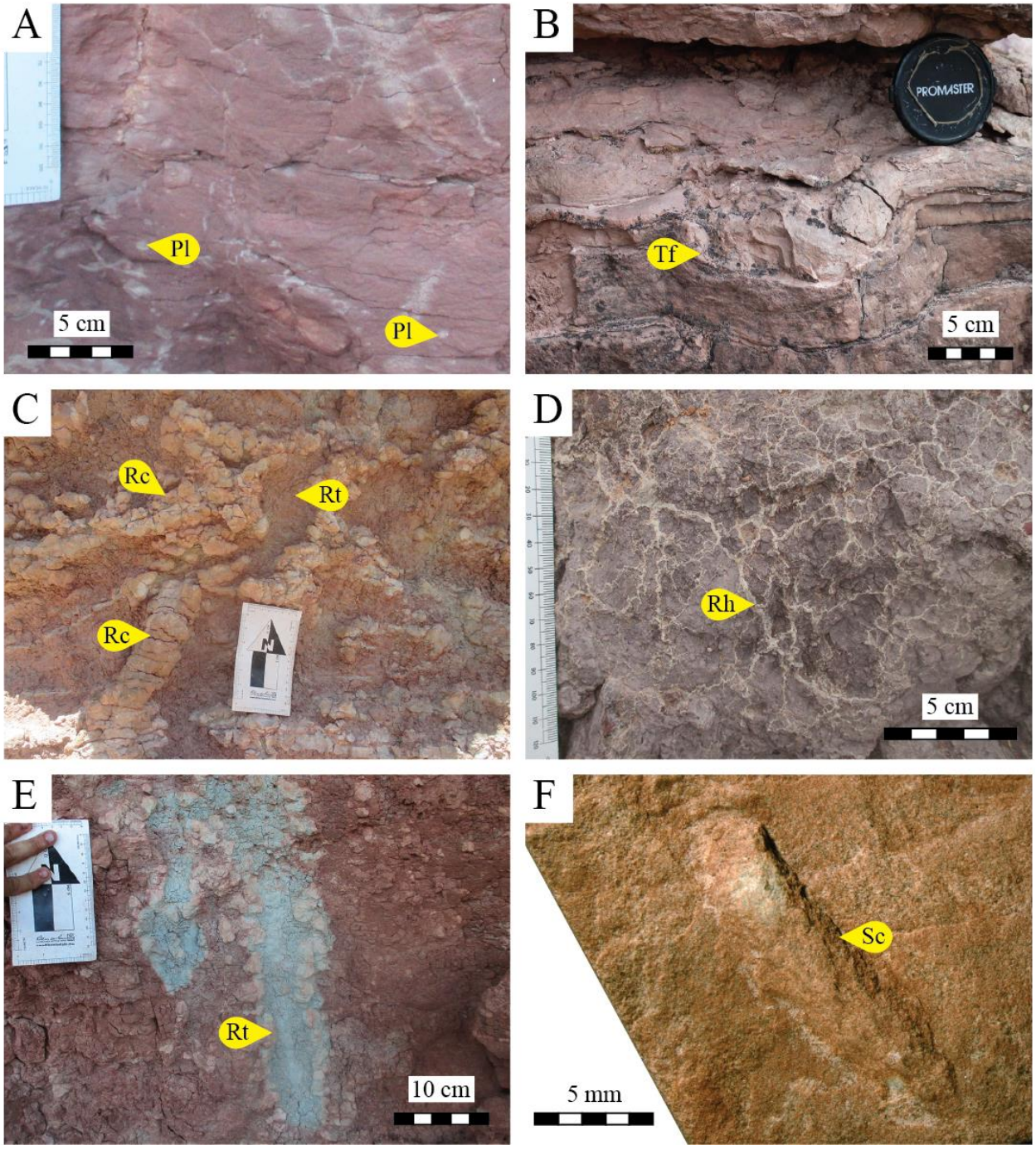
A
Pl
5 cm
Pl
B
PROMASTER
Tf
5 cm
C
Rc
Rt
Rc
D
Rh
5 cm
E
Rt
10 cm
F
Sc
5 mm

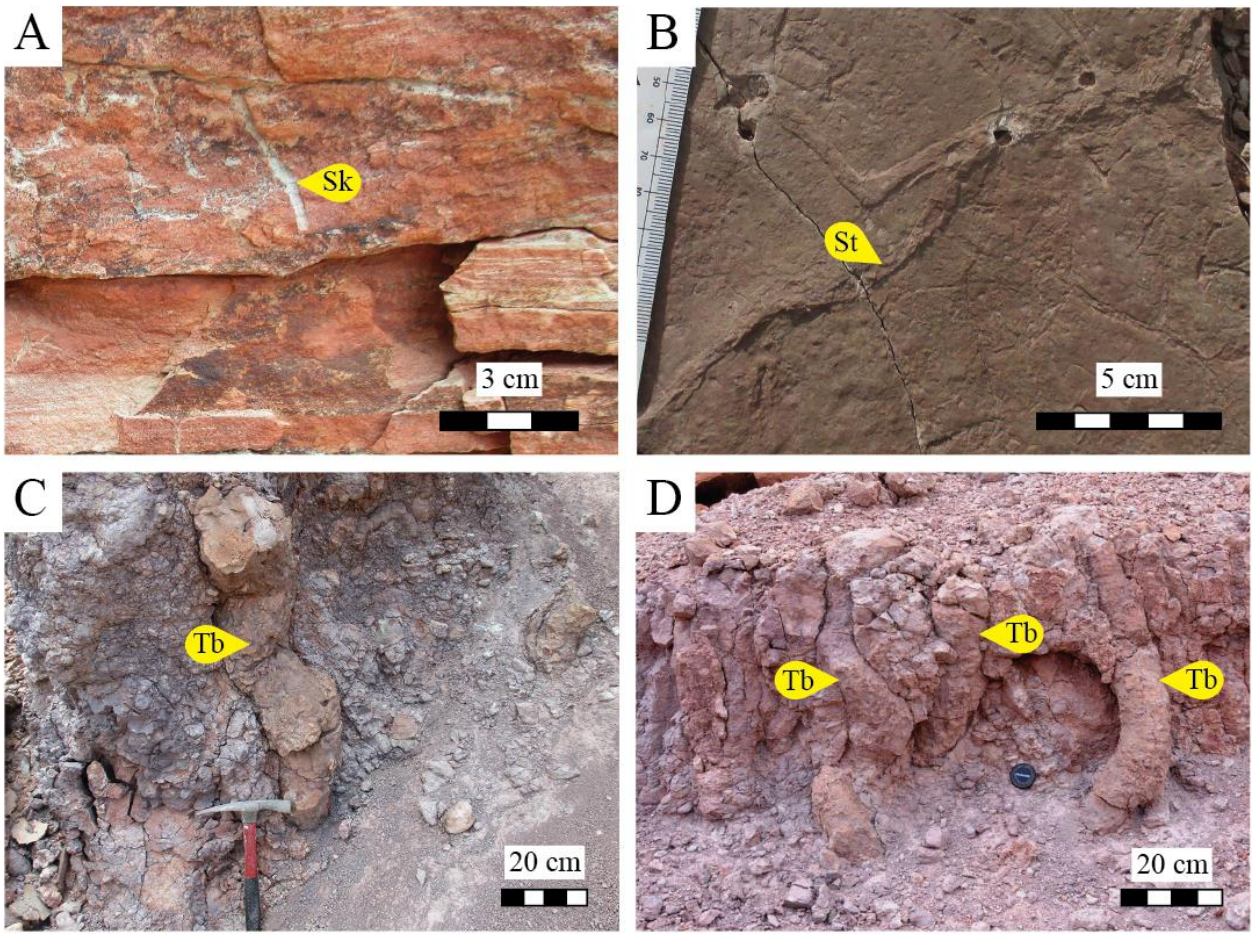
A
Sk
3 cm
B
St
5 cm
C
Tb
20 cm
D
Tb
Tb
Tb
20 cm

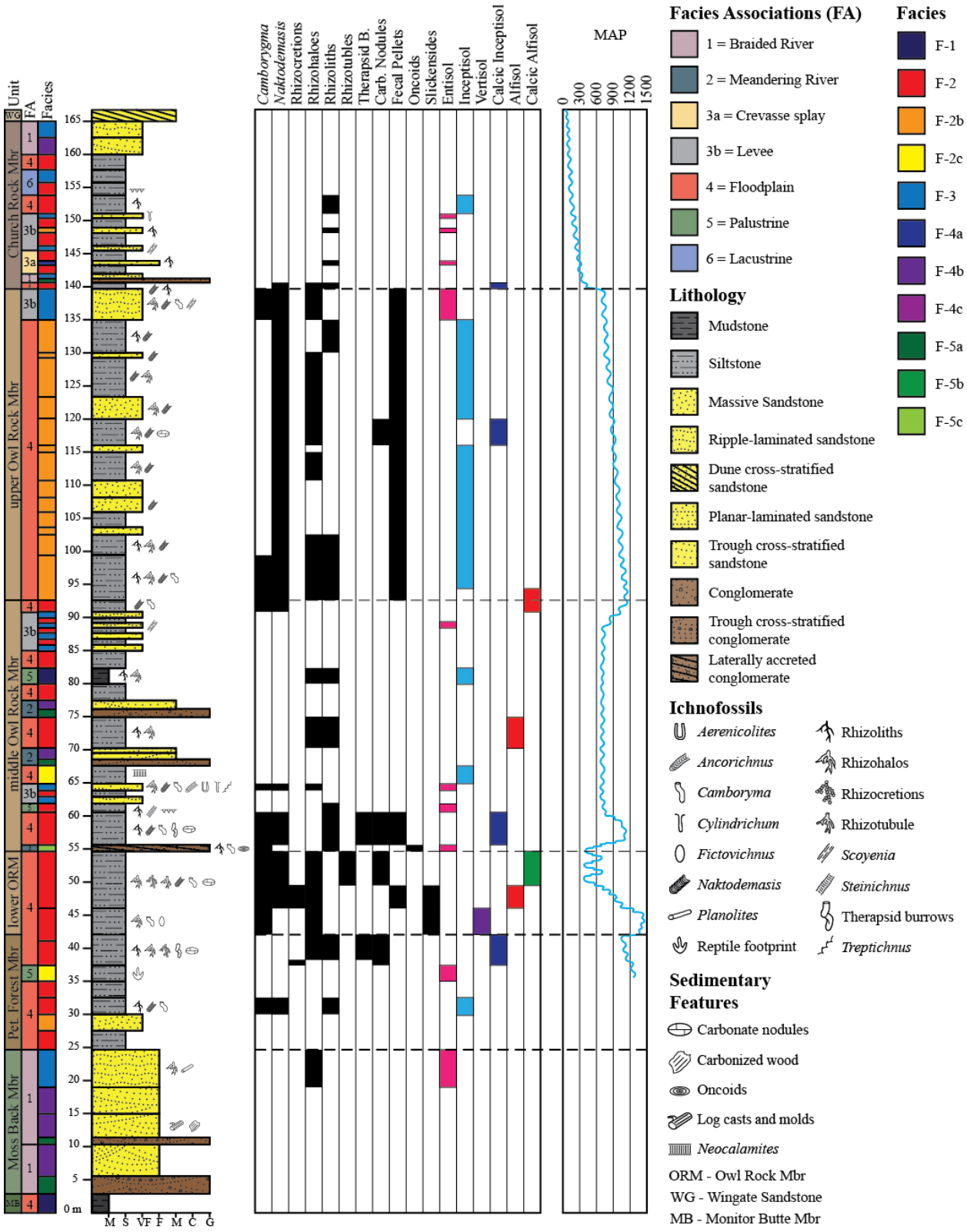
Unit
FA
Facies
Church Rock Mbr
upper Owl Rock Mbr
middle Owl Rock Mbr
lower ORM
Pet. Forest Mbr
Moss Back Mbr
WG
MB
M S VF F M C G
Camborygma
Naktodemasis
Rhizocretions
Rhizohaloes
Rhizoliths
Rhizotubles
Therapsid B.
Carb. Nodules
Fecal Pellets
Oncoids
Slickensides
Entisol
Inceptisol
Vertisol
Calcic Inceptisol
Alfisol
Calcic Alfisol
MAP
0
300
600
900
1200
1500
Facies Associations (FA)
1 = Braided River
2 = Meandering River
3a = Crevasse splay
3b = Levee
4 = Floodplain
5 = Palustrine
6 = Lacustrine
Facies
F-1
F-2
F-2b
F-2c
F-3
F-4a
F-4b
F-4c
F-5a
F-5b
F-5c
Lithology
Mudstone
Siltstone
Massive Sandstone
Ripple-laminated sandstone
Dune cross-stratified sandstone
Planar-laminated sandstone
Trough cross-stratified sandstone
Conglomerate
Trough cross-stratified conglomerate
Laterally accreted conglomerate
Ichnofossils
Aerenicolites
Ancorichnus
Camboryma
Cylindrichum
Fictovichnus
Naktodemasis
Planolites
Reptile footprint
Rhizoliths
Rhizohalos
Rhizocretions
Rhizotubule
Scoyenia
Steinichnus
Therapsid burrows
Treptichnus
Sedimentary Features
Carbonate nodules
Carbonized wood
Oncoids
Log casts and molds
Neocalamites
ORM - Owl Rock Mbr
WG - Wingate Sandstone
MB - Monitor Butte Mbr

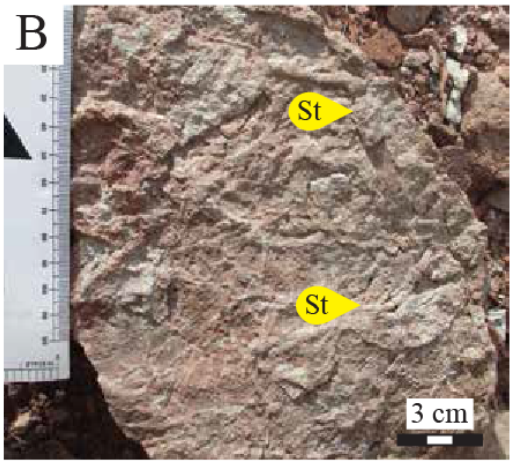

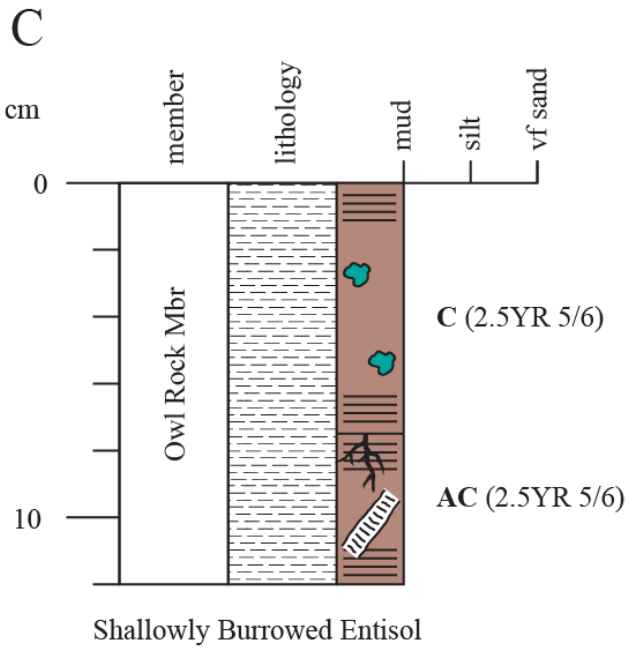

Ichnofossils

- *Aerenicolites*
- *Ancorichnus*
- *Camboryma*
- *Cylindrichum*
- *Fictovichnus*
- *Naktodemasis*
- *Planolites*
- Reptile Footprint
- Rhizoliths
- Rhizohalos
- Rhizocretions
- Rhizotubule
- *Skolithos*
- *Scoyenia*
- *Steinichnus*
- Therapsid Burrows
- *Treptichnus*

Pedogenic Features

- Blocky peds
- Carbonate nodules
- Granular peds
- Iron nodules
- Mottles
- Prismatic peds
- Relict Bedding
- Siderite nodules
- Slickensides
- Wedge peds

Sedimentary Features

- Planar-laminated bedding
- Ripple-laminated bedding

Lithology

- Mudstone
- Siltstone
- Sandstone
- Conglomerate

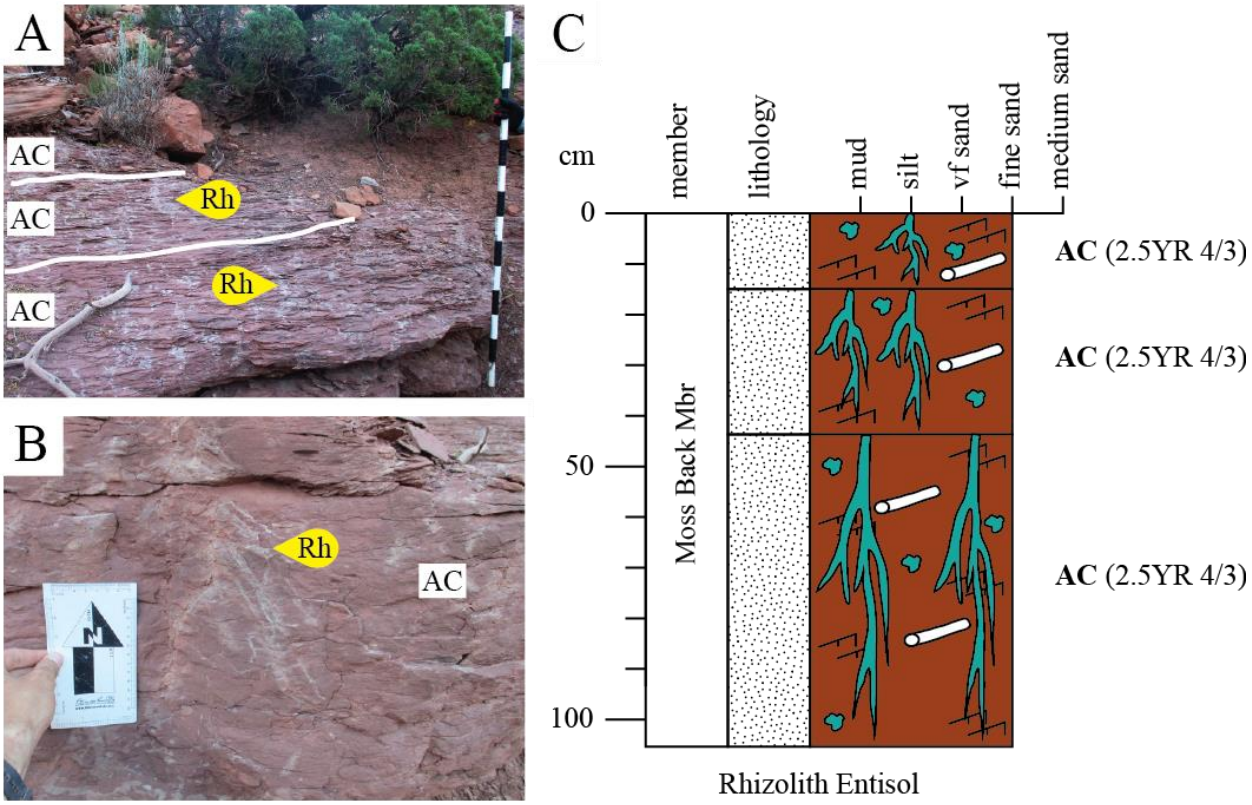
A
AC
Rh
AC
Rh
AC
B
Rh
AC
C
cm
member
lithology
mud
silt
vf sand
fine sand
medium sand
0
50
100
Moss Back Mbr
AC (2.5YR 4/3)
AC (2.5YR 4/3)
AC (2.5YR 4/3)
Rhizolith Entisol

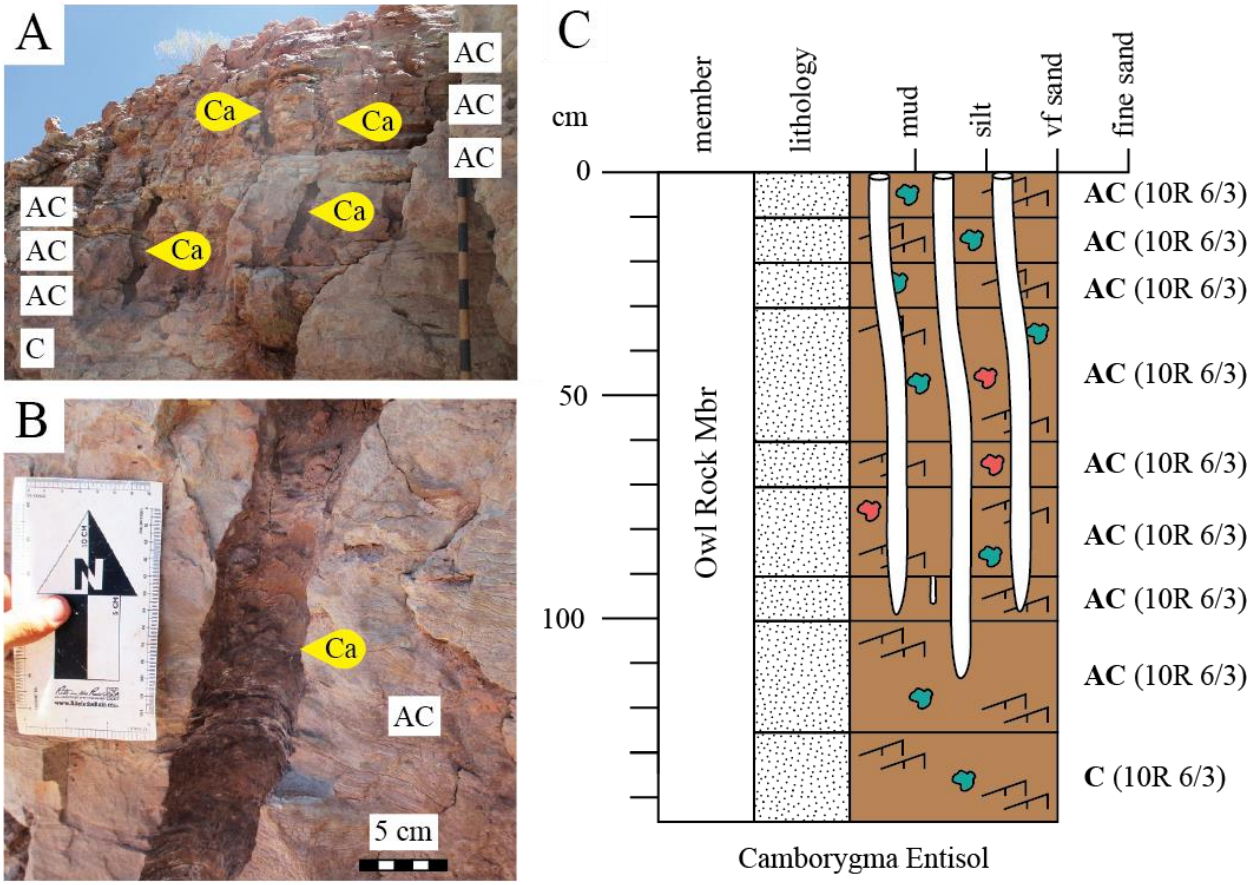
A
AC
AC
AC
Ca
Ca
Ca
Ca
AC
AC
AC
C
B
Ca
AC
5 cm
C
cm
member
lithology
mud
silt
vf sand
fine sand
0
50
100
Owl Rock Mbr
AC (10R 6/3)
AC (10R 6/3)
AC (10R 6/3)
AC (10R 6/3)
AC (10R 6/3)
AC (10R 6/3)
AC (10R 6/3)
AC (10R 6/3)
C (10R 6/3)
Camborygma Entisol

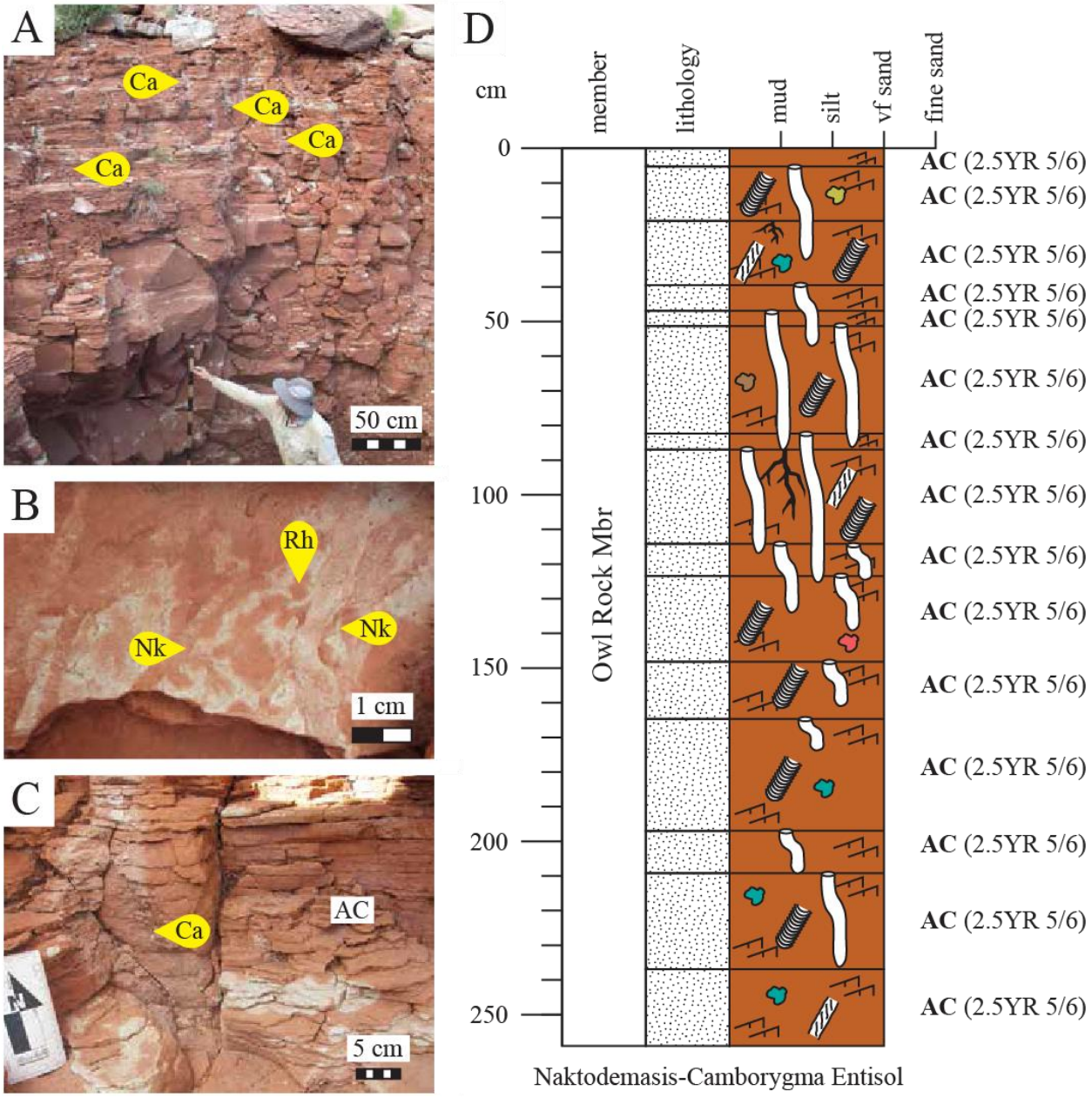
A
Ca
Ca
Ca
Ca
50 cm
B
Rh
Nk
Nk
1 cm
C
Ca
AC
5 cm
D
cm
member
lithology
mud
silt
vf sand
fine sand
0
50
100
150
200
250
Owl Rock Mbr
AC (2.5YR 5/6)
AC (2.5YR 5/6)
AC (2.5YR 5/6)
AC (2.5YR 5/6)
AC (2.5YR 5/6)
AC (2.5YR 5/6)
AC (2.5YR 5/6)
AC (2.5YR 5/6)
AC (2.5YR 5/6)
AC (2.5YR 5/6)
AC (2.5YR 5/6)
AC (2.5YR 5/6)
AC (2.5YR 5/6)
Naktodemasis-Camborygma Entisol

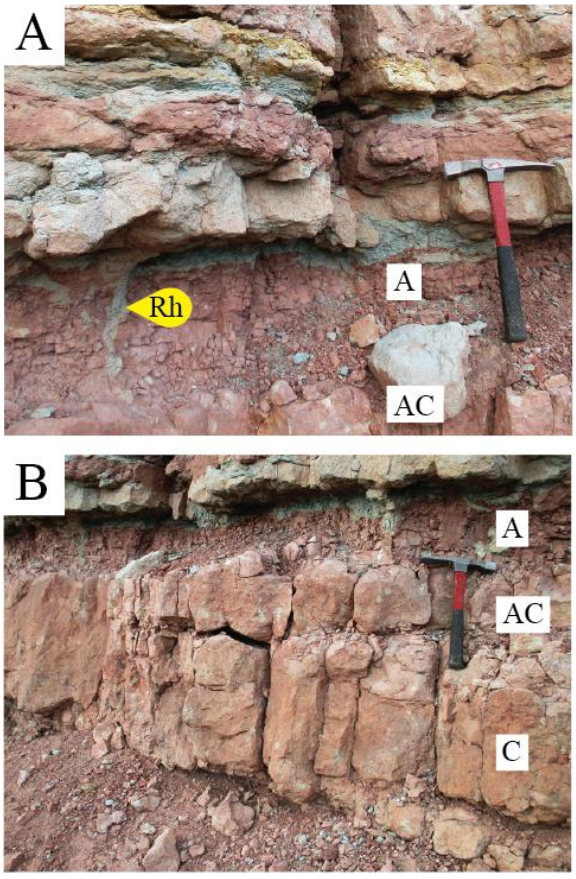
A
Rh
A
AC
B
A
AC
C
C
cm
member
lithology
mud
silt
vf sand
fine sand
0
10
20
30
40
50
60
70
80
90
Owl Rock Mbr
A (10R 5/4)
AC (5YR 7/4)
C (5YR 7/4)
Rhizolith Inceptisol

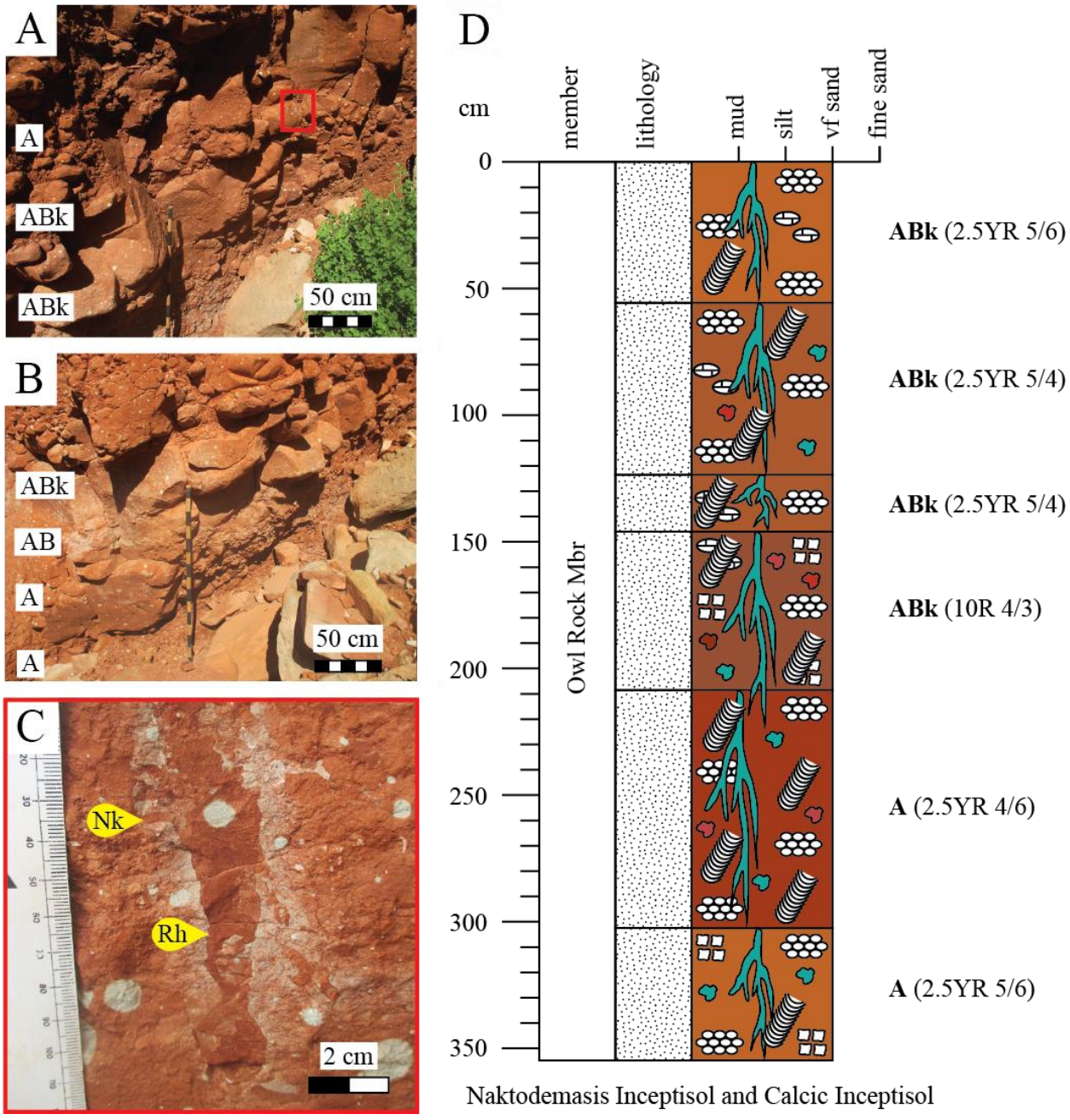
A
A
ABk
ABk
50 cm
B
ABk
AB
A
A
50 cm
C
Nk
Rh
2 cm
D
cm
member
lithology
mud
silt
vf sand
fine sand
0
50
100
150
200
250
300
350
Owl Rock Mbr
ABk (2.5YR 5/6)
ABk (2.5YR 5/4)
ABk (2.5YR 5/4)
ABk (10R 4/3)
A (2.5YR 4/6)
A (2.5YR 5/6)
Naktodemasis Inceptisol and Calcic Inceptisol

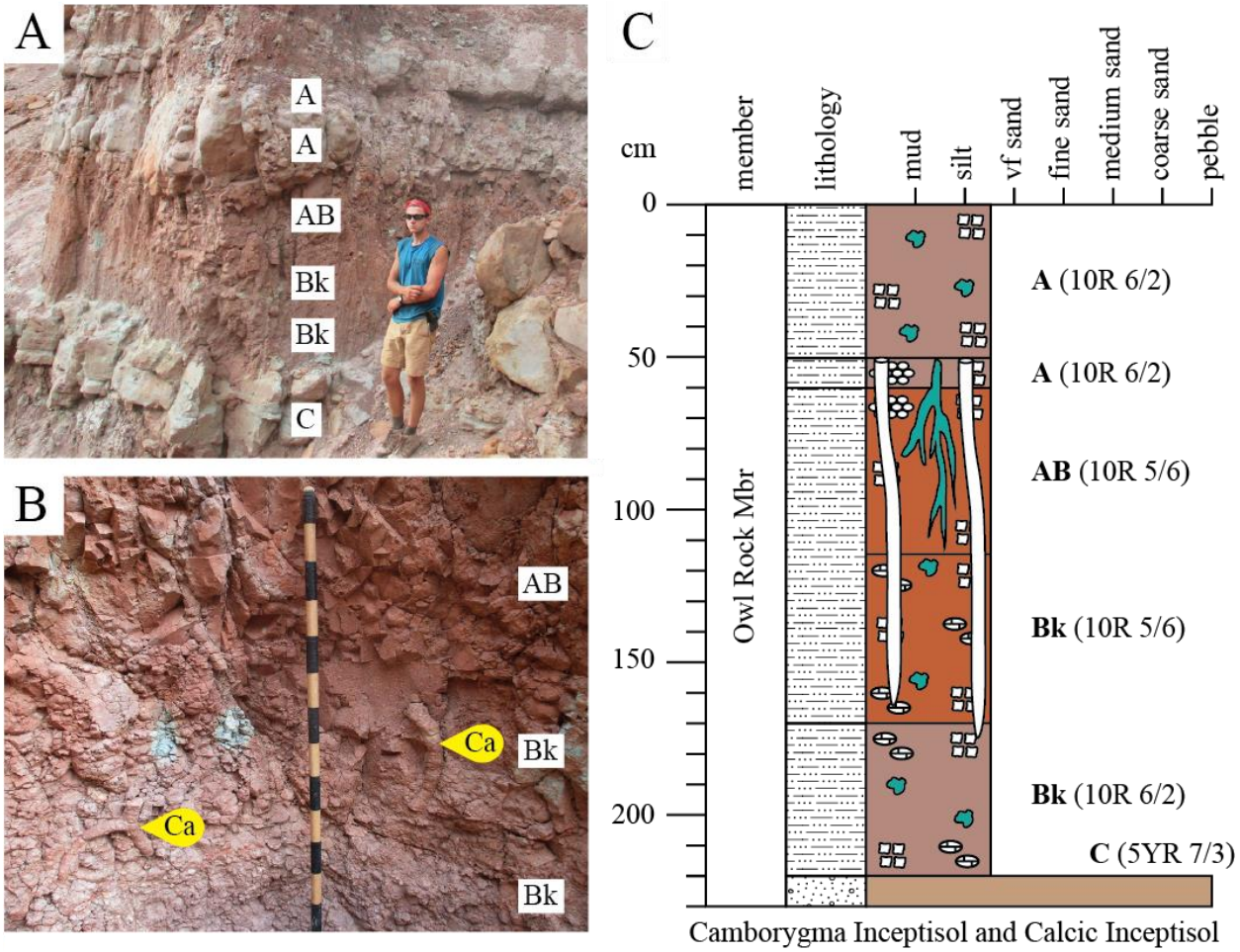
A
A
A
AB
Bk
Bk
C
B
AB
Ca
Bk
Ca
Bk
C
cm
member
lithology
mud
silt
vf sand
fine sand
medium sand
coarse sand
pebble
0
50
100
150
200
Owl Rock Mbr
A (10R 6/2)
A (10R 6/2)
AB (10R 5/6)
Bk (10R 5/6)
Bk (10R 6/2)
C (5YR 7/3)
Camborygma Inceptisol and Calcic Inceptisol

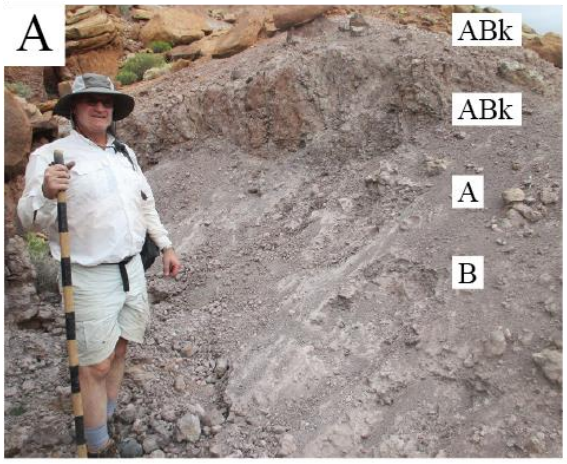

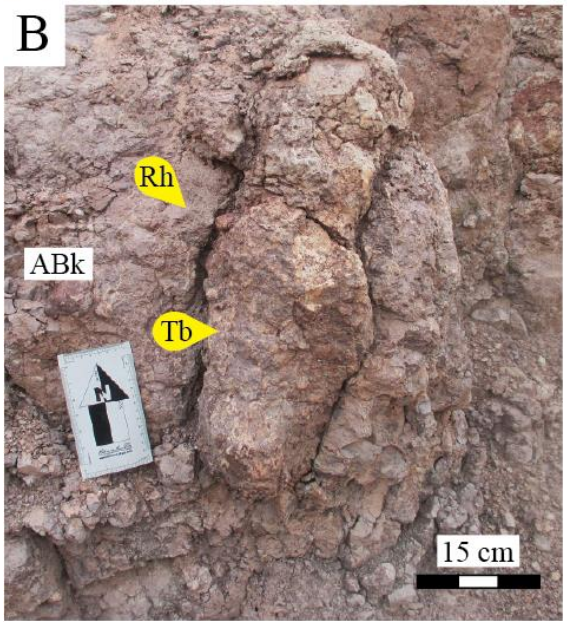

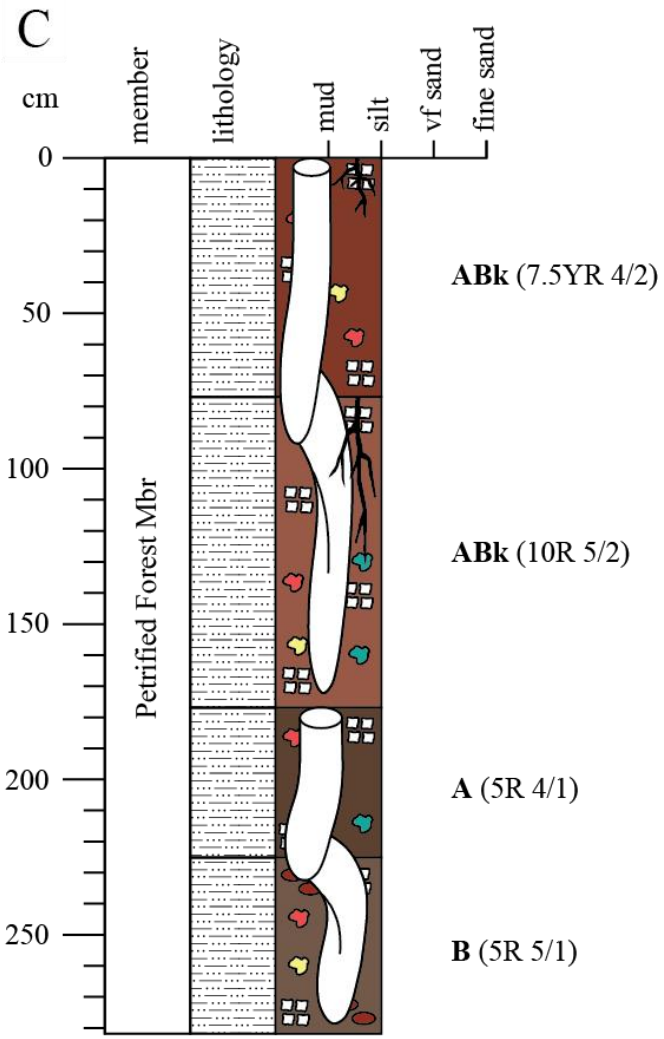

Therapsid Inceptisol and Calcic Inceptisol

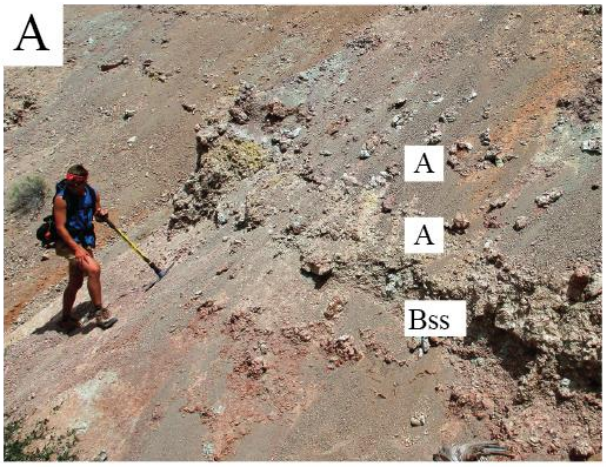
A
A
A
Bss

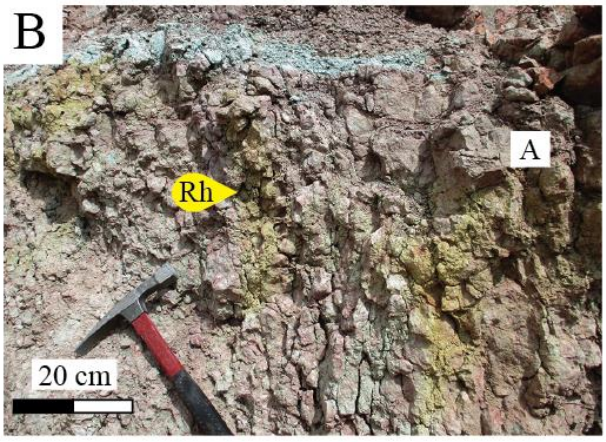
B
A
Rh
20 cm

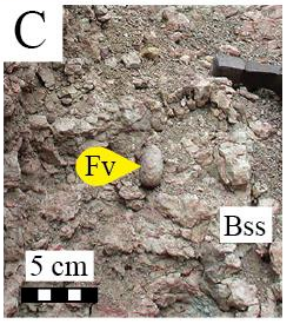
C
Fv
Bss
5 cm

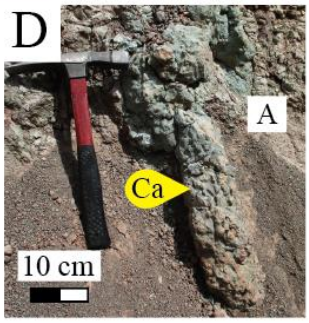
D
A
Ca
10 cm

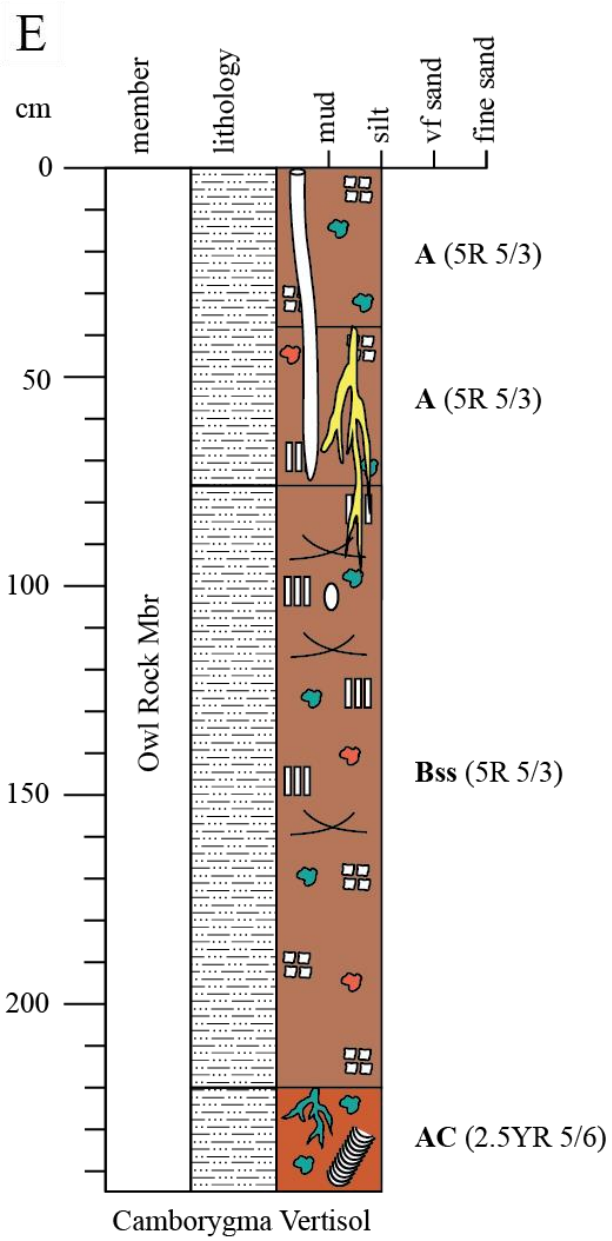
E
cm
member
lithology
mud
silt
vf sand
fine sand
0
50
100
150
200
Owl Rock Mbr
A (5R 5/3)
A (5R 5/3)
Bss (5R 5/3)
AC (2.5YR 5/6)
Camborygma Vertisol

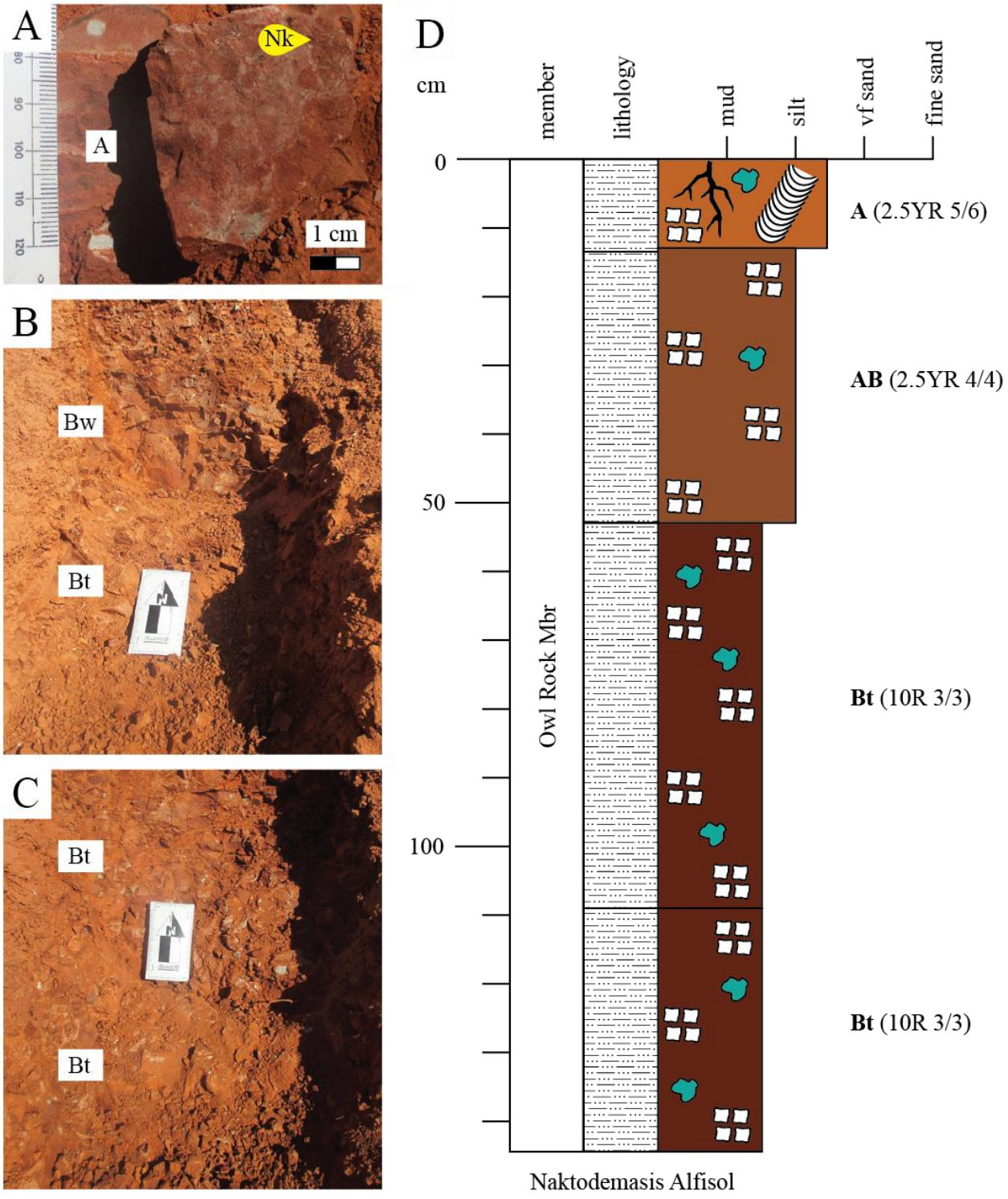
A
Nk
A
1 cm
B
Bw
Bt
C
Bt
Bt
D
cm
member
lithology
mud
silt
vf sand
fine sand
0
50
100
Owl Rock Mbr
A (2.5YR 5/6)
AB (2.5YR 4/4)
Bt (10R 3/3)
Bt (10R 3/3)
Naktodemasis Alfisol

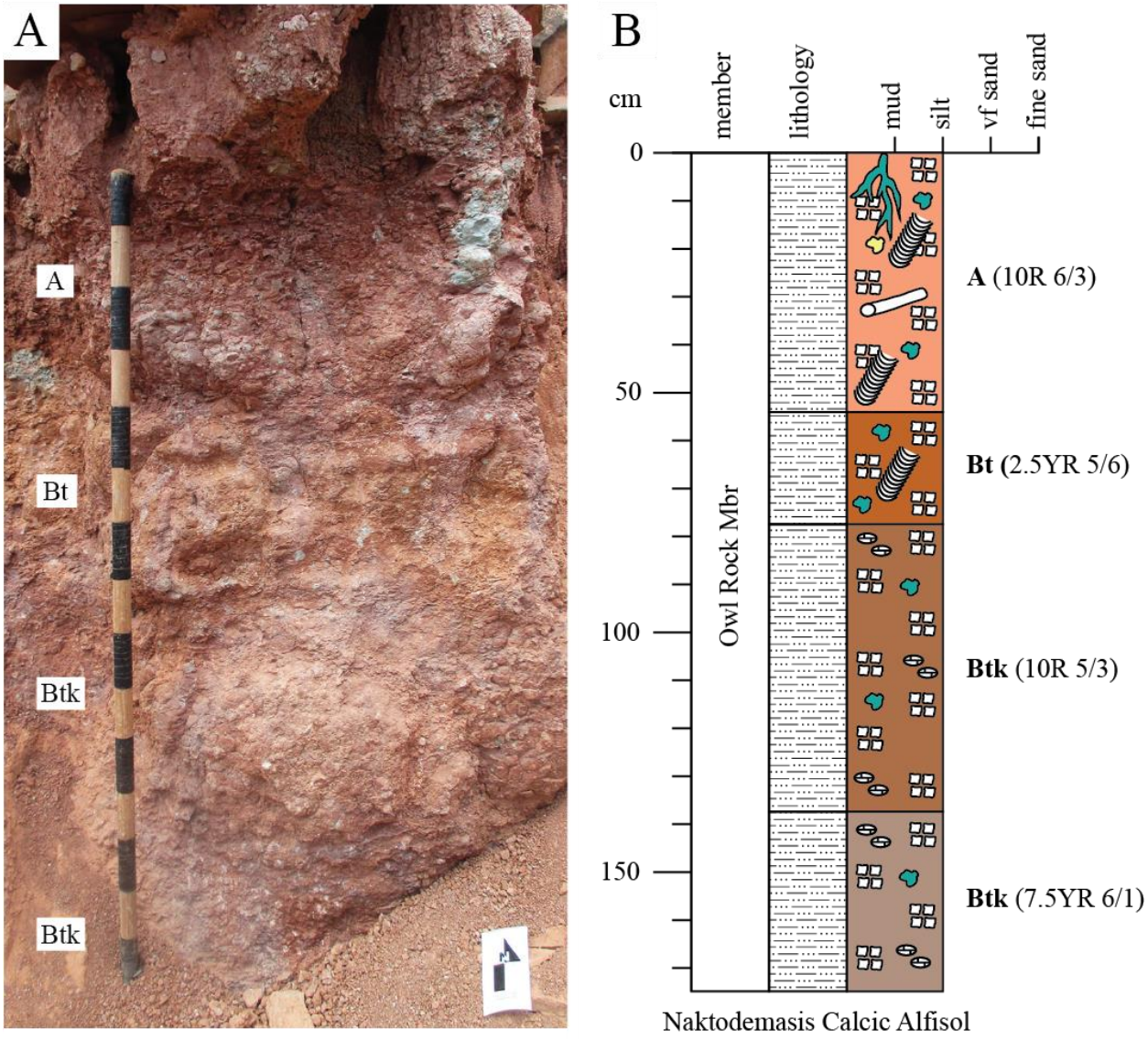
A
A
Bt
Btk
Btk
B
cm
member
lithology
mud
silt
vf sand
fine sand
0
50
100
150
Owl Rock Mbr
A (10R 6/3)
Bt (2.5YR 5/6)
Btk (10R 5/3)
Btk (7.5YR 6/1)
Naktodemasis Calcic Alfisol

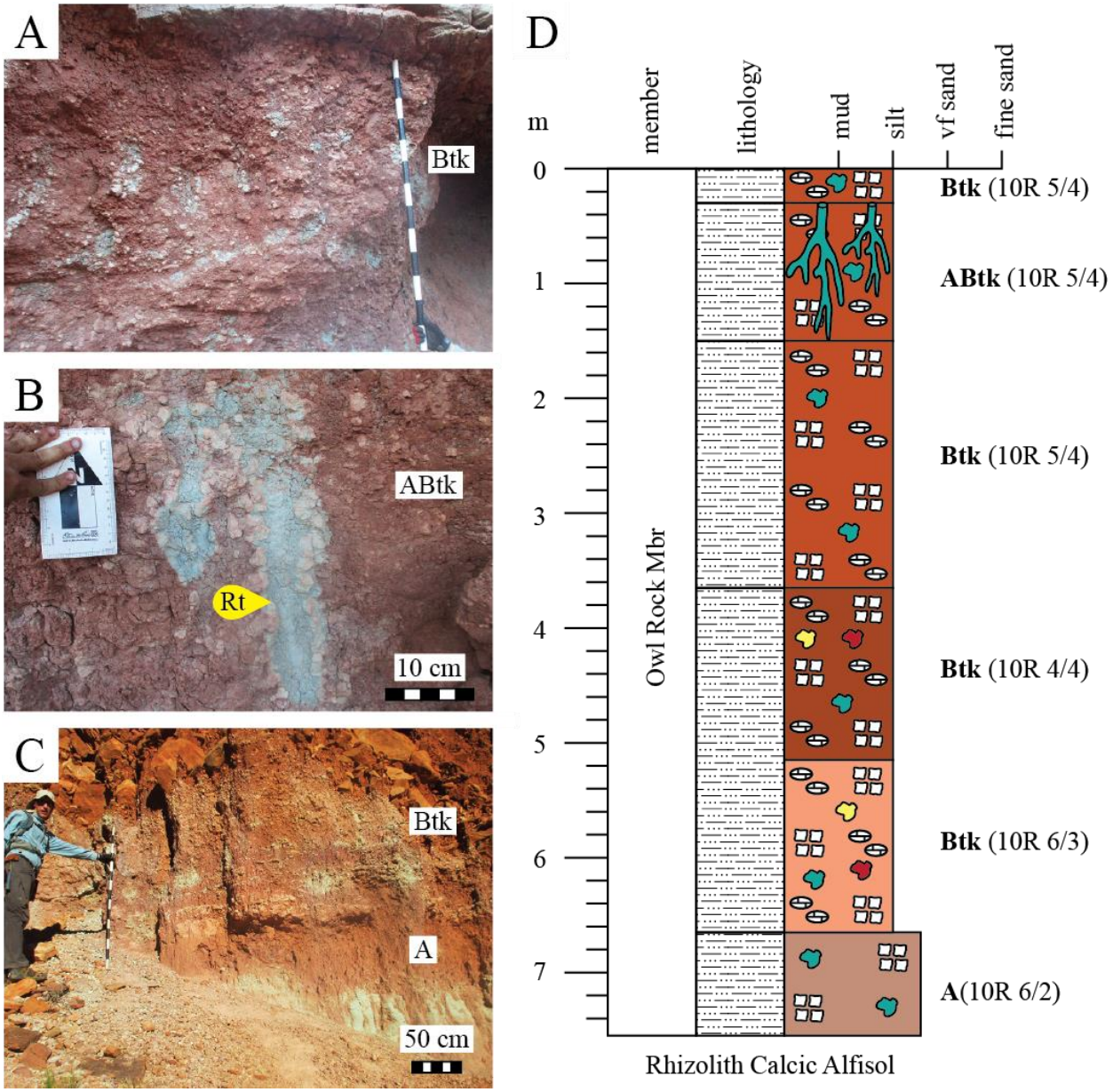
A
Btk
B
ABtk
Rt
10 cm
C
Btk
A
50 cm
D
m
member
lithology
mud
silt
vf sand
fine sand
0
1
2
3
4
5
6
7
Owl Rock Mbr
Btk (10R 5/4)
ABtk (10R 5/4)
Btk (10R 5/4)
Btk (10R 4/4)
Btk (10R 6/3)
A(10R 6/2)
Rhizolith Calcic Alfisol

CHINLE FM ICHNOPEDOFACIES ENVIRONMENTAL MODEL

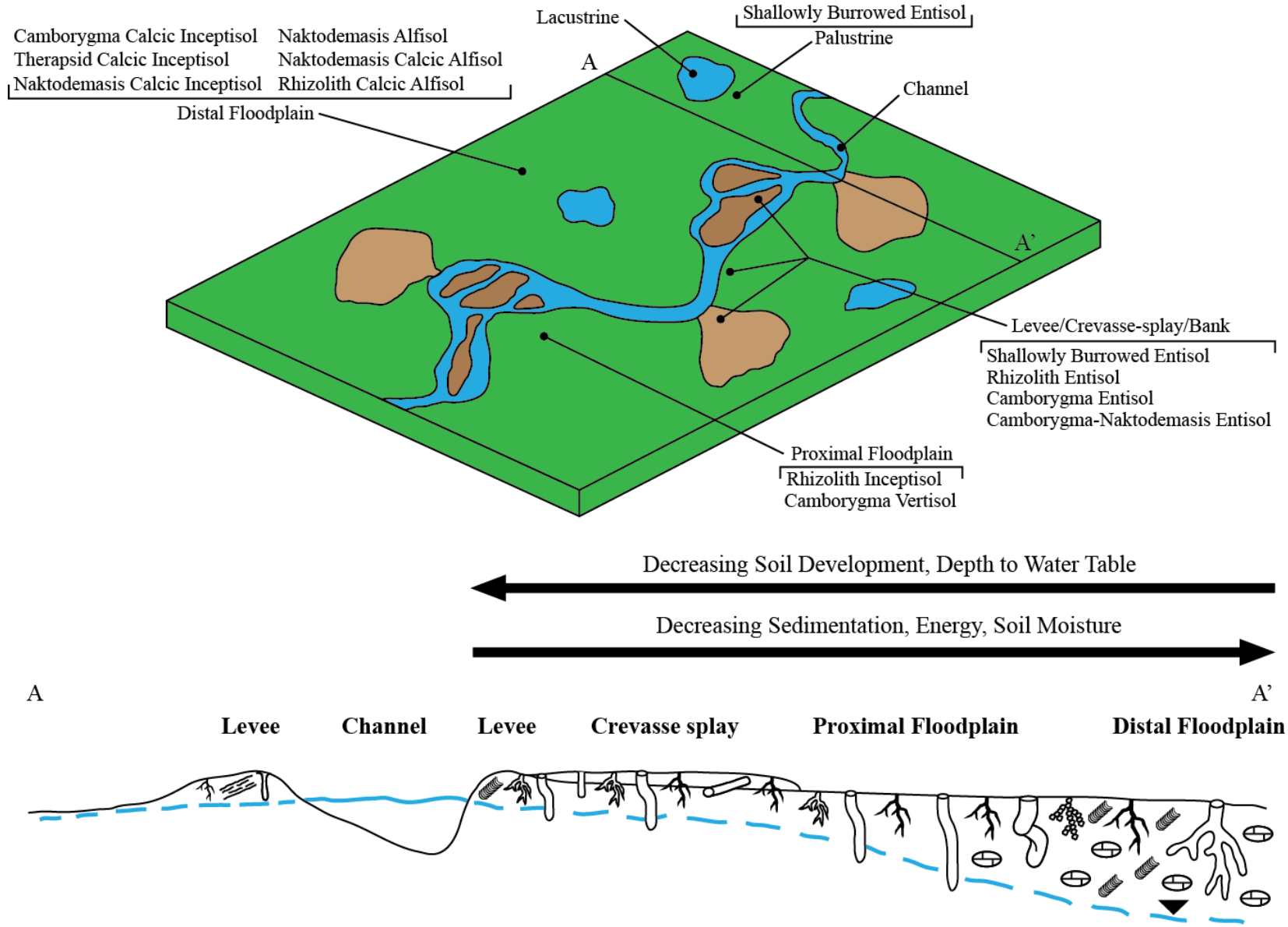

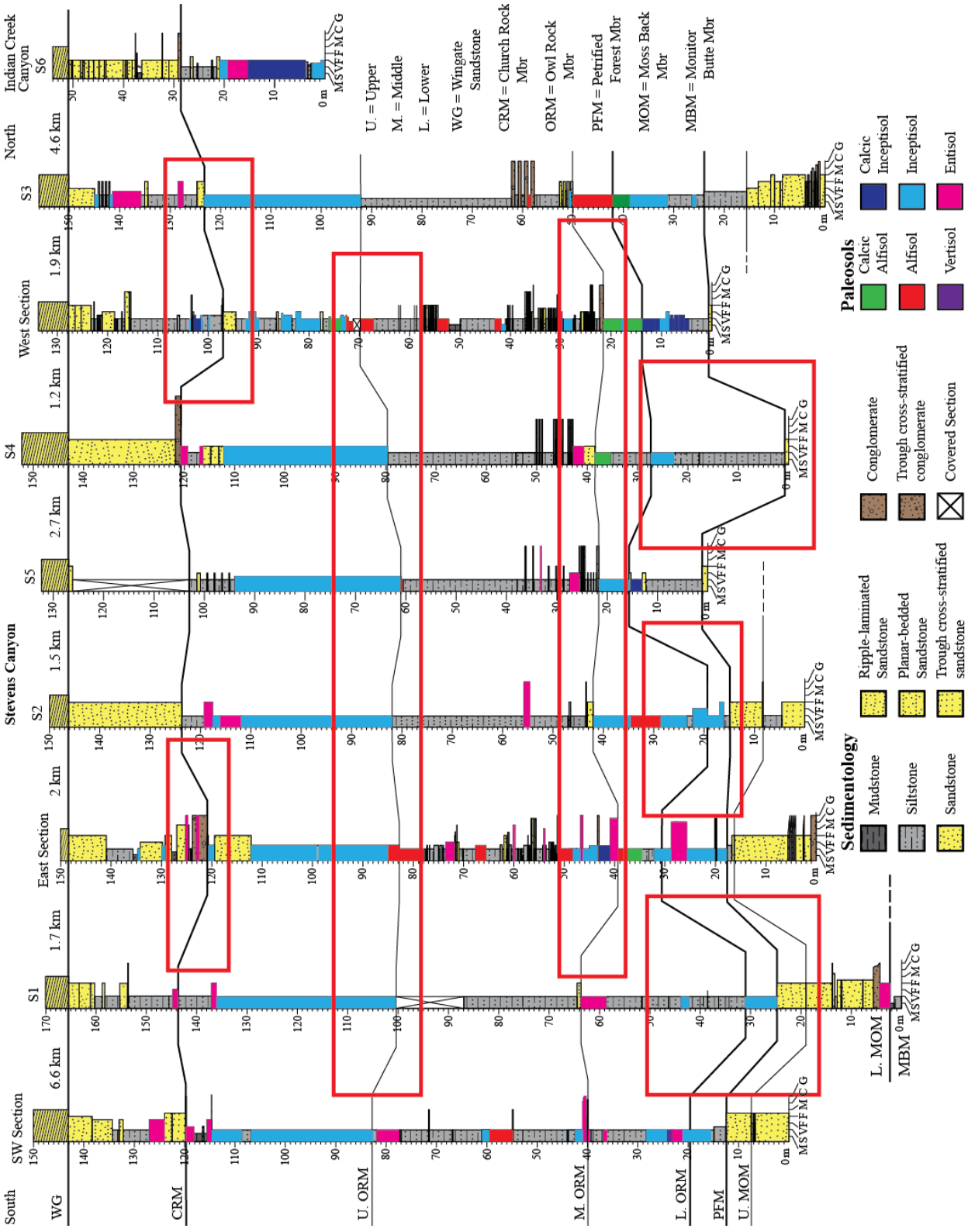
South
SW Section
6.6 km
East Section
1.7 km
2 km
Stevens Canyon
1.5 km
2.7 km
West Section
1.9 km
1.2 km
North
4.6 km
Indian Creek Canyon
S1
S2
S3
S4
S5
S6
WG
CRM
U. ORM
M. ORM
L. ORM
PFM
U. MOM
L. MOM
MBM
U. = Upper
M. = Middle
L. = Lower
WG = Wingate Sandstone
CRM = Church Rock Mbr
ORM = Owl Rock Mbr
PFM = Petrified Forest Mbr
MOM = Moss Back Mbr
MBM = Monitor Butte Mbr
Sedimentology
Mudstone
Siltstone
Sandstone
Ripple-laminated Sandstone
Planar-bedded Sandstone
Trough cross-stratified sandstone
Conglomerate
Trough cross-stratified conglomerate
Covered Section
Paleosols
Calcic
Alfisol
Calcic
Inceptisol
Alfisol
Inceptisol
Vertisol
Entisol

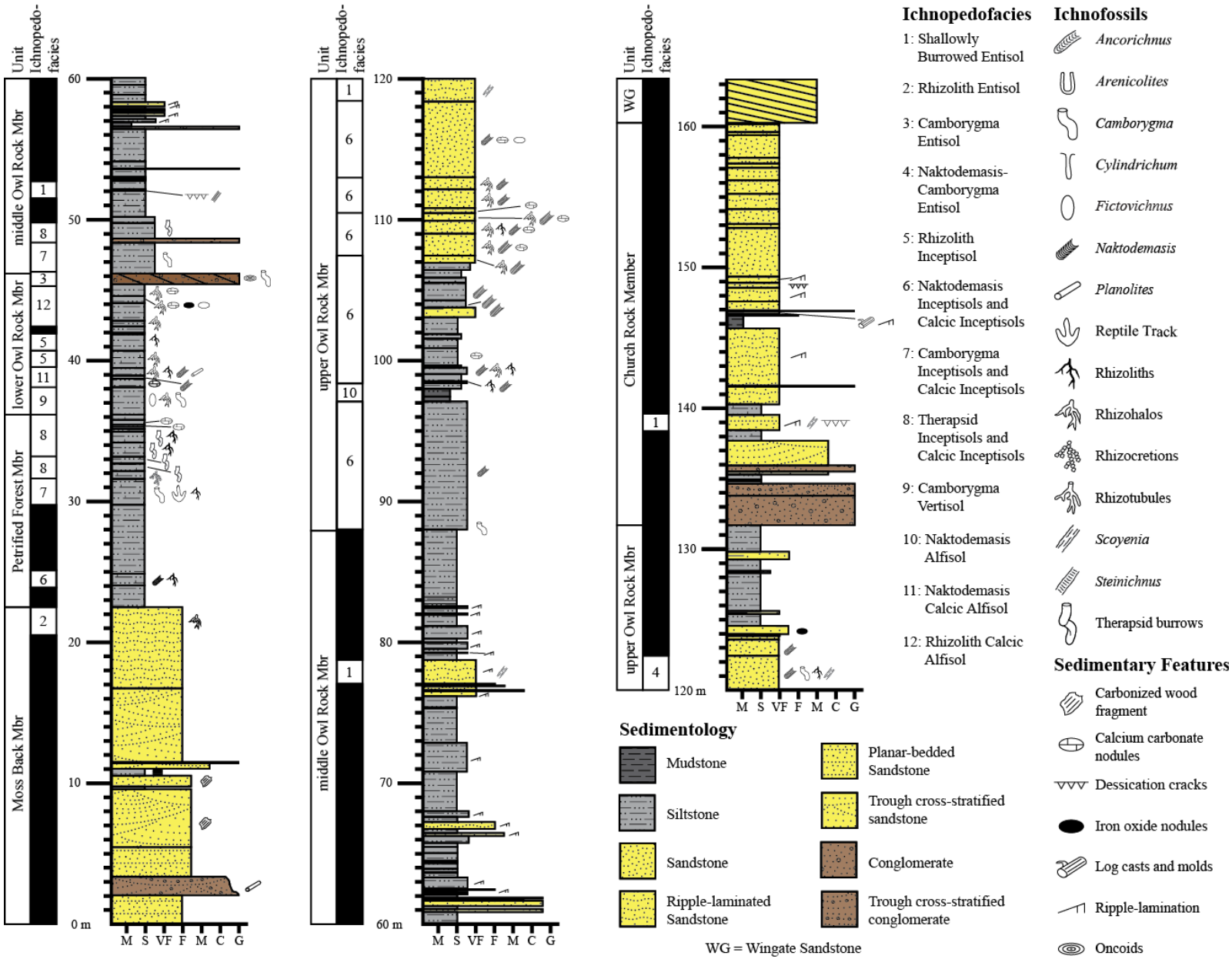
Unit
Ichnopedo-facies
Moss Back Mbr
Petrified Forest Mbr
lower Owl Rock Mbr
middle Owl Rock Mbr
upper Owl Rock Mbr
Church Rock Member
WG
M S VF F M C G
Ichnopedofacies
1: Shallowly Burrowed Entisol
2: Rhizolith Entisol
3: Camborygma Entisol
4: Naktodemasis-Camborygma Entisol
5: Rhizolith Inceptisol
6: Naktodemasis Inceptisols and Calcic Inceptisols
7: Camborygma Inceptisols and Calcic Inceptisols
8: Therapsid Inceptisols and Calcic Inceptisols
9: Camborygma Vertisol
10: Naktodemasis Alfisol
11: Naktodemasis Calcic Alfisol
12: Rhizolith Calcic Alfisol
Ichnofossils
Ancorichnus
Arenicolites
Camborygma
Cylindrichum
Fictovichnus
Naktodemasis
Planolites
Reptile Track
Rhizoliths
Rhizohalos
Rhizocretions
Rhizotubules
Scoyenia
Steinichnus
Therapsid burrows
Sedimentology
Mudstone
Siltstone
Sandstone
Ripple-laminated Sandstone
Planar-bedded Sandstone
Trough cross-stratified sandstone
Conglomerate
Trough cross-stratified conglomerate
Sedimentary Features
Carbonized wood fragment
Calcium carbonate nodules
Dessication cracks
Iron oxide nodules
Log casts and molds
Ripple-lamination
Oncoids
WG = Wingate Sandstone

TABLE 1.—*Chinle Formation Lithfacies*

Facies	Lithology	Thickness	Sediment Size and Texture	Composition
F-1	Massive to finely laminated, red, pale red, brown, and green-grey mudstone	0.3–4.75 m	Mud with rare silt and very fine sand; grains subangular to subrounded and moderately to well sorted	Mud; silt and sand grains comprised of quartz and calcite; calcium carbonate cement
F-2a	Massive red, pale red, and green-grey siltstone	0.02–12.0 m	Silt with mud and very fine sand; grains angular to subrounded and moderately to well sorted	Silt and sand grains comprised of quartz, calcite, and siltstone clasts; variable mud between grains; Fe and Mn nodules ranging from <0.1 mm to 0.3 mm in diameter; calcium carbonate cement
F-2b	Massive, red, pale red, and brown siltstone to very fine-grained sandstone	0.1–5.4 m	Silt with very fine sand and mud; grains subangular to subrounded and moderately to well sorted	Silt and sand grains comprised of quartz, calcite, siltstone clasts, and rare muscovite; variable mud between grains, Fe and Mn nodules <0.1 mm in diameter; calcium carbonate cement
F-2c	Planar-laminated, red, pale red, and brown siltstone to very fine-grained sandstone	0.02–2.5 m	Silt with very fine sand and mud; grains angular to subrounded and moderately to well sorted	Silt and sand grains comprised of quartz, calcite, and siltstone clasts; variable mud between grains, often draped along laminations; Fe and Mn nodules <0.1 mm in diameter; calcium carbonate cement
F-3	Ripple-cross-laminated, red, pale red, brown, and green-grey siltstone to medium-grained sandstone	0.02–7.5 m	Very fine to medium sand with silt and mud; grains subangular to subrounded; individual beds moderately to well sorted	Silt and sand grains comprised of quartz, calcite, siltstone clasts, and rare muscovite; variable mud between grains, often draped along laminations; Fe and Mn nodules <0.1 mm in diameter; calcium carbonate cement
F-4a	Massive, red, brown, and green-grey, fine- to very coarse-grained sandstone	0.1–2.0 m	Fine to very coarse sand; grains subrounded to rounded; individual beds well sorted	Sand grains comprised of quartz, siltstone clasts, lithic fragments, and limestone clasts; Fe and Mn nodules <0.1 mm in diameter; calcium carbonate cement
F-4b	Trough-cross-stratifed, brown, very fine- to coarse-grained sandstone	0.9–2.0 m	Very fine to coarse sand; grains subrounded to angular; individual beds moderately sorted	Sand grains comprised of quartz, lithic clasts, muscovite, and feldspar; quartz grains show overgrowth cement; Fe and Mn nodules <0.1 mm in diameter
F-4c	Planar-laminated, brown, and green-grey, fine- to coarse-grained sandstone	0.04–6.7 m	Fine to coarse sand with silt and mud; grains subangular to rounded; individual beds moderately to well sorted	Sand and silt grains comprised of quartz, siltstone clasts, lithic fragments, and limestone clasts; variable mud and siltstone between sand grains; Fe and Mn nodules <0.1 mm in diameter; calcium carbonate cement
F-5a	Trough-cross-stratified, brown and green-grey conglomerate	0.2–2.1 m	Granule to cobble clasts; poorly sorted	Quartz, lithic, and limestone clasts; Fe nodules <0.1 mm in diameter
F-5b	Massive to planar-laminated, red, brown, and green-grey conglomerate	0.01–2.1 m	Granule to pebble clasts; poorly sorted	Quartz, siltstone, lithic, and limestone clasts; calcium carbonate cement
F-5c	Incline-bedded, brown and green-grey conglomerate	0.75 m	Granule to pebble clasts; poorly sorted; beds graded and show lateral accretion	Quartz, limestone, and lithic clasts, oncoids up to 3.5 cm x 12 cm in diameter

TABLE 2.—*Chinle Formation Ichnofossils*

Ichnofossil	Size	Description	Behavior	Occurrence
Arenicolites	openings 2–7 mm diameter, 2–10 mm apart	Vertical, U-shaped burrows with paired cylindrical openings; smooth burrow walls; convex epirelief	Hydrophilic	Owl Rock Mbr
Ancorichnus	4 mm diameter	Horizontal burrows with smooth wall linings and meniscate backfill; burrows do not branch; concave and convex epirelief	Hygrophilic	Owl Rock Mbr
Camborygma	0.6–12 cm diameter, up to 185 cm long	Large vertical to subvertical, cylindrical to J-shaped burrows; show branching and chamber development; walls lined or unlined and have surficial scratch marks; full relief or concave epirelief	Hydrophilic	Petrified Forest and Owl Rock mbrs
Cylindrichum	2–7 mm diameter	Vertical, test-tube-shaped burrows with rounded lower ends; cylindrical openings in plan view; burrows infilled with sediment; convex epirelief	Terraphilic	Petrified Forest, Owl Rock, and Church Rock mbrs
Fictovichnus	1.5 cm diameter, up to 3 cm long	Ovoid capsules; walls smooth or show high density pattern of transverse scratch marks; full relief	Terraphilic	Owl Rock Mbr
Naktodemasis	0.5–6 mm diameter	Subvertical to subhorizontal, unlined, meniscate backfilled burrows; burrows filled with sediment from surrounding medium; meniscate packages thin, tightly spaced, and ellipsoidal; burrows straight to sinuous and do not branch but crosscut; does not weather differentially from surrounding matrix	Terraphilic, Hygrophilic	Petrified Forest and Owl Rock mbrs
Planolites	3–14 mm diameter	Horizontal to subhorizontal, simple, unlined, unbranched, cylindrical burrows; cylindrical openings in cross section; infilled with sediment	Hydrophilic	Moss Back, Petrified Forest, Owl Rock, and Church Rock mbrs
Rhizocretions	2–7 cm diameter, up to 3 m long	Vertical, infilled burrows which taper towards bottom; infilled by same material as surrounding matrix or by calcium carbonate nodules; have irregular bumpy surface; full relief	Terraphilic	Petrified Forest and Owl Rock mbrs
Rhizohaloes	0.4–8 cm diameter, 1 m long	Vertical to subvertical halo surrounding root trace; original root material absent	Terraphilic	Moss Back, Petrified Forest, Owl Rock, and Church Rock mbrs
Rhizoliths	Often <2 mm diameter, up to 7 mm diameter, up to 52 cm long	Vertical to subvertical, sinuous traces with regular branching that often crosscut; taper towards base; contain fragments of original root materal	Terraphilic	Moss Back, Petrified Forest, Owl Rock, and Church Rock mbrs
Rhizotubules	6–9 cm diameter, 20–60 cm long	Vertical traces of calcium carbonate nodules surrounding a central cylindrical tube; tubes branch and taper towards base	Terraphilic	Owl Rock Mbr
Scoyenia	1–6 mm diameter	Horizontal to subhorizontal, straight to sinuous, unlined, meniscate backfilled burrows; surficial morphology of ropey texture and overlapping scratch marks; do not branch but crosscut; meniscate packages thin and tightly spaced; convex epirelief	Hygrophilic	Petrified Forest, Owl Rock, and Church Rock mbrs

TABLE 2.—*Extended*

Ichnofossil	Size	Description	Behavior	Occurrence
Skolithos	2–5.5 mm diameter, 3.5–12 cm long	Vertical, simple, straight, cylindrical burrows; burrow walls smooth	Hydrophilic	Owl Rock Mbr
Steinichnus	4–9 mm diameter	Horizontal, cylindrical, sinuous burrows; width varies across a single burrow; burrows branch and cross cut; structureless burrow fill; convex epirelief	Hygrophilic	Owl Rock Mbr
Tetrapod footprint	9–20 cm long, 4–11 cm deep	Only seen in cross section where footprint preserved as depressions deforming underlying bedding	Epiterraphilic	Petrified Forest and Chruch Rock mbrs
Therapsid burrow	6–16 cm diameter, 215 cm long	Very large vertical to subvertical, helical and cylindrical burrows; surficial morphology shows V-shaped scratch marks; full relief	Terraphilic	Petrified Forest and Owl Rock mbrs
Treptichnus	7 mm diameter	Horizontal burrows consisting of shallow U-shaped segments connecting to form a zig-zag or irregular pattern; forked where segments connect; burrow infilled with sediment; convex epirelief	Hydrophilic	Owl Rock Mbr

TABLE 3.—*Chinle Formation Ichnocoenoses, traces listed in order of abundance*

Ichnocoenoses	Trace Fossils	Facies
I-1. *Camborygma*	*Camborygma*, *Naktodemasis*, rhizohaloes, and rhizoliths; rare therapsid burrows, *Scoyenia*, tetrapod tracks, *Cylindrichum*, and *Skolithos*	F-2a, F-2b, F-2c, F-3, F-4a
I-2. *Cylindrichum*	*Cylindrichum* and *Scoyenia*	F-2c, F-3
I-3. *Naktodemasis*	*Naktodemasis*, rhizohaloes, rhizoliths; rare *Camborygma*, *Planolites*	F-2a, F-2b
I-4. *Naktodemasis–Camborygma*	*Naktodemasis*, *Camborygma*, rhizoliths, and *Scoyenia*; rare *Ancorichnus*, *Arenicolites*, *Cylindrichum*, *Planolites*, and *Treptichnus*	F-2a, F-2b, F-3
I-5. Rhizolith	Rhizohaloes, rhizoliths, rhizocretions, rhizotubules; rare *Planolites*, *Naktodemasis*, and *Skolithos*	F-1, F-2a, F-2b, F-2c, F-3, F-4a
I-6. *Scoyenia*	*Scoyenia* and rhizoliths; rare *Cylindrichum*, *Planolites*, and *Camborygma*	F-2a, F-3
I-7. *Skolithos*	*Skolithos*; rare *Planolites* and *Naktodemasis*	F-2c
I-8. *Steinichnus*	*Steinichnus*; rare rhizoliths	F-1, F-4b
I-9. Therapsid	Therapsid burrows, *Camborygma*, rhizohaloes, rhizoliths; rare *Cylindrichum*, *Scoyenia*, and *Naktodemasis*	F-2a, F-2b

TABLE 4.—*Chinle Formation Paleosols*

Paleosol Order	Horizons	Color	Common Pedogenic Features	Facies	Ichnocoenoses
P-1. Entisol	AC, C	Red, pale red, red brown, and green grey	Primary bedding and sedimentary structures present; bedding disrupted by roots and burrows	F-2c, F-3, F-4a, F-4b	I-1, I-2, I-3, I-4, I-5, I-6, I-7, I-8
P-2. Inceptisol	A, AC, C	Red, pale red, and red brown	Weak horizon development; A horizon has angular blocky and granular peds	F-1, F-2a, F2b	I-3, I-5
P-3. Calcic Inceptisol	A, AB, ABk, Bk C	Red, pale red, and red brown	A horizon has angular blocky and granular peds; AB horizon has angular blocky and granular peds, redder than overlying A horizon; ABk and Bk horizons have angular blocky and granular peds, Stages 1–2 calcium carbonate accumulation; green-grey reduction halos	F-2a, F-2b	I-1, I-3, I-9
P-4. Vertisol	A, Bss	Pale red	A horizon has angular blocky and prismatic peds; Bss horizon has prismatic peds, large slickensides; red, yellow, and green-grey mottles	F-2a	I-1
P-5. Alfisol	A, AB, Bt	Red and red brown	A horizon has angular blocky and granular peds; Bt horizon has angular blocky, wedge, and granular peds, clay accumulation and slickensides; green-grey reduction halos	F-2a, F-2b	I-1, I-3, I-4, I-5
P-6. Calcic Alfisol	A, ABtk, Bt, Btk	Red, pale red, and red brown	A horizon has angular blocky peds; Bt horizon has angular blocky peds, clay accumulation; ABtk and Btk horizons have angular blocky peds, clay accumulation, sparse to numerous Stages 2–3 calcium carbonate nodules, rare slickensides; green-grey reduction halos	F-2a, F-2b	I-1, I-3, I-5, I-9

TABLE 5.—*Chinle Formation Facies Associations*

Facies Association	Lithofacies	Ichnocoenoses	Paleosols	Other Features	Paleoenvironment
FA-1	F-2a, F-3, F-4b, F-4c, F-5a, F-5b	I-5	P-1	Prevalence of coarse-grained lithofacies and trough-cross-stratification; sand bodies form interconnected, stacked, laterally extensive sand sheets; contain wood fragments and log casts; basal erosive contact	Braided River
FA-2	F-5c	N/A	N/A	Incline-bedded conglomerates; ribbon and thin sand sheet bodies surrounded by mudstones and siltstones; large oncoids as clasts	Meandering River
FA-3	F-2a, F-2c, F-3, F-4a, F-5b	I-1, I-2, I-4, I-6, I-7	P-1	Interbedded ripple-cross-laminated sandstone and siltstone; thin, laterally discontinuous sand sheet and ribbon sand bodies; basal erosive contact	Crevasse Splay and Levee
FA-4	F-1, F-2a, F-2b, F-2c, F-3, F-4a	I-1, I-3, I-5, I-9	P-1, P-2, P-3, P-4, P-5, P-6	Predominance of fine-grained lithofacies; high variety of trace fossils; well-developed paleosols	Overbank and Floodplain
FA-5	F-1, F-2a, F-2c	I-1, I-2, I-5, I-8	P-1, P-2	Planar-laminated siltstone and very fine-grained sandstone; disruption of bedding by tetrapod tracks and rhizoliths; shallow, horizontal burrows along bedding planes; *Neocalamites*	Palustrine
FA-6	F-2a, F-2c	N/A	N/A	Planar-laminated siltstone and very fine-grained sandstone; rare trace fossils; desiccation cracks	Lacustrine